

國立交通大學

物理研究所

碩士論文

半古典方法於自旋弛豫和自旋傳輸之應用

Semiclassical Method Applied to
Spin Relaxation and Spin Transport



研究生：蔡政展

指導教授：張正宏 教授

中華民國九十五年七月

半古典方法於自旋弛豫和自旋傳輸之應用

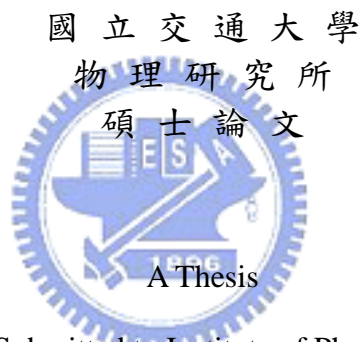
Semiclassical Method Applied to
Spin Relaxation and Spin Transport

研究生：蔡政展

Student : Jengjan Tsai

指導教授：張正宏

Advisors : Cheng-Hung Chang



Submitted to Institute of Physics

College of Science

National Chiao Tung University

in partial Fulfillment of the Requirements

for the Degree of

Master

in

Physics

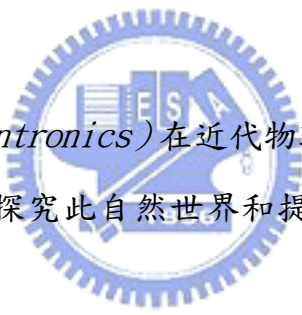
July 2006

Hsinchu, Taiwan, Republic of China

ABSTRACT

Semiclassical Method Applied to Spin Relaxation and Spin Transport

Tsai, Jengjan



自旋電子學 (*Spintronics*) 在近代物理中是如此活躍的一道學門，其提供豐富的素材來探究此自然世界和提供推進下一個電子世代之發展的舞臺。

本文主要涉及在自旋電子學中極其重要的自旋弛豫 (*spin relaxation, SR*) 和自旋傳輸 (*spin transport, ST*) 之課題。本文以半古典方法 (*semiclassical method*) 來探討介觀系統 (*mesoscopic system*) 於自旋-迴旋交互作用 (*spin-orbit interaction*) 下的電子自旋行為。半古典方法之應用乃是此文的關鍵所在。應用此方法我們獲得許多有趣的結果, 諸如：於各式的自旋-迴旋交互作用下的電子自旋弛豫和自旋傳輸的範型 (*pattern*)，我們分別探討此範型於自旋-迴旋交互作用 (即有效磁場, *effective magnetic field*) 之配置 (*configuration*) 及其實際大小之作用下的情形；由自旋弛豫和自旋

傳輸之範型得到規則系統 (*regular system*) 和混沌系統 (*chaotic system*) 的本質性差異；有效磁場的方均根 (*root-mean-square, RMS*) 和其配置之等值性 (*equivalence*)；自旋弛豫時間 (*spin relaxation time, T1*) 和自旋去相時間 (*spin dephasing time, T2*) 於自旋弛豫例子下之探討；*Rashba* 項 (*Rashba term*) 和 *Dresselhouse* 一次項 (*Dresselhouse linear term*) 的等值性；自旋弛豫和自旋傳輸衰竭之減緩 (*slow down*)；自旋弛豫和自旋傳輸衰竭之遏止 (*stop*)；自旋波形編輯器 (*Spin Waveform Editor, SWE*) 等等。



ABSTRACT

Semiclassical Method Applied to Spin Relaxation and Spin Transport

Tsai, Jengjan

Spintronics the so much active research region in modern physics, offers the matter to explore the fundamental nature of the world and the possible application in next electronic generation.

In this thesis we try to explore some aspects about spintronics, especially focus on spin relaxation (SR) and spin transport (ST) in mesoscopic systems under the spin-orbit coupling effect in terms of modern semiclassical approach. The semiclassical approach is the hinge of this thesis. Applying the semiclassical method in spin relaxation and spin transport we obtain some interesting results, e.g. spin relaxation and spin transport patterns under nine (or ten) kinds of different effective magnetic field B_{eff} which deduced from D'yakonov-Perel' spin-orbit interaction mechanism (i.e. the Rashba term and Dresselhaus term) treated from two kinds of points of view – normalized and realistic mimic, intrinsic distinguishableness

between regular and chaotic systems from the patterns of SR and ST, the equivalence between root-mean-square (RMS) of B_{eff} and B_{eff} configuration, revelation of spin relaxation time T_1 (often called longitudinal or spin-lattice time) and spin dephasing time T_2 (also called transverse or decoherence time) in spin relaxation, equivalence between Rashba term case and Dresselhaus linear term case in SR and ST, slow down the spin relaxation and spin transport decay, creating cases of never relaxed and decayable in spin relaxation case and spin transport case, spin waveform editor (SWE), and so on.



Acknowledgements

I think that I should thank *everything!* My parents, my relatives, my teachers, my friends, my classmates, my staff, living objects, matters, environment et al. they bring so wonderful encounter to me. At this moment I thank especially for my dear parents, my dear instructor (C. H. Chang et al.), my dear friends, my dear staff in NCTU and NTHU (Miss Nora et al.), my dear classmates in NCTU and NTHU, the unique world and so on. Thank you for bringing me so wonderful life! 881 ~



Contents

ABSTRACT	iii
ABSTRACT	v
Acknowledgements	vii
List of Tables	xii
List of Figures	xiii
Introduction	1
Part 1. Concepts and Formulism	8
Chapter 1. Spintronics	9
1.1. Foreword	9
1.2. Spin Relaxation and Spin Dephasing	11
1.3. Spin Transport	19
Chapter 2. Operation Environment	21
2.1. Two-dimensional Electron Gas (2DEG)	21
2.2. Proposed Sample Preparation	25



Chapter 3. Spin	28
3.1. Lead-in	28
3.2. Spin 1/2	31
3.3. Electron in A Magnetic Field	35
3.4. Time Evolution and Spin Rotation	41
3.5. Spin Precession Extension	45
Chapter 4. Spin-orbit Coupling	48
4.1. Spin-orbit Coupling Effect	48
4.2. Spin-orbit Coupling in Solid-state Physics	48
4.3. Spin-orbit Coupling in Quasi-two-dimensional Systems	51
4.4. Inversion-Asymmetry-Induced Spin Splitting	52
4.5. B=0 Spin Splitting and Spin-Orbit Interaction	54
4.6. BIA Spin Splitting in Zinc Blende Semiconductors	56
4.7. SIA Spin Splitting	58
Chapter 5. Spin Dynamics	62
5.1. Preface	63
5.2. Rashba and Dresselhouse SOI Effect	64
5.3. Spin Evolution	70
Chapter 6. Semiclassical Approach	72
6.1. Chaotic Scattering	72
6.2. Scattering Approach to the Electric Conductance	75

6.3. Semiclassical Transmission Amplitudes	81
6.4. Spin Conductance	85
6.5. Spin Evolution	89
Part 2. Simulation and Discussion	94
Chapter 7. Spin Relaxation	95
7.1. Overview of Spin Relaxation Pattern (\mathbf{B}_{eff} Configuration Normalized Case)	97
7.2. Some Aspects of Spin Relaxation Patterns (\mathbf{B}_{eff} Configuration in Real Material)	104
7.3. Equivalence between R and $D - k1$ Modified Cases	107
7.4. Equivalence between RMS of \mathbf{B}_{eff} and \mathbf{B}_{eff} Configuration	108
7.5. Relaxation Rate Slow Down Case	110
7.6. Relaxation Rate Never Decay Case	111
Chapter 8. Spin Transport	113
8.1. Overview of the Conductance Decay Patterns (\mathbf{B}_{eff} Configuration Normalized Case)	115
8.2. Some Aspects of Conductance Decay Patterns (\mathbf{B}_{eff} Configuration in Real Material)	128
8.3. Equivalence between R and $D - k1$ Modified Cases	133
8.4. Slow Down Conductance Decay Pattern Case	140
8.5. Never Decay Pattern Case	142

Chapter 9. Spin Waveform Editor (SWE)	146
Part 3. Conclusion and Outlook	150
Chapter 10. Conclusion and Outlook	151
References	154
Vita	158



List of Tables

4.1 B=0 spin degeneracy is due to the combined effect of inversion symmetry in space and time.	52
---	----



List of Figures

0.1 Typical ballistic cavities.	2
1.1 Qualitative sketch of a Datta-Das spin field-effect transistor (SFET).	10
2.1 Conduction and valence band line-up at a junction between an n -type AlGaAs and intrinsic GaAs.	23
2.2 Schematic layer structure of an inverted $\text{In}_{0.53}\text{Ga}_{0.47}/\text{In}_{0.52}\text{Al}_{0.48}\text{As}$ heterostructure and profile of the Datta-Das-like SFET.	26
2.3 Schematic layer structure of an inverted $\text{In}_{0.53}\text{Ga}_{0.47}/\text{In}_{0.52}\text{Al}_{0.48}\text{As}$ heterostructure and profile of the quantum dot for simulation.	27
3.1 \mathbf{n} is a unit vector lies in $3D$ real space.	34
3.2 Magnetic field sweeps around on a cone, at angular velocity ω .	36
4.1 Qualitative sketch of the band structure of GaAs close to the fundamental gap.	49
4.2 Qualitative sketch of a wave function, Eq. 4.2, in the envelope function approximation.	55

4.3 Lowest-order spin orientation $\langle \sigma \rangle$ of the eigenstates $ \psi_{\pm}(\mathbf{k}_{\parallel})\rangle$ in the presence of BIA.	56
4.4 Lowest-order spin orientation $\langle \sigma \rangle$ of the eigenstates $ \psi_{\pm}(\mathbf{k}_{\parallel})\rangle$ in the presence of SIA.	59
5.1 A quantum dot, shows an electron trajectory constituted by straight-line segments.	62
5.2 A quantum ring, shows an electron trajectory constituted by straight-line segments.	62
6.1 Classical distribution of length for stadium (solid line) and rectangular (dash line) billiards.	74
7.1 Configuration of \mathbf{B}_{eff}	95
7.2 Five operation systems.	96
7.3 Spin relaxation rate under the viewpoint of effect of direction of \mathbf{B}_{eff} .	99
7.4 Sum up of nine operation cases into one under the viewpoint of effect of direction of \mathbf{B}_{eff} .	100
7.5 The effect of L_{so} .	101
7.6 Cases of the initial spinor input in $+x$ and $+y$ directions for spin relaxation discussion.	102
7.7 The effects of l_m (length of mean free path) and size of system.	104



7.8 Spin relaxation rate under the viewpoint of effect of real (calculated) aspect of \mathbf{B}_{eff} .	105
7.9 Sum up of nine operation cases into one under the viewpoint of effect real (calculated) aspect of \mathbf{B}_{eff} .	106
7.1 Equivalence between <i>RMS</i> of \mathbf{B}_{eff} and \mathbf{B}_{eff} configuration in the relaxation.	108
7.1 Relaxation rate slow down case.	110
7.1 Relaxation rate never decay case.	111
8.1 Operation systems for spin transport.	113
8.2 $\langle g_{xx} \rangle$ v.s. $1/L_{so}$ under the action of normalized B_{eff} in more narrow circular ring system.	116
8.3 $\langle g_{yy} \rangle$ v.s. $1/L_{so}$ under the action of normalized B_{eff} in more narrow circular ring system.	117
8.4 $\langle g_{zz} \rangle$ v.s. $1/L_{so}$ under the action of normalized B_{eff} in more narrow circular ring system.	118
8.5 $\langle g_{xx} \rangle$ v.s. $1/L_{so}$ under the action of normalized B_{eff} in less narrow circular ring system.	121
8.6 $\langle g_{yy} \rangle$ v.s. $1/L_{so}$ under the action of normalized B_{eff} in less narrow circular ring system.	122

8.7 $\langle g_{zz} \rangle$ v.s. $1/L_{so}$ under the action of normalized B_{eff} in less narrow circular ring system.	123
8.8 $\langle g_{xx} \rangle$ v.s. $1/L_{so}$ under the action of normalized B_{eff} in more narrow Sinai billiard system.	124
8.9 $\langle g_{yy} \rangle$ v.s. $1/L_{so}$ under the action of normalized B_{eff} in more narrow Sinai billiard system.	125
8.10 $\langle g_{zz} \rangle$ v.s. $1/L_{so}$ under the action of normalized B_{eff} in more narrow Sinai billiard system.	126
8.11 Sum up of $\langle g_{xx} \rangle$ v.s. $1/L_{so}$ under the action of nine kinds of normalized B_{eff} in more narrow Sinai billiard system.	127
8.12 Sum up of $\langle g_{yy} \rangle$ v.s. $1/L_{so}$ under the action of nine kinds of normalized B_{eff} in more narrow Sinai billiard system.	127
8.13 Sum up of $\langle g_{zz} \rangle$ v.s. $1/L_{so}$ under the action of nine kinds of normalized B_{eff} in more narrow Sinai billiard system.	128
8.14 $\langle g_{xx} \rangle$ v.s. $1/L_{so}$ under the action of normalized B_{eff} in less narrow Sinai billiard system.	129
8.15 $\langle g_{yy} \rangle$ v.s. $1/L_{so}$ under the action of normalized B_{eff} in less narrow Sinai billiard system.	130
8.16 $\langle g_{zz} \rangle$ v.s. $1/L_{so}$ under the action of normalized B_{eff} in less narrow Sinai billiard system.	131

8.17	Sum up of $\langle g_{xx} \rangle$ v.s. $1/L_{so}$ under the action of nine kinds of normalized B_{eff} in less narrow Sinai billiard system.	132
8.18	Sum up of $\langle g_{yy} \rangle$ v.s. $1/L_{so}$ under the action of nine kinds of normalized B_{eff} in less narrow Sinai billiard system.	132
8.19	Sum up of $\langle g_{zz} \rangle$ v.s. $1/L_{so}$ under the action of nine kinds of normalized B_{eff} in less narrow Sinai billiard system.	133
8.20	Comparison between the normalized \mathbf{B}_{eff} configuration and \mathbf{B}_{eff} configuration in real material for $D - k2$ case in circular ring system.	134
8.21	Comparison between the normalized \mathbf{B}_{eff} configuration and \mathbf{B}_{eff} configuration in real material for $RD - k4$ case in circular ring system.	135
8.22	Comparison between the normalized \mathbf{B}_{eff} configuration and \mathbf{B}_{eff} configuration in real material for $D - k1$ case in Sinai billiard.	136
8.23	Comparison between the normalized \mathbf{B}_{eff} configuration and \mathbf{B}_{eff} configuration in real material for $RD - k4$ case in Sinai billiard.	137
8.24	Equivalence between R and $D - k1$ modified cases.	138
8.25	Example of equivalence between R and $D - k1$ modified cases in circular ring system.	139
8.26	Example of equivalence between R and $D - k1$ modified cases in Sinai billiard system.	140

8.27	Example of slow down conductance decay pattern case in $RD - k1$ and $RD - k4$ cases.	141
8.28	Examples of never decay spin conductance pattern case.	144
9.1	Square waveform patterns.	146
9.2	Design of Spin Waveform Editor (SWE) device 1.	147
9.3	Design of Spin Waveform Editor (SWE) device 2.	147



Introduction

It is so excited to touch and explore the natural world. *Spintronics* the so much active research region in modern physics, offers the matter to explore the fundamental nature of the world and the possible application in next electronic generation. In this thesis we try to explore some aspects about spintronics, especially focus on spin relaxation (SR) and spin transport (ST) in mesoscopic systems, see Fig. 0.1, under the spin-orbit coupling effect in terms of modern semiclassical approach. Due to the flush development in theoretical and experimental research in spintronics, we strongly expect oncoming of experimental breakthrough to verify the so much theoretical prediction and advance the spintronics research. We also hope that our research in the thesis could nudge spintronics towards a more fulgent future.

The semiclassical approach is the hinge of our thesis. Applying the semiclassical method in spin relaxation and spin transport we obtain some interesting results, e.g. spin relaxation and spin transport patterns under nine (or ten) kinds of different effective magnetic field B_{eff} which deduced from D'yakonov-Perel' spin-orbit interaction mechanism (i.e. the Rashba term and Dresselhaus term) treated from

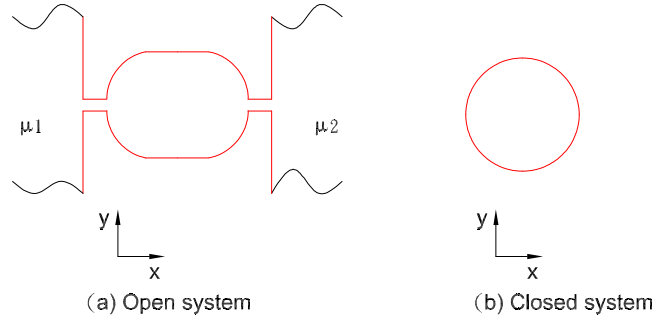


Figure 0.1. (a) Typical ballistic cavity coupled to reservoirs characterized by chemical potential μ_1 and μ_2 for mesoscopic structure. (b) Typical ballistic cavity for closed mesoscopic structure.

two kinds of points of view – normalized and realistic mimic, intrinsic distinguish-ability between regular and chaotic systems from the patterns of SR and ST, the equivalence between root-mean-square (RMS) of B_{eff} and B_{eff} configuration, revelation of spin relaxation time T_1 (often called longitudinal or spin-lattice time) and spin dephasing time T_2 (also called transverse or decoherence time) in spin relaxation, equivalence between Rashba term case and Dresselhaus linear term case in SR and ST, slow down the spin relaxation and spin transport decay, creating cases of never relaxed and decayable in spin relaxation case and spin transport case, spin waveform editor (SWE), and so on. Since the significant role of semi-classical method in this thesis, here we shortly talk about something relevant to it and then we give an rough outline of this thesis to be as an introduction.

The mesoscopic regime is attained in small condensed matter systems at sufficiently low temperature for the electrons to propagate coherently across the sample [1]. The phase coherence of the electron wave-function is broken by an inelastic

event (coupling to an external environment, electron-phonon or electron-electron scattering, etc.) over a distance L_ϕ larger than the size of the system a . In a more precise language, we should not talk of electrons, which are strongly interacting, but of Landau quasiparticles, which are the weakly interacting carriers (at low energies and small temperature) moving in a self consistent field. The quasiparticle lifetime gives the limitation on L_ϕ arising from electron-electron interactions. Following the standard practice, we will refer to the carriers as *electrons* and we will not distinguish between the electrostatically imposed external potential and the self consistent field.

The view of a mesoscopic system as a single phase-coherent unit allow us to deal with a one-particle problem, where the theoretical concepts of *Quantum Chaos* are more simply applied. However, this simplistic approach does not describe the physical reality completely since in real life L_ϕ is larger than a but never strictly infinite. The fact that Mesoscopic Physics is not such an ideal laboratory for Quantum Chaos makes the richness of their relationship. Mesoscopic system are extremely useful to study the interplay between quantum and classical mechanics.

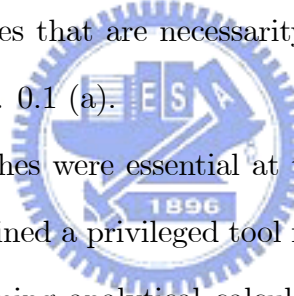
Mesoscopic Physics was initially focused on disordered metals, where the classical motion of electrons is a random walk between the impurities. The phase-coherence in the multiple scattering of electrons gives rise to corrections to the classical (Drude) conductance. The small parameter is $k_F l$, with $k_F = 2\pi/\lambda_F$ the

Fermi wave-vector and l the elastic mean-free-path (i.e. the typical distance traveled by the electron between successive collision with the impurities). Mesoscopic disordered conductors are then characterized by $\lambda_F \ll l \ll a \ll L_\phi$.

It is in a *second generation* of mesoscopic systems, semiconductor microstructures, that the connection with Quantum Chas has been more successfully developed. Extremely pure semiconductor (GaAs/AlGaAs) heterostructures make it possible to create a two-dimensional electron gas (2DEG) by quantizing the motion perpendicular to the interphase. Given the crystalline perfection and the fact that the dopants are away from the plane of the carriers, an electron can travel a long distance before its initial momentum is randomized. This typical distance, the transport mean-free-path l_T , is generally larger than the elastic mean-free-path (due to small-angle scattering [2]) and it can achieve values of $5 - 15\mu m$.

Various techniques have been developed to produce a lateral confinement in the 2DEG and define one-dimensional (quantum wire) and zero-dimensional (quantum boxes or cavities) structure. Spatial resolutions of the order of a micro allow to define, at the level of the 2DEG, mesoscopic structures smaller than the elastic mean-free-path, paving the way to the ballistic regime [3][4][5]. When $a \ll l_T$ the classical motion of the two-dimensional electrons is given by the collisions with the walls defining the cavity, with a very small drift due to the weak impurity potential. In usual ballistic transport the disorder effects are very small, and the distinction between ballistic and clean regimes is often skipped.

It is important to realize that the constraints arising from the measurement limit the type of problems to study. We do not try to deal with microscopic systems where the level spacing Δ can become larger than the temperature broadening $k_B T$. The fruitful connection between Quantum Chaos and Mesoscopic Physics has to be established from the observables that are accessible in the laboratory. The physical property of ballistic microstructures which is most easily measured is their electrical resistance, and as a consequence, an important wealth of experimental results on ballistic transport has been obtained in the last decade [6][7][8][9][10][11][12]. In order to measure the electrical resistance we have to open the cavities, connecting them to measuring devices that are necessarily macroscopic and can be thought as electron reservoirs Fig. 0.1 (a).



Semiclassical approaches were essential at the advent of Quantum Mechanics and have ever since remained a privileged tool for developing our intuition on new problems and for performing analytical calculations as well [13]. The semiclassical approximation in one-dimensional is referred in standard textbooks as the WKB (Wentzel-Kramers-Brillouin) method and allows to obtain closed expressions for eigenenergies and eigenfunctions. The extension to higher dimensions is built from the Van Vleck approximation to the propagator, expressed as a sum over classical trajectories, each of them associated with a weight given by a stability prefactor and a phase depending on the classical action. The consistent use of the stationary-phase method whenever an integral has to be evaluated allows us to link classical mechanics with other quantum protagonists, like the Green

function, the density of states, matrix elements, scattering amplitudes, etc. the dependence of the properties of a quantum system on the underlying classical mechanics can then be established, and this is why the semiclassical approach is so widely used in the studies of Quantum Chaos. For the usual densities of the 2DEG ($\approx 10^{12} \text{cm}^{-2}$) [1] the Fermi wave-length are of the order of 40nm . The semiclassical approximation is therefore justified in the study of mesoscopic ballistic cavities since $\lambda_F \ll a \ll l_T \ll l_\phi$.

We note that the first generation of mesoscopic systems, the disordered metals, have mainly been analyzed within diagrammatic perturbation theory. Since the scattering centers of disorder metals (defects, impurities, interstitials, etc.) are of atomic dimensions the single scattering events have to be treated quantum mechanically. Therefore the semiclassical description of disordered system is mixed one, built from a classical propagation between quantum scatterings. Assuming that the classical single scattering events have a random outcome and invoking an ensemble average, we are lead to a diffusive motion of electrons. The situation is then quite different from that of ballistic systems, were the classical trajectories are completely determined by the geometry and the dynamics can be chaotic or integrable depending on the shape of the cavity. Also, the notion of impurity average, so crucial in disordered systems, is usually replaced in the ballistic regime by averages over energy or over samples.

This thesis is organized as follows. It is divided by three parts. First part, *Concepts and Formulism*, we talk about the minimal necessary relevant concepts

and formulism to this thesis and deduce some expressions for understanding the thesis. It includes *Spintronics, Operation Environment, Spin, Spin-orbit Coupling, Spin Dynamics*, and *Semiclassical Approach* of spin transport and spin relaxation, and so on. Second part, *Simulation and Discussion*, we present our simulation results and deduce some expressions relevant to the corresponsive topics. It is mainly divided by three portions. First portion we discuss the *Spin Relaxation*. Here we explore both the regular and chaotic systems and different collision (scattering) situation under the effect of Rashba and Dresselhouse terms. We find some very interesting and surprising results about the spin relaxation decay rate. We get an expression which depicts satisfactory aspects for these spin relaxation rate and so on. Second portion we focus on the *Spin Transport*, the regular systems and chaotic systems under Rashba and Dresselhouse (linear and/or cubic) terms effect are discussed. We also examine the equivalence between Rashba and Dresselhouse linear terms in spin transport and relaxation under some point of view and mention a special case of the arrangement of Rashba and Dresselhouse linear terms to produce the never decay spin transport current and so forth. Final portion we propose and design a spintronic device – *Spin Waveform Editor (SWE)*. This device can be applied as a switch or/and as a resource for research and instruction usage. Part 3, *Conclusion and Outlook*, we give a conclusion that talks about some defect and leakage in our research, and the outlook which indicates something interesting and hopeful respect in further research. Reference is lay in the final.

Part 1

Concepts and Formulism



CHAPTER 1

Spintronics

1.1. Foreword

Spintronics is a multidisciplinary field whose central theme is the active manipulation of spin degrees of freedom in solid-state systems. Here the term *spin* stands for either the spin of a single electron or the average spin of an ensemble of electrons, manifested by magnetization. The control of spin is then a control of either the population and the phase of the spin of an ensemble of particles, or a coherent spin manipulation of a single or a few-spin system. The goal of spintronics is to understand the interaction between the particle spin and its solid-state environments and to make useful devices using the acquired knowledge. Fundamental studies of spintronics include investigations of spin transport in electronic materials, as well as of spin dynamics and spin relaxation. Typical questions that are posed are (a) what is an effective way to polarize a spin system? (b) how long is the system able to remember its spin orientation? and (c) how can spin be detected?

Now let us illustrate the generic spintronic scheme on a prototypical device, the Datta-Das spin field-effect transistor (SFET, [14]), depicted in Fig. 1.1. The scheme shows the structure of the usual FET, with a drain, a source, a narrow

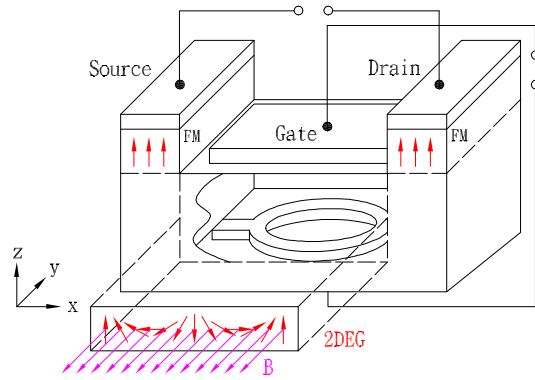


Figure 1.1. Qualitative sketch of a Datta-Das spin field-effect transistor (SFET) [14]. Larger black arrows indicate the spin polarization in the ferromagnetic contact (FM) and the semiconducting channel. Smaller black arrows indicate the effective magnetic field $\mathbf{B}_{eff}(k_x)$ in the semiconducting channel. A top gate is used to tune the spin precession by applying an electric ϵ perpendicular to the channel, and a gate for controlling the current. The gate either allows the current to flow (ON) or does not (OFF). The spin transistor is similar in that the result is also a control of the charge current. The difference, however, is in the physical realization of the current control. In the Datta-Das SFET the source and the drain are ferromagnets acting as the injection and detection of the electron spin. The drain injects electrons with spins perpendicular to the transport direction. The electrons are transported ballistically through the channel. When they arrive at the drain, their spin is detected. In simplified picture, the electron can enter the drain (ON) if its spin points in the same direction as the spin of the drain. Otherwise it is scattered away (OFF). The role of the gate is to generate an effective magnetic field as Figure 1.1 shown, arising from the spin-orbit coupling in the substrate material,

channel, and a gate for controlling the current. The gate either allows the current to flow (ON) or does not (OFF). The spin transistor is similar in that the result is also a control of the charge current. The difference, however, is in the physical realization of the current control. In the Datta-Das SFET the source and the drain are ferromagnets acting as the injection and detection of the electron spin. The drain injects electrons with spins perpendicular to the transport direction. The electrons are transported ballistically through the channel. When they arrive at the drain, their spin is detected. In simplified picture, the electron can enter the drain (ON) if its spin points in the same direction as the spin of the drain. Otherwise it is scattered away (OFF). The role of the gate is to generate an effective magnetic field as Figure 1.1 shown, arising from the spin-orbit coupling in the substrate material,

from the confinement geometry of the transport channel, and the electrostatic potential of the gate. This effective magnetic field causes the electrons spins to precess. By modifying the voltage, one can cause the precession to lead to either parallel or antiparallel (or anything between) electron spin at the drain, effectively controlling the current.

Well! Even though the name *Spintronics* is rather novel (the term was coined by Wolf, S. A. in 1996, as a name for a DARPA initiative for novel magnetic materials and devices), contemporary research in spintronics relies closely on a long tradition of results obtained in diverse areas of physics (e.g., magnetism, semiconductor physics, superconductivity, optics, and mesoscopic physics) and establishes new connections between its different subfields. Spintronics also benefits from a large class of emerging materials, such as ferromagnetic semiconductors [15][16], organic semiconductors [17], organic ferromagnets [18], high-temperature superconductors, and carbon nanotubes [19][20], which can bring novel functionalities to the traditional devices. In one word, there is a continuing need for fundamental studies before the potential of spintronic applications can be fully realized [21]. This is right part of the goal of this thesis.

1.2. Spin Relaxation and Spin Dephasing

Spin relaxation and spin dephasing are process that lead to spin equilibration and are thus of great important for spintronics. The fact that nonequilibrium electronic spin in metals and semiconductors lives relatively long (typically

a nanosecond), allowing for spin-encoded information to travel macroscopic distances, is what makes spintronics a viable option for technology. After introducing the concepts of spin relaxation and spin dephasing time respectively, which are commonly called τ_s , we just briefly talk about the major physical mechanisms responsible for spin equilibration in nonmagnetic electronic systems: Elliott-Yafet, D'yakonov-Perel', Bir-Aronov-Pikus, and hyperfine interaction processes [21].

1.2.1. Spin Relaxation Time and Spin Dephasing Time

Spin relaxation and spin dephasing of a spin ensemble are traditionally defined within the framework of the Bloch-Torrey equations [22][23] for magnetization dynamics. For mobile electrons, spin relaxation time T_1 (often called longitudinal or spin-lattice time) and spin dephasing time T_2 (also called transverse or decoherence time) are defined via the equation for the spin precession, decay, and diffusion of electronic magnetization \mathbf{M} in an applied magnetic field $\mathbf{B}(t) = B_0\hat{z} + \mathbf{B}_1(t)$, with a static longitudinal components B_0 (conventionally in the \mathbf{z} direction), and frequently, a transverse oscillating part \mathbf{B}_1 perpendicular to \mathbf{z} [23][24]:

$$(1.1) \quad \frac{\partial M_x}{\partial t} = \gamma(\mathbf{M} \times \mathbf{B})_x - \frac{M_x}{T_2} + D\nabla^2 M_x,$$

$$(1.2) \quad \frac{\partial M_y}{\partial t} = \gamma(\mathbf{M} \times \mathbf{B})_y - \frac{M_y}{T_2} + D\nabla^2 M_y,$$

$$(1.3) \quad \frac{\partial M_z}{\partial t} = \gamma(\mathbf{M} \times \mathbf{B})_z - \frac{M_z - M_z^0}{T_1} + D\nabla^2 M_z,$$

Here $\gamma = \mu_B g / \hbar$ is the electron gyromagnetic ratio (μ_B is the Bohr magneton and g is the electronic g factor), D is the diffusion coefficient (for simplicity we assume an isotropic or a cubic solid with scalar D), and $M_z^0 = \chi B_0$ is the thermal equilibrium magnetization with χ denoting the system's static susceptibility. The Bloch equations are phenomenological, describing quantitatively very well the dynamics of mobile electron spins (more properly, magnetization) in experiments such as conduction-electron spin resonance and optical orientation. Although relaxation and decoherence processes in a many-spin system are generally too complex to be fully described by only two parameters, T_1 and T_2 are nevertheless an extremely robust and convenient measure for quantifying such processes in many cases of interest. To obtain microscopic expressions for spin relaxation and dephasing times, one starts with a microscopic description of the spin system (typically using the density-matrix approach), derives the magnetization dynamics, and compares it with the Bloch equations to extract T_1 and T_2 .

Time T_1 is the time it takes for the longitudinal magnetization to reach equilibrium. Equivalently, it is the time of thermal equilibration of the spin population with the lattice. In T_1 processes an energy has to be taken from the spin system, usually by phonons, to the lattice. Time T_2 is classically the time it takes for

an ensemble of transverse electron spins, initially precessing in phase about the longitudinal field, to lose their phase due to spatial and temporal fluctuations of the precessing frequencies. For an ensemble of mobile electrons the measured T_1 and T_2 come about by averaging spin over the thermal distribution of electron momenta. Motional (dynamical) narrowing is an inhibition of phase change by random fluctuations. Consider a spin rotating with frequency ω_0 . The spin phase changes by $\Delta\phi = \omega_0 t$ over time t . If the spin is subject to a random force that makes spin precession equally likely clockwise and anticlockwise, the average spin phase does not change, but the root-mean-square phase change increases with time as $(\langle \Delta^2\phi \rangle)^{1/2} \approx (\omega_0\tau_c)(t/\tau_c)^{1/2}$, where τ_c is the correlation time of the random force, or the average time of spin precession in one direction. This is valid for rapid fluctuations, $\omega_0\tau_c \ll 1$. The phase relaxation time t_ϕ is defined as the time over which the phase fluctuations reach unity: $1/t_\phi = \omega_0^2\tau_c$.

In isotropic and cubic solids $T_1 = T_2$ if $\gamma B_0 \ll 1/\tau_c$, where τ_c is the so-called correlation or interaction time: $1/\tau_c$ is the rate of change of the effective dephasing magnetic field. Phase losses occur during time intervals of τ_c . If the system is anisotropic, the equality $T_1 = T_2$ no longer holds, even in the case of full motional narrowing of the spin-spin interactions and g -factor broadening. Using simple qualitative analysis Yafey in 1963 showed that, while there is no general relation between the two times, the inequality $T_2 \leq 2T_1$ holds, and that T_2 changes with the direction by at most a factor of 2. The equality of the two times is very convenient for comparing experiment and theory, since measurements usually

yield T_2 , while theoretically it is often more convenient to calculate T_1 . In many cases a single symbol τ_c is used for spin relaxation and dephasing (and called indiscriminately either of these terms), if it does not matter what experimental situation is involved, or if one is working at small magnetic fields.

In our simulation I think that we mainly calculate (simulate) spin relaxation time T_1 (or called longitudinal or spin-lattice time), in Chapter 7 we also simulate few illustrative cases which show the aspects of spin dephasing time T_2 (or called transverse or decoherence time), we find a reasonable explanation to reach the consistency about the statement $T_2 \leq 2T_1$.

Experiments detecting spin relaxation and decoherence of conduction electrons can be grouped into two broad categories: (a) those measuring spectral characteristics of magnetization depolarization and (b) those measuring time or space correlations of magnetization [21]. Well! Here we do not attempt to discuss the aspects of experiments, so we stop discussing further more.

1.2.2. Mechanism of Spin Relaxation

Four mechanisms for spin relaxation of conduction electrons have been found relevant for metals and semiconductors: the Elliott-Yafet, D'yakonov-Perel', Bir-Aronov-Pikus, and hyperfine-interaction mechanisms. (Here we do not consider magnetic scattering, that is, scattering due to an exchange interaction between conduction electrons and magnetic impurities.) In the Elliott-Yafet mechanism electron spins relax because the electron wave functions normally associated with

a given spin have an admixture of the opposite-spin states, due to spin-orbit coupling induced by ions. The D'yakonov-Perel' mechanism explains spin dephasing in solids without a center of symmetry. Spin dephasing occurs because electrons feel an effective magnetic field, resulting from the lack of inversion symmetry and from the spin-orbit interaction, which changes in random directions every time the electron scatters to a different momentum state. The Bir-Aronov-Pikus mechanism is important for p-doped semiconductors, in which the electron-hole exchange interaction gives rise to fluctuating local magnetic fields flipping electron spins. Finally, in semiconductor heterostructures (quantum wells and quantum dots and so on) based on semiconductors with a nuclear magnetic moment, it is the hyperfine interaction of the electron spins and nuclear moments which dominates spin dephasing of localized or confined electron spins [21]. In this thesis, we mainly consider the spin relaxation in two-dimensional III-V semiconductor heterostructures due to D'yakonov-Perel' mechanism, so we just exhibit the D'yakonov-Perel' Mechanism a little more, and ignore to talk about other mechanisms more detailedly.

An efficient mechanism of spin relaxation due to spin-orbit coupling in systems lacking inversion symmetry was found by D'yakonov and Perel' in 1971. Without inversion symmetry the momentum states of the spin-up and spin-down electrons are not degenerate: $E_{\mathbf{k}+} \neq E_{\mathbf{k}-}$. Kramer's theorem still dictates that $E_{\mathbf{k}+} = E_{-\mathbf{k}-}$. Most prominent examples of materials without inversion symmetry come from groups III-V (such as GaAs) and II-VI (ZnSe, etc.) semiconductor, where inversion symmetry is broken by the presence of two distinct atoms in the Bravais

lattice. Elemental semiconductors like Si possess inversion symmetry in the bulk, so the D'yakonov-Perel' mechanism does not apply to them. In heterostructures the symmetry is broken by the presence of asymmetric confining potentials.

Spin splittings induced by inversion asymmetry can be described by introducing an intrinsic \mathbf{k} -dependent magnetic field $\mathbf{B}_i(\mathbf{k})$ around which electron spins precess with Larmor frequency $\boldsymbol{\Omega}(\mathbf{k}) = e/m \mathbf{B}_i(\mathbf{k})$. The intrinsic field derives from the spin-orbit coupling in the band structure. The corresponding Hamiltonian term describing the precession of electrons in the conduction band is

$$(1.4) \quad H(\mathbf{k}) = \frac{1}{2} \hbar \boldsymbol{\sigma} \cdot \boldsymbol{\Omega}(\mathbf{k})$$

where $\boldsymbol{\sigma}$ are the Pauli matrices. Momentum-dependent spin precession described by H , together with momentum scattering characterized by momentum relaxation time τ_p , leads to spin dephasing. While the microscopic expression for $\boldsymbol{\Omega}(\mathbf{k})$ needs to be obtained from the band structure, treating the effects of inversion asymmetry by introducing intrinsic precession helps to give a qualitative understanding of spin dephasing. It is important to note, however, that the analogy with real Larmor precession is not complete. An applied magnetic field induces a macroscopic spin polarization and magnetization, while H of Eq. (1.4) produces an equal number of spin-up and spin-down states.

Two limiting cases can be considered: (a) $\tau_p \Omega_{av} \geq 1$ and (b) $\tau_p \Omega_{av} \leq 1$, where Ω_{av} is an average magnitude of the intrinsic Larmor frequency $\Omega(\mathbf{k})$ over the actual momentum distribution. Case (a) corresponds to the situation in which individual electron spins process a full cycle before being scattered to another momentum state. The total spin in this regime initially dephases reversibly due to the anisotropy in $\Omega(\mathbf{k})$. The spin dephasing rate, which depends on the distribution of values of $\Omega(\mathbf{k})$, is in general proportional to the $\Delta\Omega$ of the distribution: $1/\tau_s \approx \Delta\Omega$. The spin is irreversibly lost after time τ_p , when randomizing scattering takes place.

Case (b) is what is usually meant by the D'yakonov-Perel' mechanism. This regime can be viewed from the point of view of individual electrons as a spin precession about fluctuating magnetic fields, whose magnitude and direction change randomly with the average time step of τ_p . The electron rotates about the intrinsic field at an angle $\delta\phi = \Omega_{av}\tau_p$, before experiencing another field and starting to rotate with a different speed and in a different direction. As a result, the spin phase follows a random walk: after time t , which amounts to t/τ_p steps of the random walk, the phase progresses by $\Phi(t) \approx \delta\phi\sqrt{t/\tau_p}$. Defining τ_s at the time at which $\Phi(t) = 1$, the usual motional narrowing result is obtained: $1/\tau_s \approx \Omega_{av}^2\tau_p$.

The faster the momentum relaxation, the slower the spin dephasing. The difference between cases (a) and (b) is that in case (a) the electron spins form an ensemble that directly samples the distribution of $\Omega(\mathbf{k})$, while in case (b) it is the distribution of the sums of the intrinsic Larmor frequencies (the total phase

of a spin after many steps consists of a sum of randomly selected frequencies multiplied by τ_p), which, according to the central-limit theorem, has a significantly reduced variance. Both limits (a) and (b) and the transition between them have been experimentally demonstrated in n -GaAs/AlGaAs quantum wells by observing temporal spin oscillations over a large range of temperatures (and thus τ_p) [26].

1.3. Spin Transport

Maybe *Transport* will be not a simple topic for master graduate student. Under different operation environment, the various transport aspects could be exhibited. For example, comparing mean free path l with characteristic dimensions of the system a , one can discriminate between *diffusive*, $l \ll a$, *quasi-ballistic*, $l > a$, and *ballistic*, $l \gg a$, transport. Such a classification appears incomplete in the situation where different dimensions of the sample are substantially different. If phase coherence is taken into account, the scales L_ϕ and L_T become important, and the situation appears more rich and interesting. In our thesis we assume the electron exhibits the ballistic transport, so here we don't intend to show the content of diffusive transport, we just indicate the key point of ballistic transport, that is a very powerful method in physics of small systems the so-called Landauer approach.

The main principle of this approach is the assumption that the system in question is coupled to large reservoirs where all inelastic processes take place. Consequently, the transport through the systems can be formulated as a quantum

mechanical scattering problem. Thus one can reduce the non-equilibrium transport problem to a quantum mechanical one. Another important assumption is that the system is connected to reservoirs by ideal quantum wires which behave as waveguides for the electron waves. And we also give an very important assumption for the transport topics, we assume that the *charge* transport is independent (un-coupled) to *spin* transport which it is attached to the wave functions of charge particle. This assumption offers the base to consider the spin evolution independently to the charge (electron) traveling. Our simulations are all established under this such assumption. We should discuss this more detailedly in Chapter 6.



CHAPTER 2

Operation Environment

2.1. Two-dimensional Electron Gas (2DEG)

By dynamically two-dimensional we mean that the electrons or holes have quantized energy levels for one spatial dimension, but are free to move in two spatial dimensions. Thus the wave vector is a good quantum number for two dimensions, but not for the third. These systems are not two-dimensional in a strict sense, both because wave functions have a finite spatial extent in the third dimension and because electromagnetic fields are not confined to a plane but spill out into the third dimension. Theoretical predictions for idealized two-dimensional systems must therefore be modified before they can be compared with experiment.

Here we shall generally confine our discussion to systems for which parameters can be varied in a given sample, usually by application of an electrical stress. Systems of this sort generally occur in what may broadly be called heterostructures. The best known example are carriers confined to the vicinity of junctions between insulators and semiconductors, between layers of different semiconductors, and between vacuum and liquid helium. For most of these systems the carrier concentration can be varied, so that a wealth of information can be obtained from one

sample. They all have at least one well-defined interface which is usually sharp to a nanometer or less.

The effects of changes in surface conditions on the conductance of a semiconductor sample have been studied for many years. Such measurements are usually called field-effect measurements because a major physical variable is the electric field normal to the semiconductor surface. One important way to change the surface condition, and therefore the surface electric field, is through the control of gaseous ambients, see for example: Brattain, W. H.-Bardeen, J. cycle experiment in 1953, and Mary, A. experiment in 1974. A disadvantage of the early measurements was that the conductance of the entire sample was measured, and the surface effects were extracted by taking differences or derivatives as the ambient was changed. In conjunction with field-effect measurements, theories for the dependence of the mobility of carriers near the surface on the surface conditions were developed and refined. Most of the early work was based on the phenomenological notion of diffuse and specular reflection at the surface, as first used by Fuchs, K. in 1938 in studying transport in metal films. .

Investigation of space-charge layers on narrow-gap III-V semiconductors also started in the mid-1960s. However, the difficulty of obtaining samples with good quality has long prevented progress in this system. After many people effort and many years later, the development on heterostructure growth techniques made it possible to fabricate high-quality-double heterostructures with ultrathin layers. Two main methods of growth with very precise control of thickness, planarity,

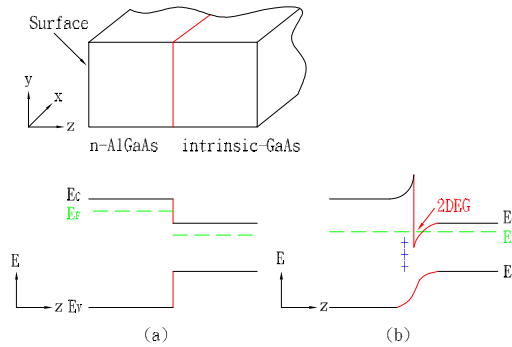


Figure 2.1. Conduction and valence band line-up at a junction between an n -type AlGaAs and intrinsic GaAs (a) before and (b) after charge transfer has taken place. Note that this is a cross-section view. Patterning is done on the surface (x - y plane) using lithographic techniques [1].

compositions etc. were developed in the 1970s. A modern molecular-beam epitaxy method became practically important for III-V heterostructure technology due first of all to the pioneering work of Cho, A. in 1971. Metal-organic chemical-vapor deposition originated from the early work of Manasevit, H. in 1968 and found broad application in III-V heterostructure research after Dupuis, R. and Dapkus, P. in 1977 reported the room-temperature injection of AlGaAs DH lasers which had been grown by the metal-organic chemical-vapor deposition method. Here we do not discuss the progress of the techniques development more forward, we turn our attention to the formation aspects of 2DEG in GaAs-AlGaAs heterojunctions. Recent work on mesoscopic conductors has largely been based on GaAs-AlGaAs heterojunctions where a thin two-dimensional conducting layer is formed at the interface between GaAs and AlGaAs. To understand why this layer is formed

consider the conduction and valence band line-up in the z -direction when first bring the layers in contact Fig. 2.1 (a). The Fermi energy E_F in the widegap AlGaAs layer is higher than that in the narrowgap GaAs layer. Consequently electrons spill over from the n -AlGaAs leaving behind positively charged donors. This space charge gives rise to an electrostatic potential that causes the bands to bend as shown. At equilibrium the Fermi energy is constant everywhere. The electron density is sharply peaked near the GaAs-AlGaAs interface (where the Fermi energy is inside the conduction band) forming a thin conducting layer which is usually referred to as the two-dimensional electron gas Fig. 2.1 (b). The carrier concentration in a 2DEG typically ranges from $2.0 \times 10^{11}/\text{cm}^2$ to $2.0 \times 10^{12}/\text{cm}^2$ and can be depleted by applying a negative voltage to a metallic gate deposited on the surface. The practical importance of this structure lies in its use as a field effect transistor which goes under a variety of names such as MODFET (Modulation Doped Field Effect Transistor) or HEMT (High Electron Mobility Transistor).

Note that this structure is similar to standard silicon MOSFETs, where the 2DEG is formed in silicon instead of GaAs. The role of the wide-gap AlGaAs is played by a thermally grown oxide layer (SiO_x). Indeed much of the pioneering work on the properties of two-dimensional conductors was performed using silicon MOSFETs.

Except for the space-charge layers investigation in Si and narrow-gap III-V semiconductors, there are many other systems to be investigated, like two-dimensional electron crystal, InSb, InAs, InP, $\text{Hg}_{1-x}\text{Cd}_x\text{Te}$ systems and Ge, Te,

PbTe, ZnO systems. And the investigated systems also include heterojunctions, quantum wells, superlattices, thin film, and layer compounds, for example, GaSe and related materials and TaSe₂ and related materials, and graphite and intercalated graphite, and even for electron-hole system. And the electrons on liquid helium also constitute a special kind of quasi-two-dimensional space-charge layer. And the magnetic-field-induced surface states in metals also be consider in point of view of inversion two-dimensional layer [1].

2.2. Proposed Sample Preparation

In this thesis, we explore mainly the spin relaxation in closed quantum systems and the spin transport in open quantum systems. Here we just mention the minimal description to give a contour to understand our proposed sample for exploring.

- Open quantum system

Figure 2.2 shows the layer structure of the inverted In_{0.53}Ga_{0.47}As/In_{0.52}Al_{0.48}As modulation doped structure. The heterostructure proposed to be used in this thesis was grown by molecular beam epitaxy (MBE) on a Fe-doped semi-insulating (100) InP substrate. All InGaAs and InAlAs layers were lattice matched to InP. The doping density of the 7-*nm*-thick In_{0.52}Al_{0.48}As carrier supply layer which is underneath a 2DEG channel was $4.0 \times 10^{18} \text{ cm}^{-3}$. The 2DEG channel was formed in an undoped In_{0.53}Ga_{0.47}As channel layer of 20-*nm* thickness. The channel layer is separated by an undoped In_{0.52}Al_{0.48}As spacer layer of 6-*nm* thickness to reduce

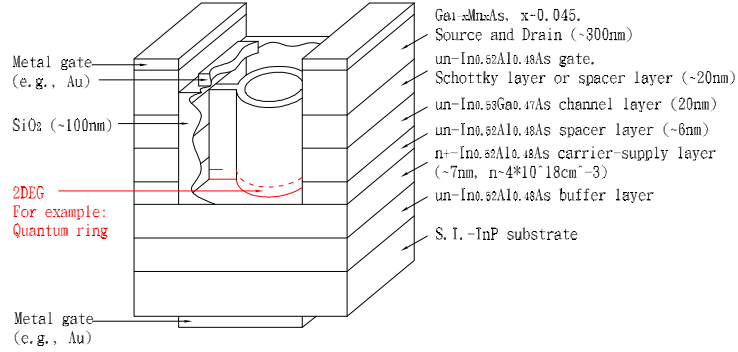


Figure 2.2. Schematic layer structure of an inverted $\text{In}_{0.53}\text{Ga}_{0.47}/\text{In}_{0.52}\text{Al}_{0.48}\text{As}$ heterostructure and profile of the Datta-Das-like SFET.

ionized donor scattering. Then we can apply MBE technique to grow an about 300- nm -thick $\text{Ga}_{1-x}\text{Mn}_x\text{As}$ layer with $x \approx 0.045$. GaAs and (In, Ga) As layers were grown at $T \approx 540 - 580^\circ\text{C}$, while the (Ga, Mn) As layer was grown at $T \approx 250^\circ\text{C}$. The 4.5% Mn concentration is determined from the lattice constant measured by X-ray diffraction, and is expected to yield Curie temperature T_c in the range of 40 – 90K with a hole concentration $p \sim 10^{20}\text{cm}^{-3}$. The easy axis of the (Ga, Mn) As magnetization is in the plane of the sample, verified by a superconducting quantum interference device (SQUID) magnetometer. Then we may use electron beam (EB) lithography, Lift off technique and Ar sputter etching to shape the desired 2DEG structure, for example, various sized mesoscopic rings, dots, and so on [27], and reveal the electrical spin injection source and spin detection drain electrodes. Next we grow about a 100- nm -thick SiO_2 insulating layer which covers the shaped 2DEG structure, finally the gate electrode was made on the top of the

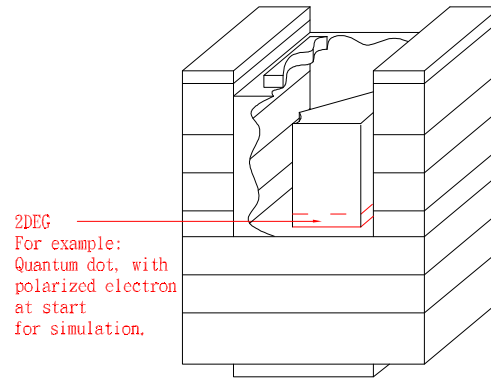


Figure 2.3. Schematic layer structure of an inverted $\text{In}_{0.53}\text{Ga}_{0.47}/\text{In}_{0.52}\text{Al}_{0.48}\text{As}$ heterostructure and profile of the quantum dot for simulation.

source and drain and the SiO_2 insulating layer [28]. Here we see a Datta-Das-like spin field-effect transistor (SFET) in Fig. 1.1 as described in Section *Spintronics*.

- Closed quantum system

For the closed Quantum system, the procedure of the preparation of sample is almost the same to the description of open quantum system, the only differences are we need not fabricate the source and drain electrodes, and we just imagine that polarized electrons have existed before the simulation. Figure 2.3 shows the layer structure and profile of one of the simulation sample.

CHAPTER 3

Spin

3.1. Lead-in

Spin is a fundamental property of all elementary particle [29]. In classical mechanics, a rigid object admits two kinds of angular momentum: orbital ($\mathbf{L} = \mathbf{r} \times \mathbf{p}$), associated with the motion of the center of mass, and spin ($\mathbf{S} = I\boldsymbol{\omega}$), associated with motion about the center of mass. We have an example, the earth has orbital angular momentum attributable to its annual revolution around the sun, and spin angular momentum coming from its daily rotation about the north-south axis. We find that in the classical context this distinction is largely a matter of convenience, for when you come right down to it, \mathbf{S} is nothing but the sum total of the "orbital" angular momenta of all the rocks and dirt clods that go to make up the earth, as they circle around the axis. But an analogous thing happens in quantum mechanics, and here the distinction is absolutely fundamental. In addition to orbital angular momentum, associated (in the case of hydrogen) with the motion of the electron around the nucleus (and described by the spherical harmonics), the electron also carries another form of angular momentum, which has nothing to do with motion in space (and which is not, therefore, described by any function of the position variable r, θ, ϕ) but which is somewhat analogous to classical spin (and

for which, therefore, we use the same word). It doesn't pay to press this analogy too far: The electron (as far as we know) is a structureless point particle, and its spin angular momentum cannot be decomposed into orbital angular momenta of constituent parts. Suffice it to say that elementary particles carry intrinsic angular momentum (\mathbf{S}) in addition to their "extrinsic" angular momentum (\mathbf{L}) [30].

We also could find one of contrary interpretations about spin described by Ohanian, H. C. [31]. The point of view of Ohanian's paper is stated below. The lack of a concrete picture of the spin leaves a grierous gap in our understanging of quantum mechanics. The prevailing acquiescence to this unsatisfactory situation becomes all the more puzzling when one realizes that the means for filling the gap have been at hand since 1939, when Belinfante established that the spin could be regarded as due to a circulating flow of energy, or a momentum density, in the electron wave field. He established that this picture of the spin is valid not only for electrons, but also for photons, vector mesons, and gravitons – in all cases the spin angular momentum is due to a circulating energy flow in the fields. Thus contrary to the common prejudice, the spin of the electron has a close classical analogy: It is an angular momentum of exactly the same kind as carried by the fields of a circularly polarized electromagnetic wave. Furthermore, according to a result established by Gordon in 1928, the magnetic moment of the electron is due to the circulating flow of charge in the electron wave field. This means that neither the spin nor the magnetic moment are internal properties of the electron – they have nothing to do with the internal structure of the electron, but only with the

structure of its wave field. Here one thing must be emphasized that, in contrast to some other attempts at explaining the spin [32], the present explanation is completely consistent with the standard interpretation of quantum mechanics.

The algebraic theory of spin is a carbon copy of the theory of orbital angular momentum, beginning with the fundamental commutation relations [30]:

$$(3.1) \quad [S_x, S_y] = i\hbar S_z, \quad [S_y, S_z] = i\hbar S_x, \quad [S_z, S_x] = i\hbar S_y.$$

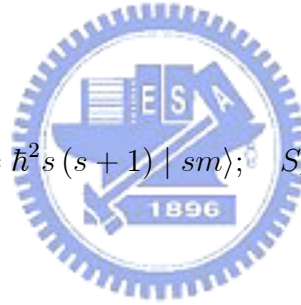
It follows that the eigenvectors of S^2 and S_z satisfy

$$(3.2) \quad S^2 |sm\rangle = \hbar^2 s(s+1) |sm\rangle; \quad S_z |sm\rangle = \hbar m |sm\rangle,$$

and

$$(3.3) \quad S_{\pm} |sm\rangle = \hbar \sqrt{s(s+1) - m(m \pm 1)} |s(m \pm 1)\rangle,$$

where $S_{\pm} \equiv S_x \pm iS_y$. But here the eigenvectors are not spherical harmonics (they're not functions of θ and ϕ at all), and there is no a priori reason to exclude the half-integer values of s and m :



$$(3.4) \quad s = 0, \frac{1}{2}, 1, \frac{3}{2}, \dots; \quad m = -s, -s + 1, \dots, s - 1, s.$$

It so happens that every elementary particle has a specific and immutable value of s , which we call the spin of that particular species: π mesons have spin 0; electrons have spin 1/2; photons have spin 1; deltas have spin 3/2; gravitons have spin 2; and so on. By contrast, the orbital angular momentum quantum number l (for an electron in a hydrogen atom, say) can take on any (integer) value we please, and will change from one to another when the system is perturbed. But s is fixed, for any given particle, and this makes the theory of spin comparatively simple.



3.2. Spin 1/2

Here the most important case is $s = 1/2$, for this is the spin of the particles that make up ordinary matter (protons, neutron, and electrons), as well as all quarks and all leptons. Moreover, once we understand spin 1/2, it is a simple matter to work out the formalism for any higher spin. There are just two eigenstates: $|\frac{1}{2}\frac{1}{2}\rangle$ (or denoted as $|+\rangle$), which we call spin up (informally, \uparrow), and $|\frac{1}{2}(-\frac{1}{2})\rangle$ (or denoted as $|-\rangle$), which we call spin down (informally, \downarrow). Using these as basis vectors, the general state of a spin-1/2 particle can be expressed as a two-element column matrix (or *spinor*):

$$(3.5) \quad \chi = \begin{pmatrix} a \\ b \end{pmatrix} = a\chi_+ + b\chi_-,$$

with

$$(3.6) \quad \chi_+ = \begin{pmatrix} 1 \\ 0 \end{pmatrix}, \quad \chi_- = \begin{pmatrix} 0 \\ 1 \end{pmatrix}$$

representing spin up and for spin down.

Meanwhile, the spin operators become 2×2 matrices, which we can work out by noting their effect on χ_+ and χ_- ; Equation 3.2 says

$$(3.7) \quad S^2\chi_+ = \frac{3}{4}\hbar^2\chi_+; \quad S^2\chi_- = \frac{3}{4}\hbar^2\chi_-; \quad S_z\chi_+ = \frac{\hbar}{2}\chi_+; \quad S_z\chi_- = -\frac{\hbar}{2}\chi_-;$$

and Equation 3.3 gives

$$(3.8) \quad S_+\chi_- = \hbar\chi_+; \quad S_-\chi_+ = \hbar\chi_-; \quad S_+\chi_+ = S_-\chi_- = 0.$$

Now, $S_{\pm} = S_x \pm iS_y$, so

$$(3.9) \quad S_x = \frac{1}{2}(S_+ + S_-) \text{ and } S_y = \frac{1}{2i}(S_+ - S_-),$$

and it follows that

$$(3.10) \quad S_x \chi_+ = \frac{\hbar}{2} \chi_-; \quad S_x \chi_- = \frac{\hbar}{2} \chi_+; \quad S_y \chi_+ = -\frac{\hbar}{2i} \chi_-; \quad S_y \chi_- = \frac{\hbar}{2i} \chi_+.$$

Thus

$$(3.11) \quad S^2 = \frac{3}{4} \hbar^2 \begin{pmatrix} 1 & 0 \\ 0 & 1 \end{pmatrix}; \quad S_+ = \hbar \begin{pmatrix} 0 & 1 \\ 0 & 0 \end{pmatrix}; \quad S_- = \hbar \begin{pmatrix} 0 & 0 \\ 1 & 0 \end{pmatrix};$$

while

$$(3.12) \quad S_x = \frac{\hbar}{2} \begin{pmatrix} 0 & 1 \\ 1 & 0 \end{pmatrix}; \quad S_y = \frac{\hbar}{2} \begin{pmatrix} 0 & -i \\ i & 0 \end{pmatrix}; \quad S_z = \frac{\hbar}{2} \begin{pmatrix} 1 & 0 \\ 0 & -1 \end{pmatrix}.$$

It's a little tidier to divide off the factor of $\hbar/2$: $\mathbf{S} = (\hbar/2)\boldsymbol{\sigma}$, where

$$(3.13) \quad \sigma_x = \begin{pmatrix} 0 & 1 \\ 1 & 0 \end{pmatrix}; \quad \sigma_y = \begin{pmatrix} 0 & -i \\ i & 0 \end{pmatrix}; \quad \sigma_z = \begin{pmatrix} 1 & 0 \\ 0 & -1 \end{pmatrix}.$$

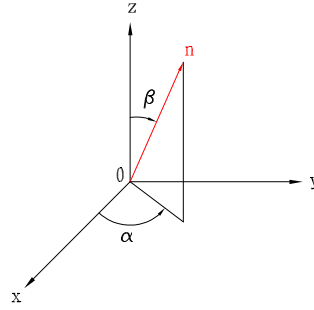


Figure 3.1. \mathbf{n} is a unit vector lies in $3D$ real space.

These are the famous Pauli spin matrices. Notice that S_x , S_y , S_z and S^2 are all Hermitian (as they should be, since they represent observables). On the other hand, S_+ and S_- are not hermitian – evidently they are not observable.

If we try to construct $|\mathbf{S} \cdot \mathbf{n}; +\rangle$ where it is one of the eigenstates which measured in the direction parallel to \mathbf{n} , such that

$$(3.14) \quad \mathbf{S} \cdot \mathbf{n} |\mathbf{S} \cdot \mathbf{n}; +\rangle = \left(\frac{\hbar}{2}\right) |\mathbf{S} \cdot \mathbf{n}; +\rangle$$

where \mathbf{n} is the unit vector and characterized by the angle shown in the Figure 3.1.

By applying the eigenvalue and eigenstate idea and skill, we can get

$$(3.15) \quad |\mathbf{S} \cdot \mathbf{n}; +\rangle = \cos\left(\frac{\beta}{2}\right) |+\rangle + \sin\left(\frac{\beta}{2}\right) e^{i\alpha} |-\rangle$$

Well! This equation can be used as the initial spinor input for calculation and simulation in this thesis.

3.3. Electron in A Magnetic Field

A spinning charged particle constitutes a magnetic dipole. Its magnetic dipole moment $\boldsymbol{\mu}$ is proportional to its spin angular momentum \mathbf{S} :

$$(3.16) \quad \boldsymbol{\mu} = \gamma \mathbf{S},$$

the proportionality constant γ is called the gyromagnetic ratio. (Classically, the gyromagnetic ratio of a rigid objects is $q/2m$, where q is its charge and m is its mass. For reasons that are fully explained only in relativistic quantum theory, the gyromagnetic ratio of the electron is almost exactly twice the classical value [33].) When a magnetic dipole is placed in a magnetic field \mathbf{B} , it experiences a torque, $\boldsymbol{\mu} \times \mathbf{B}$, which tends to line it up parallel to the field (just like a compass needle). The energy associated with this torque is [33]

$$(3.17) \quad H = -\boldsymbol{\mu} \cdot \mathbf{B},$$

so the Hamiltonian of a spinning charged particle, at least in a magnetic field \mathbf{B} (If the particle is allowed to move, there will also be kinetic energy to consider;

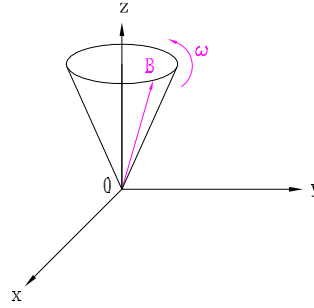


Figure 3.2. Magnetic field sweeps around on a cone, at angular velocity ω , Eq. 3.19.

moreover, it will be subject to the Lorentz force ($q\mathbf{v} \times \mathbf{B}$), which is not derivable from a potential energy function and hence does not fit the Schrödinger equation as we have formulated it so far. Anyhow, for the moment let's just assume that the particle is free to rotate, (but otherwise stationary.), becomes

$$(3.18) \quad H = -\gamma \mathbf{B} \cdot \mathbf{S},$$

where \mathbf{S} is the appropriate spin matrix (Eq. 3.12, in the case of spin 1/2).

Now let us see two cases which relevant to our thesis.

- Cses 1

Imagine an electron (charge $-e$, mass m) at rest at the origin in the presence of a magnetic field whose magnitude (B_0) is constant but whose direction sweeps out a cone, of opening angle α , at constant angular velocity ω , Fig. 3.2.

The magnetic field is

$$(3.19) \quad \mathbf{B}(t) = B_0 [\sin \alpha \times \cos(\omega t)\mathbf{i} + \sin \alpha \times \sin(\omega t)\mathbf{j} + \cos \alpha \mathbf{k}].$$

The Hamiltonian (Eq. 3.18) is

$$(3.20) \quad \begin{aligned} H(t) &= \frac{e}{m} \mathbf{B} \cdot \mathbf{S} \\ &= \frac{e\hbar B_0}{2m} [\sin \alpha \times \cos(\omega t)\boldsymbol{\sigma}_x + \sin \alpha \times \sin(\omega t)\boldsymbol{\sigma}_y + \cos \alpha \boldsymbol{\sigma}_z] \\ &= -\frac{\hbar\omega_1}{2} \begin{pmatrix} \cos \alpha & e^{-i\omega t} \sin \alpha \\ e^{i\omega t} \sin \alpha & -\cos \alpha \end{pmatrix} \end{aligned}$$

where

$$(3.21) \quad \omega_1 \equiv -\frac{eB_0}{m}.$$

The normalized eigenspinors of $H(t)$ are

$$(3.22) \quad \chi_+(t) = \begin{pmatrix} \cos(\alpha/2) \\ e^{i\omega t} \sin(\alpha/2) \end{pmatrix}$$

and

$$(3.23) \quad \chi_{\pm}(t) = \begin{pmatrix} \sin(\alpha/2) \\ -e^{i\omega t} \cos(\alpha/2) \end{pmatrix};$$

they represent spin up and spin down, respectively, along the instantaneous direction of $\mathbf{B}(t)$. The corresponding eigenvalues are

$$(3.24) \quad E_{\pm} = \mp \frac{\hbar\omega_1}{2}.$$

Suppose the electron starts out with spin up, along $\mathbf{B}(0)$:

$$(3.25) \quad \chi(0) = \begin{pmatrix} \cos(\alpha/2) \\ \sin(\alpha/2) \end{pmatrix}.$$

The exact solution to the time-dependent Schrödinger equation is

$$(3.26) \quad \chi(t) = \begin{pmatrix} \left[\cos(\lambda t/2) + i \frac{(\omega_1 + \omega)}{\lambda} \sin(\lambda t/2) \right] \cos(\alpha/2) e^{-i\omega t/2} \\ \left[\cos(\lambda t/2) + i \frac{(\omega_1 - \omega)}{\lambda} \sin(\lambda t/2) \right] \sin(\alpha/2) e^{i\omega t/2} \end{pmatrix},$$

where

$$(3.27) \quad \lambda = \sqrt{\omega^2 + \omega_1^2 + 2\omega\omega_1 \cos \alpha},$$

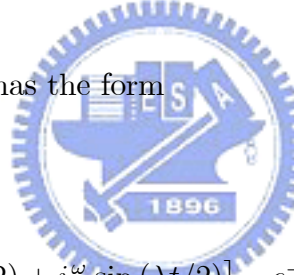
or, writing it as a linear combination of χ_+ and χ_- ,

$$(3.28) \quad \chi(t) = \left[\cos(\lambda t/2) + i \frac{(\omega_1 + \omega \cos \alpha)}{\lambda} \sin(\lambda t/2) \right] e^{-i\omega t/2} \chi_+(t) \\ + i \left[\frac{\omega}{\lambda} \sin \alpha \sin(\lambda t/2) \right] e^{-i\omega t/2} \chi_-(t).$$

Now if we assume an spin evolution operator S_s which with the relationship

$$(3.29) \quad \chi(t) = S_s \chi(0),$$

then we find that S_s has the form



$$(3.30) \quad S_s = \begin{pmatrix} e^{-i\omega t/2} \left[\cos(\lambda t/2) + i \frac{\omega}{\lambda} \sin(\lambda t/2) \right] & e^{-i\omega t/2} \left[i \frac{\omega_1}{\lambda} \sin(\lambda t/2) \cot(\lambda/2) \right] \\ e^{i\omega t/2} \left[i \frac{\omega_1}{\lambda} \sin(\lambda t/2) \tan(\lambda/2) \right] & e^{i\omega t/2} \left[\cos(\lambda t/2) - i \frac{\omega}{\lambda} \sin(\lambda t/2) \right] \end{pmatrix},$$

we should see that the operator S_s is just the one S_p see Eq. 5.20 in view of someone extreme situation (i.e. the trajectory of someone particle (electron) exhibited as a smooth curve).

- Case 2

An electron is at rest at the origin, in the presence of a magnetic field whose magnitude (B_0) is constant but whose direction rides around at constant angular velocity ω on the lip of a cone of opening angle α as Case 1, Fig. 3.2:

$$(3.31) \quad \mathbf{B}(t) = B_0 [\sin \alpha \times \cos(\omega t)\mathbf{i} + \sin \alpha \times \sin(\omega t)\mathbf{j} + \cos \alpha \mathbf{k}],$$

where it is the same to Eq. 3.19.

Then assuming the particle starts out with spin up (says in z direction), we can find its exact solution to the time-dependent Schrödinger equation is

$$(3.32) \quad \chi(t) = \begin{pmatrix} [\cos(\lambda t/2) + i[(\omega + \omega_1 \cos \alpha) / \lambda] \sin(\lambda t/2)] e^{-i\omega t/2} \\ i[(\omega_1 \cos \alpha) / \lambda] \sin(\lambda t/2) e^{i\omega t/2} \end{pmatrix},$$

where

$$(3.33) \quad \omega_1 \equiv -\frac{eB_0}{m}$$

and

$$(3.34) \quad \lambda = \sqrt{\omega^2 + \omega_1^2 + 2\omega\omega_1 \cos \alpha},$$

are also the same to Equations 3.21 and 3.27 [30].

As the Case 1, if we assume an spin evolution operator S_s which with the relationship $\chi(t) = S_s\chi(0)$, we could get the similar equation as Eq. 3.30.

3.4. Time Evolution and Spin Rotation

Suppose we have a physical system whose state ket at t_0 is represented by $|\alpha, t_0\rangle$. At later times, we do not, in general, expect the system to remain in the same state $|\alpha, t_0\rangle$. Let us denote the ket corresponding to the state at some later time by

$$(3.35) \quad |\alpha, t_0; t\rangle, \quad t > t_0.$$



The two kets are related by an operator which we call the time-evolution operator $U(t, t_0)$;

$$(3.36) \quad |\alpha, t_0; t\rangle = U(t, t_0) |\alpha, t_0\rangle.$$

Due to the unitary requirement and the composition property and borrow from classical mechanics idea that the Hamiltonian is the generator of time evolution [34], we can find out the infinitesimal time-evolution operator is written as

$$(3.37) \quad U(t_0 + dt, t_0) = 1 - \frac{iHdt}{\hbar},$$

where H , the Hamiltonian operator, is assumed to be Hermitian, and then we exploit the composition property of the time-revolution operator, we could get

$$(3.38) \quad i\hbar \frac{\partial}{\partial t} U(t, t_0) = HU(t, t_0).$$

This is the Schrödinger equation for the time-revolution operator. If the Hamiltonian operator is independent of time. By this we mean that even when the parameter t is changed; the H operator remains unchanged. The Hamiltonian for a spin-magnetic moment interacting with a time-independent magnetic field is an example of this.

In the Schrödinger picture the operators corresponding to observables like x , p_y , and S_z are fixed in time, while state kets vary with time. By solving Eq. 3.38, we get

$$(3.39) \quad U(t, t_0) = \exp \left[\frac{-iH(t - t_0)}{\hbar} \right].$$

In contrast, in the Heisenberg picture the operators corresponding to observables vary with time; the state kets are fixed, frozen so to speak, at what they

were at to. It is convenient to set in $U(t, t_0)$ to zero for simplicity and work with $U(t)$, which is defined by [35]

$$(3.40) \quad U(t, t_0 = 0) \equiv U(t) = \exp \left[\frac{-iH(t)}{\hbar} \right]$$

Now let us talk about the spin rotation. Following the exploration, we think that because rotations affect physical systems, the state ket corresponding to a rotated is expected to look different from the state ket corresponding to the original unrotated system. Given a rotation operator R , characterized by a 3×3 orthogonal matrix R , we associate an operator $D(R)$ in the appropriate ket space such that

$$(3.41) \quad |\alpha\rangle_R = D(R) |\alpha\rangle$$

where $|\alpha\rangle_R$ and $|\alpha\rangle$ stand for the kets of the rotated and original system, respectively. Note that the 3×3 orthogonal matrix R acts on a column matrix made up of the three components of a classical vector, while the operator $D(R)$ acts on state vectors in ket space. The matrix representation of $D(R)$ depends on the dimensionality N of the particular ket space in question. For $N = 2$, appropriate for describing a spin $1/2$ system with no other degree of freedom, $D(R)$ is represented by a 2×2 matrix; for a spin 1 system, the appropriate representation is a 3×3 unitary matrix, and so forth.

Then following the generator concept for deducing translations and time evolution, and the implicated group properties of general rotations R and other necessary skills. We get for spin 1/2 system with finite rotations, if a rotation about the direction characterized by a unit vector \mathbf{n} by a finite angle ϕ , the rotation operator $D(\mathbf{n}, \phi)$ can be written as

$$(3.42) \quad D(\mathbf{n}, \phi) = \exp\left(\frac{-i\mathbf{S} \cdot \mathbf{n}\phi}{\hbar}\right) \\ \doteq \exp\left(\frac{-i\boldsymbol{\sigma} \cdot \mathbf{n}\phi}{2}\right).$$

Using

$$(3.43) \quad (\boldsymbol{\sigma} \cdot \mathbf{n})^n = \begin{cases} 1 & \text{for } n \text{ even} \\ \boldsymbol{\sigma} \cdot \mathbf{n} & \text{for } n \text{ odd} \end{cases},$$

we could write

$$\begin{aligned}
 (3.44) \quad \exp\left(\frac{-i\boldsymbol{\sigma} \cdot \mathbf{n}\phi}{2}\right) &= \left[1 - \frac{(\boldsymbol{\sigma} \cdot \mathbf{n})^2}{2!} \begin{pmatrix} \phi \\ 2 \end{pmatrix}^2 + \frac{(\boldsymbol{\sigma} \cdot \mathbf{n})^4}{4!} \begin{pmatrix} \phi \\ 2 \end{pmatrix}^4 - \dots \right] \\
 &\quad - i \left[(\boldsymbol{\sigma} \cdot \mathbf{n}) \begin{pmatrix} \phi \\ 2 \end{pmatrix} - \frac{(\boldsymbol{\sigma} \cdot \mathbf{n})^3}{3!} \begin{pmatrix} \phi \\ 2 \end{pmatrix}^3 + \dots \right] \\
 &= \mathbf{1} \cos\left(\frac{\phi}{2}\right) - i\boldsymbol{\sigma} \cdot \mathbf{n} \sin\left(\frac{\phi}{2}\right).
 \end{aligned}$$

Explicitly, in 2×2 form we have [35]

$$(3.45) \quad \exp\left(\frac{-i\boldsymbol{\sigma} \cdot \mathbf{n}\phi}{2}\right) = \begin{pmatrix} \cos\left(\frac{\phi}{2}\right) - in_z \sin\left(\frac{\phi}{2}\right) & (-in_x - n_y) \sin\left(\frac{\phi}{2}\right) \\ (-in_x + n_y) \sin\left(\frac{\phi}{2}\right) & \cos\left(\frac{\phi}{2}\right) + in_z \sin\left(\frac{\phi}{2}\right) \end{pmatrix}.$$

3.5. Spin Precession Extension

Imagine an electron (charge $-e$, mass m) at rest at the origin, in the presence of a uniform magnetic field, which points in the z -direction:

$$(3.46) \quad \mathbf{B} = B\mathbf{k}$$

The hamiltonian is

$$\begin{aligned}
 (3.47) \quad H &= -\gamma \mathbf{B} \cdot \mathbf{S} \\
 &= \frac{e}{m} \mathbf{S} \cdot \mathbf{B} = \frac{e}{m} \mathbf{S} \cdot B \mathbf{n}_B = \frac{e}{m} B \mathbf{S} \cdot \mathbf{n}_B \\
 &= \omega S_{\mathbf{n}_B},
 \end{aligned}$$

where

$$(3.48) \quad \omega = \frac{eB}{m},$$

it is called the Larmor Frequency [33].

The time-evolution operator based on this Hamiltonian is given by

$$\begin{aligned}
 (3.49) \quad U(t, 0) &= \exp \left[\frac{-iHt}{\hbar} \right] \\
 &= \exp \left[\frac{-iS_z \omega t}{\hbar} \right].
 \end{aligned}$$

And consider a rotation by a finite angle ϕ about the z -axis. If the ket of a spin 1/2 system (e.g. an electron) before rotation is given by $|\alpha\rangle$, due to Eq. 3.41 the ket after rotation is given by

$$(3.50) \quad |\alpha\rangle_R = D_z(\phi) |\alpha\rangle$$

with

$$(3.51) \quad D_z(\phi) = \exp\left[\frac{-iS_z\phi}{\hbar}\right].$$

Comparing Eq. 3.49 with Eq. 3.51, we see that the time-evolution operator here is precisely the same as the rotation operator in Eq. 3.51 with ϕ set equal to ωt . In this manner we see immediately why this Hamiltonian causes spin precession [35].

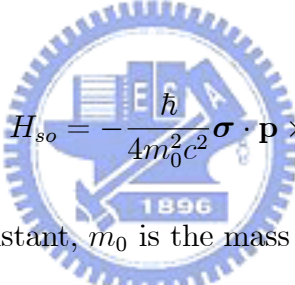
Under our discussion in 2DEG systems, the electrons behave ballistically, that is for each free moving path, it moves like a straight-line segment. Later we will discuss the spin dynamics for each straight-line segment, we will find that during the electron movement in each straight-line segment, the magnitude and direction of effective magnetic field (\mathbf{B}_{eff}) is fixed. That is we could treat the electron precession during the moving to be just like an electron at rest at the origin, in the presence of a uniform magnetic field.

CHAPTER 4

Spin-orbit Coupling

4.1. Spin-orbit Coupling Effect

In atomic physics, spin-orbit (SO) interaction enters into the Hamiltonian from a nonrelativistic approximation to the Dirac equation [36]. This approach gives rise to the Pauli SO term


$$(4.1) \quad H_{so} = -\frac{\hbar}{4m_0^2c^2} \boldsymbol{\sigma} \cdot \mathbf{p} \times (\nabla V_0)$$

where \hbar is Planck's constant, m_0 is the mass of a free electron, c is the velocity of light, \mathbf{p} is the momentum operator, V_0 is the Coulomb potential of the atomic core, and $\boldsymbol{\sigma}$ is the vector of Pauli spin matrices. It is well known that atomic spectra are strongly affected by SO coupling.

4.2. Spin-orbit Coupling in Solid-state Physics

In a crystalline solid, the motion of electrons is characterized by energy bands $E_n(\mathbf{k})$ with band index n and wave vector \mathbf{k} . Here also, SO coupling has a very

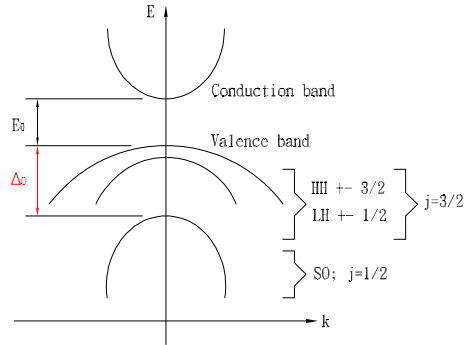


Figure 4.1. Qualitative sketch of the band structure of GaAs close to the fundamental gap.

profound effect on the energy band structure $E_n(\mathbf{k})$. For example, in semiconductors such as GaAs, SO interaction gives rise to a splitting of the topmost valence band, see Fig. 4.1.

In a tight-binding picture without spin, the electron states at the valence band edge are p -like (orbital angular momentum $l = 1$). With SO coupling taken into account, we obtain electronic states with total angular momentum $j = 3/2$ and $j = 1/2$. These $j = 3/2$ and $j = 1/2$ states are split in energy by a gap Δ_0 , which is referred to as the SO gap.

This example illustrates how the orbital motion of crystal electrons is affected by SO coupling. (We use the term "orbital motion" for Bloch electrons in order to emphasize the close similarity we have here between atomic physics and solid-state physics.) It is less obvious in what sense the spin degree of freedom is affected by the SO coupling in a solid. Here we shall analyze both questions for quasi-two-dimensional semiconductors such as quantum wells (QWs) and heterostructures.

It was first emphasized by Elliot [37] and by Dresselhouse et al. [38] that the Pauli SO coupling, Eq. 4.1, may have important consequences for the one-electron energy levels in bulk semiconductors. Subsequently, SO coupling effects in a bulk zinc blende structure were discussed in two classic papers by Parmenter [39] and Dresselhouse [40]. Unlike the diamond structure of Si and Ge, the zinc blende structure does not have a center of inversion, so that we can have a spin splitting of the electron and hole states at nonzero wave vectors \mathbf{k} even for a magnetic field $B = 0$. In the inversion-symmetric Si and Ge crystals we have, on the other hand, a twofold degeneracy of the Bloch states for every wave vector \mathbf{k} . Clearly, the spin splitting of the Bloch states in the zinc blende structure must be a consequence of SO coupling, because otherwise the spin degree of freedom of the Bloch electrons would not *know* whether it was moving in an inversion-symmetric diamond structure or an inversion-asymmetric zinc blende structure.

In the solid-state physics, it is a considerable task to analyze a microscopic Schrödinger equation for the Bloch electrons in a lattice-periodic crystal potential. (We note that in a solid (as in atomic physics) the dominant contribution to the Pauli SO term, Eq. 4.1, stems from the motion in the bare Coulomb potential in the innermost region of the atomic cores. In a pseudopotential approach the bare Coulomb potential in the core region is replaced by a smooth pseudopotential.) Often, band structure calculations for electron states in the vicinity of the fundamental gap are based on the $\mathbf{k} \cdot \mathbf{p}$ method and the envelope function approximation (EFA). Here SO coupling enters solely in terms of matrix elements of the operator,

Eq. 4.1, between bulk band-edge Bloch states, such as the SO gap Δ_0 in Figure 4.1. These matrix elements provide a convenient parameterization of SO coupling effects in semiconductor structures.

4.3. Spin-orbit Coupling in Quasi-two-dimensional Systems

Quasi-two-dimensional (2D) semiconductor structures such as QWs and heterostructures are well suited for a systematic investigation of SO coupling effects. Increasing perfection in crystal growth techniques such as molecular-beam-epitaxy (MBE) and metal-organic chemical vapor deposition (MOCVD) allows one to design and investigate tailor-made quantum structures. Moreover, the size quantization in these systems gives rise to many completely new phenomena that do not exist in three-dimensional semiconductors. We remark here that whenever we talk about 2D systems, in fact we in mind quasi-2D systems with 2 finite spatial extension in the z direction, the growth direction of these system.

A detailed understanding of SO-related phenomena in 2D systems is important both in fundamental research and in applications of 2D systems in electronic devices. For instance, for many years it was accepted that no metallic phase could exist in a disordered 2D carrier system. This was due to the scaling arguments of Abrahams et al. and the support of subsequent experiments. In the past few years, however, experiments on high-quality 2D systems have provided us with reason to revisit the question of whether or not a metallic phase can exist in 2D system [41]. At present, these new findings are controversial. Following the observation that

Space inversion symmetry:	$E_+(\mathbf{k}) = E_+(-\mathbf{k})$	\implies	B = 0 spin degeneracy:
Time inversion symmetry:	$E_+(\mathbf{k}) = E_-(-\mathbf{k})$		$E_+(\mathbf{k}) = E_-(\mathbf{k})$
(Kramers degeneracy)			

Table 4.1. B=0 spin degeneracy is due to the combined effect of inversion symmetry in space and time.

an in-plane magnetic field suppresses the metallic behavior, it was suggested by Pudalov that the metallic behavior could be a consequence of SO coupling [42]. Using samples with tunable spin splitting, it could be shown that the metallic behavior of the resistivity depends on the symmetry of the confinement potential and the resulting spin splitting of the valence band [43]. Datta and Das [14] have proposed a new type of electronic device where the current modulation arises from spin precession due to the SO coupling in a narrow-gap semiconductor, while magnetized contacts are used to preferentially inject and detect specific spin orientation. Recently, extensive research aiming at the realization of such a device has been under way [44].

4.4. Inversion-Asymmetry-Induced Spin Splitting

Spin degeneracy of electron and hole states in a semiconductor is the combined effect of inversion symmetry in space and time [45]. Both symmetry operations change the wave vector \mathbf{k} into $-\mathbf{k}$, but time inversion also flips the spin, so that when we combine both we have a two fold degeneracy of the single-particle energies, $E_+(\mathbf{k}) = E_-(\mathbf{k})$, see Table 4.1.

When the potential through which the carriers move is inversion-asymmetric, however, the spin degeneracy is removed even in the absence of an external magnetic field \mathbf{B} . We then obtain two branches of the energy dispersion, $E_+(\mathbf{k})$ and $E_-(\mathbf{k})$. In quasi-2D quantum wells (QWs) and dots (QDs), and heterostructures, this spin splitting can be the consequence of a bulk inversion asymmetry (BIA) of the underlying crystal (e.g., a zinc blende structure [40]), and of a structure inversion asymmetry (SIA) of the confinement potential [46]. A third contribution to $B = 0$ spin splitting can be the low microscopic symmetry of the atoms at an interface [47]. We emphasize that even in inversion-asymmetric systems with $B = 0$ spin splitting we still have the Kramers degeneracy, see Table 4.1.

For a given wave vector \mathbf{k} , we can always find a spin orientation axis $\mathbf{S}(\mathbf{k})$, local in \mathbf{k} space, such that we have spin-up and spin-down eigenstates with respect to the axis $\mathbf{S}(\mathbf{k})$. But we do not call the branches $E_{\pm}(\mathbf{k})$ spin-up and spin-down, because the direction of \mathbf{S} varies as a function of \mathbf{k} such that, when averaged over all occupied states, the branches contain equal contributions of up and down spinor components. This reflects the fact that in nonmagnetic materials we have a vanishing magnetic moment at $B = 0$. While we shall focus on the effect of $B = 0$ spin splitting on the energy $E(\mathbf{k})$ and the spin degree of freedom, it has been investigated in [48] how $B = 0$ spin splitting affects also the orbital parts of the wave function.

4.5. $B=0$ Spin Splitting and Spin-Orbit Interaction

How can we visualize the fact that the electron spins are *feeling* the inversion symmetry of the spatial environment? In the EFA the full wave function

$$(4.2) \quad \Psi(\mathbf{r}) = \sum_{\nu', \sigma'} \psi_{\nu', \sigma'}(\mathbf{r}) u_{\nu', \mathbf{0}}(\mathbf{r}) |\sigma'\rangle$$

is the product of the quickly oscillating lattice-periodic part $u_{\nu', \mathbf{0}}(\mathbf{r})$ of the Bloch functions times a slowly varying envelop function $\psi_n(\mathbf{r})$. When we have SIA spin splitting, the Bloch part *feels* the atomic fields that enter into the Pauli SO term, Eq. 4.1, and the envelope function *feels* the macroscopic environment, see Figure 4.2. Therefore, we obtain SIA spin splitting only if we have both a macroscopic electric field and a microscopic electric field from the atomic cores. This is consistent with the explicit expressions for SIA spin splitting derived in the R. Winkler's book [49], where the splitting is always proportional to the macroscopic field times a prefactor that depends on the matrix elements $\Delta_{\sigma\sigma'}^{\nu\nu'}$ of the microscopic SO interaction. BIA spin splitting is independent of any macroscopic electric field. It depends only on the matrix elements $\Delta_{\sigma\sigma'}^{\nu\nu'}$ of the microscopic SO interaction. Both SIA and BIA spin splitting disappear in the limit of vanishing bulk SO gaps $\Delta_{\sigma\sigma'}^{\nu\nu'} = 0$ [49].

Several authors have suggested an intuitive picture for the $B = 0$ spin splitting, the electrons are moving with a velocity $\mathbf{v}_{\parallel} = \hbar\mathbf{k}_{\parallel}/m^*$ perpendicular to the

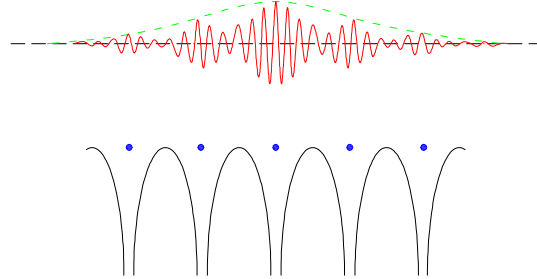
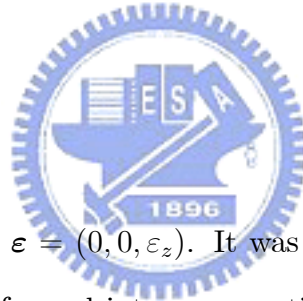


Figure 4.2. Qualitative sketch of a wave function, Eq. 4.2, in the envelope function approximation. The lower part shows the crystal potential $V_0(\mathbf{r})$. The upper part shows the slowly varying envelope function $\psi_{\nu\sigma}(\mathbf{r})$ that modulates the quickly oscillating lattice-periodic part $u_{\nu\sigma}(\mathbf{r})$ of the Bloch function.



macroscopic electric field $\boldsymbol{\varepsilon} = (0, 0, \varepsilon_z)$. It was argued that in the electron's rest frame, $\boldsymbol{\varepsilon}$ is Lorentz transformed into a magnetic field \mathbf{B} , so that the $B = 0$ spin splitting becomes a Zeeman splitting in the electron's rest frame. However, this magnetic field is given by $B = (v_{\parallel}/c^2) \varepsilon_z$ (SI units) and for typical values of ε_z and v_{\parallel} we have $B \approx 2 - 20 \times 10^{-7} T$, which would result in a spin splitting of the order of $5 \times 10^{-9} - 5 \times 10^{-5} meV$. On the other hand, the experimentally observed spin splitting is of the order of $0.1 - 10 meV$. It is clear from the discussion above that this discrepancy is due to the fact that the idea of a Lorentz transformation neglects the contribution of the atomic cores to the SO interaction felt by a Bloch electron in a solid [49].

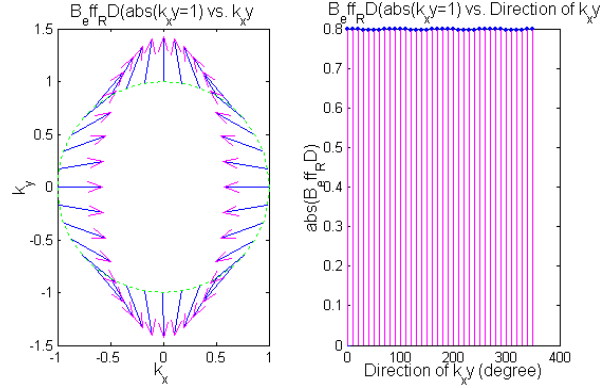


Figure 4.3. Lowest-order spin orientation $\langle \sigma \rangle$ of the eigenstates $|\psi_{\pm}(\mathbf{k}_{\parallel})\rangle$ in the presence of BIA. The circle shows $\langle \sigma \rangle$ along contours of constant energy for the upper branch E_+ of the spin-split dispersion. Here we don't show $\langle \sigma \rangle$ along contours of constant energy for the lower branch E_- of the spin-split dispersion. Left plot shows the magnitude of $\langle \sigma \rangle$ (or B_{eff}) along the direction of \mathbf{k}_{\parallel} .

4.6. BIA Spin Splitting in Zinc Blende Semiconductors

Unlike Si and Ge, which have a diamond structure, the zinc blende structure of III-V and II-VI compounds such as GaAs, InSb, and $\text{Hg}_x\text{Cd}_{1-x}\text{Te}$ does not have a center of inversion. (Strictly speaking, the diamond structure does not have a center of inversion either.) Therefore, SO interaction gives rise to a spin splitting of the bulk energy dispersion. This BIA spin splitting is well known from early theoretical studies [40][51]. It has been observed experimentally by analyzing the Shubnikov-de Haas effect in uniaxially strained bulk InSb [52] and by detecting the precession of the spin polarization of electrons photoexcited from a GaAs [110] surface [53].

For quasi-2D systems in a quantum well (QW) grown in the crystallographic direction [001] the Dresselhouse term becomes [54]

$$(4.3) \quad H_{BIA} = \eta [\sigma_x k_x (k_y^2 - \langle k_z^2 \rangle) + \sigma_y k_y (\langle k_z^2 \rangle - k_x^2)],$$

with a material-specific coefficient η . This equation can easily be diagonalized.

We obtain a spin splitting

$$(4.4) \quad E_{\pm}^{BIA}(\mathbf{k}_{\parallel}) = \pm \eta k_{\parallel} \sqrt{\langle k_z^2 \rangle^2 + \left(\frac{1}{4} k_{\parallel}^2 - \langle k_z^2 \rangle\right) k_{\parallel}^2 \sin^2(2\phi)}$$

$$(4.5) \quad \approx \pm \eta \langle k_z^2 \rangle k_{\parallel} \pm O(\mathbf{k}_{\parallel}^3)$$

We see here that in leading order of \mathbf{k}_{\parallel} the Dresselhouse term Eq. 4.3 gives rise to a spin splitting independent of the direction of \mathbf{k}_{\parallel} that is apparently very similar to the Rashba spin splitting, Eq. 4.9. Nevertheless, the corresponding wave functions are qualitatively different due to the different symmetries of the terms, Eqs. 4.3 and 4.8. If we neglect the terms cubic in \mathbf{k}_{\parallel} , the eigenfunctions in the presence of Dresselhouse spin splitting are

$$(4.6) \quad |\psi_{\pm}^{BIA}(\mathbf{k}_{\parallel})\rangle = \frac{e^{i\mathbf{k}_{\parallel} \cdot \mathbf{r}_{\parallel}}}{2\pi} \xi_{\mathbf{k}_{\parallel}}(z) \frac{1}{\sqrt{2}} \begin{pmatrix} 1 \\ \mp e^{-i\phi} \end{pmatrix}$$

so that

$$(4.7) \quad \langle \boldsymbol{\sigma}(\mathbf{k}_{\parallel}) \rangle_{\pm} = \mp \begin{pmatrix} \cos(-\phi) \\ \sin(-\phi) \\ 0 \end{pmatrix}.$$

The spin orientation Eq. 4.7 of the eigenfunctions Eq. 4.6 as a function of the direction of the in-plane wave vector is indicated by arrows in Figure 4.3. For the Rashba spin splitting we see in Figure 4.4 that if we moving clockwise on a contour of constant energy $E(\mathbf{k}_{\parallel})$ the spin vector is rotating in the same direction, consistent with axial symmetry of the Rashba term. On the other hand, Eq. 4.7 and Fig. 4.3 show that in the presence of BIA the spin vector is rotating counterclockwise for a clockwise motion in \mathbf{k}_{\parallel} space [55].

4.7. SIA Spin Splitting

In semiconductor quantum structures, the spin degeneracy can be lifted not only because of a bulk inversion asymmetry of the underlying crystal structure, but also because of a structure inversion asymmetry of the confining potential $V(\mathbf{r})$. This potential may contain a built-in or external potential, as well as the

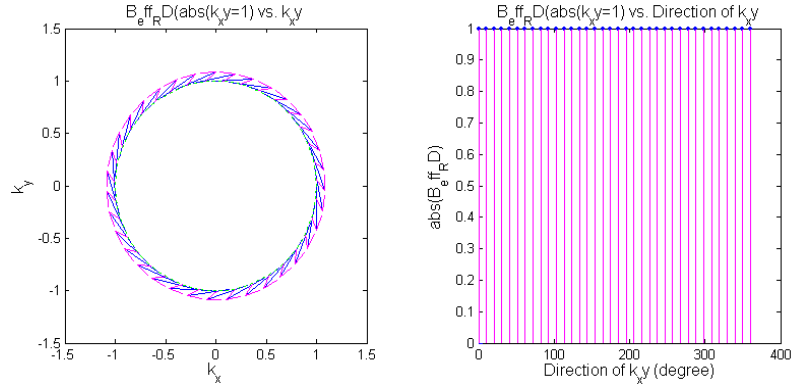


Figure 4.4. Lowest-order spin orientation $\langle \sigma \rangle$ of the eigenstates $|\psi_{\pm}(\mathbf{k}_{\parallel})\rangle$ in the presence of SIA. The circle shows $\langle \sigma \rangle$ along contours of constant energy for the upper branch E_+ of the spin-split dispersion. Here we don't show $\langle \sigma \rangle$ along contours of constant energy for the lower branch E_- of the spin-split dispersion. Left plot shows the magnitude of $\langle \sigma \rangle$ (or B_{eff}) along the direction of \mathbf{k}_{\parallel} .

effective potential from the position-dependent band edges. Recent experiments have shown that the SIA spin splitting can even be tuned continuously by means of external gates [28].

Here to lowest order in the in-plane wave vector $\mathbf{k}_{\parallel} = (k_x, k_y, 0)$ the spin splitting is characterized by the Rashba Hamiltonian [46]

$$(4.8) \quad H_{SIA} = \alpha (\sigma_x k_y - \sigma_y k_x),$$

where σ_x and σ_y are Pauli spin matrices and α is a prefactor that depends on the constituting materials and on the geometry of the quasi-2D system. If we use

polar coordinates for the in-plane wave vector, $\mathbf{k}_{\parallel} = k_{\parallel} (\cos \phi, \sin \phi, 0)$, the spin splitting is given by

$$(4.9) \quad E_{\pm}^{SIA}(\mathbf{k}_{\parallel}) = \pm \alpha k_{\parallel},$$

independent of the angle ϕ , and the eigenstates are

$$(4.10) \quad |\psi_{\pm}^{SIA}(\mathbf{k}_{\parallel})\rangle = \frac{e^{i\mathbf{k}_{\parallel} \cdot \mathbf{r}_{\parallel}}}{2\pi} \xi_{\mathbf{k}_{\parallel}}(z) \frac{1}{\sqrt{2}} \begin{pmatrix} 1 \\ \mp i e^{i\phi} \end{pmatrix},$$

where $\mathbf{r}_{\parallel} = (x, y, 0)$ and envelope function $\xi_{\mathbf{k}_{\parallel}}(z)$. In Eq. 4.10 we have assumed that the Rashba coefficient α is positive. The spin orientation of the eigenstates Eq. 4.10 is given by the expectation value of the vector $\boldsymbol{\sigma}$ of Pauli spin matrices:

$$(4.11) \quad \langle \boldsymbol{\sigma}(\mathbf{k}_{\parallel}) \rangle_{\pm} \equiv \langle \psi_{\pm}(\mathbf{k}_{\parallel}) | \boldsymbol{\sigma} | \psi_{\pm}(\mathbf{k}_{\parallel}) \rangle$$

$$(4.12) \quad = \begin{pmatrix} \pm \sin \phi \\ \mp \cos \phi \\ 0 \end{pmatrix} = \begin{pmatrix} \pm \sin(\phi - \frac{\pi}{2}) \\ \mp \cos(\phi - \frac{\pi}{2}) \\ 0 \end{pmatrix}.$$

Note that Eqs. 4.11 and 4.12 are independent of the envelope function $\xi_{\mathbf{k}_{\parallel}}(z)$ and the magnitude \mathbf{k}_{\parallel} of the in-plane wave vector. The spin orientation Eqs. 4.11 and 4.12 of the eigenfunctions 4.10 as a function of the direction of the in-plane wave vector indicated by arrows in Figure 4.4 [49].



CHAPTER 5

Spin Dynamics

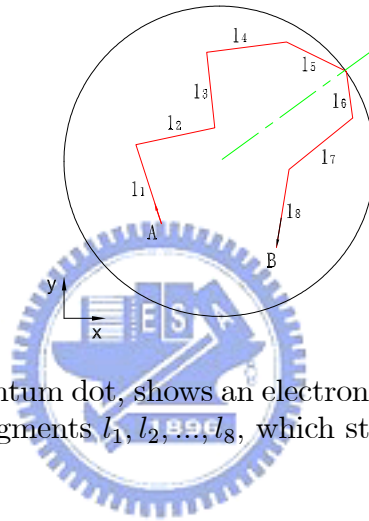


Figure 5.1. A quantum dot, shows an electron trajectory constituted by straight-line segments l_1, l_2, \dots, l_8 , which starts from point A and end at point B .

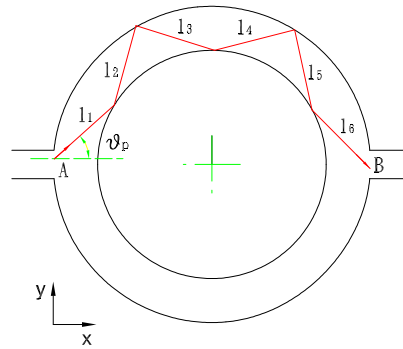


Figure 5.2. A quantum ring, shows an electron trajectory constituted by straight-line segments l_1, l_2, \dots, l_6 , which starts from point A and end at point B .

5.1. Preface

Now let us discuss the spin dynamics, that is how the spin precess in any one of straight-line segments under the effect of spin-orbit coupling interaction (SOI). In principle, we should divide the statement into four parts, they are Rashba SOI effect, Dresselhouse SOI effect with only linear term considered, Dresselhouse SOI effect with linear and cubic terms considered, and the combination of Rashba and Dresselhouse (includes linear and cubic terms) SOI effect, but for constricting the content of this thesis we just represent the part of the combination of Rashba and Dresselhouse (includes linear and cubic terms) SOI effect as representation. For the all four cases, at first, we assume an electron transmits in a 2DEG system which it may be a quantum well (or quantum dot), Fig. 5.1, or a quantum ring, Fig. 5.2. We assume there is none of an external magnetic field and the energy of the electron is conserved and the collisions of the electron with the boundary is elastic. That is the magnitude of the wave vector \mathbf{k}_{\parallel} is fixed, it implies the velocity of the electron is also fixed under the period of action. We assume the electron moves along the p trajectory and label each moving straight-line segment as \mathbf{l}_i , $i = 1, 2, 3, \dots, N$. We just focus on one of these straight-line segments, say \mathbf{l}_i , where its length is l_i and its vector is $\mathbf{k}_{\parallel,i}$, or simply denoted by \mathbf{k}_{\parallel} (and its velocity is $\mathbf{v}_{\parallel,i}$, or simply denoted by \mathbf{v}_{\parallel}) which they are fixed in this segment.

5.2. Rashba and Dresselhouse SOI Effect

Now, let us discuss the combination case of both SIA and BIA spin splitting, that is the combination case of Rashba SOI effect and Dresselhouse SOI effect. We want to find its spin orientation, i.e., the direction of the effective magnetic field \mathbf{B}_{eff} and spin evolution operator in one of the straight-line, say l_i , under the presence of SIA and BIA spin splitting. For quasi-2D systems in a quantum well (QW) grown in the crystallographic direction [001] and apply the external electrical field, we have the total Hamiltonian



$$\begin{aligned}
 (5.1) \quad H_{so} &= H_{SIA} + H_{BIA} \\
 &= \alpha (\sigma_x k_y - \sigma_y k_x) + \eta [\sigma_x k_x (k_y^2 - \langle k_z^2 \rangle) + \sigma_y k_y (\langle k_z^2 \rangle - k_x^2)] \\
 &= [\alpha k_y + \eta k_x (k_y^2 - \langle k_z^2 \rangle)] \sigma_x + [-\alpha k_x + \eta k_y (\langle k_z^2 \rangle - k_x^2)] \sigma_y
 \end{aligned}$$

with $\alpha \geq 0$ and a material-specific coefficient η , and we assume $\eta > 0$.

Then by applying the Eq. 3.18 [50], we get

$$\begin{aligned}
 (5.2) \quad H(t) &= \frac{e}{m} \mathbf{B} \cdot \mathbf{S} \\
 &= \frac{e \hbar}{m 2} (\sigma_x B_x + \sigma_y B_y + \sigma_z B_z)
 \end{aligned}$$

that is

(5.3)

$$[\alpha k_y + \eta k_x (k_y^2 - \langle k_z^2 \rangle)] \sigma_x = \frac{e \hbar}{m} \frac{1}{2} \sigma_x B_x \implies B_x = \frac{2m}{e \hbar} [\alpha k_y + \eta k_x (k_y^2 - \langle k_z^2 \rangle)]$$

(5.4)

$$[-\alpha k_x + \eta k_y (\langle k_z^2 \rangle - k_x^2)] \sigma_y = \frac{e \hbar}{m} \frac{1}{2} \sigma_y B_y \implies B_y = \frac{2m}{e \hbar} [-\alpha k_x + \eta k_y (\langle k_z^2 \rangle - k_x^2)]$$

(5.5)

$$0 = \frac{e \hbar}{m} \frac{1}{2} \sigma_z B_z \implies B_z = 0$$

Here we get the corresponding effective magnetic field $\mathbf{B}_{eff} = \mathbf{B}$.

$$(5.6) \mathbf{B}_{eff} = B \mathbf{n}_B$$

$$\begin{aligned} &= \frac{2m}{e \hbar} \sqrt{[\alpha k_y + \eta k_x (k_y^2 - \langle k_z^2 \rangle)]^2 + [-\alpha k_x + \eta k_y (\langle k_z^2 \rangle - k_x^2)]^2} \mathbf{n}_B \\ &= \frac{2m}{e \hbar} k_B \mathbf{n}_B \end{aligned}$$

where

$$(5.7) \quad k_B \equiv \sqrt{[\alpha k_y + \eta k_x (k_y^2 - \langle k_z^2 \rangle)]^2 + [-\alpha k_x + \eta k_y (\langle k_z^2 \rangle - k_x^2)]^2},$$

$$(5.8) \quad k_{\parallel} = \sqrt{k_x^2 + k_y^2},$$

$$(5.9) \quad B = \frac{2m}{e\hbar} k_B,$$

we find even η , $\langle k_z^2 \rangle$ and k_{\parallel} (or v_{\parallel}) are fixed, B is not fixed. We note that for Rashba SOI effect case (or Dresselhouse linear term SOI effect case), we have $\eta = 0$ (or $\alpha = 0$) then we find that if α (or η) and k_{\parallel} or v_{\parallel} is fixed, then B is fixed. And for Dresselhouse (linear and cubic term) SOI effect case, we find even η , $\langle k_z^2 \rangle$ and k_{\parallel} (or v_{\parallel}) are fixed, B is not fixed, we get the same situation as Rashba and Dresselhouse SOI effect case discussed here.

And then according to the relationship between spin rotation operator and time evolution operator as the discussion in Section *Spin Precession Extension*, we have

$$(5.10) \quad H(t) = \frac{e}{m} \mathbf{S} \cdot B \mathbf{n}_B = \frac{e}{m} B \mathbf{S} \cdot \mathbf{n}_B = \omega_B S_{\mathbf{n}_B}; \quad \omega_B \equiv \frac{eB}{m}$$

we find that since B is not fixed, so ω_B is also not fixed.

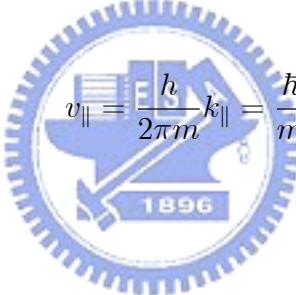
We also have

$$(5.11) \quad U(t, 0) = \exp \left[\frac{-iHt}{\hbar} \right] = \exp \left[\frac{-iS_{\mathbf{n}_B} \omega_B t}{\hbar} \right] = \exp \left[\frac{-iS_{\mathbf{n}_B} \phi}{\hbar} \right]; \quad \phi = \omega_B t$$

and from the knowledge of fundamental quantum physics, we obtain

$$(5.12) \quad k_{\parallel} = \frac{2\pi}{\lambda}; \quad \lambda = \frac{h}{p} = \frac{h}{mv_{\parallel}}$$

so then we find the velocity of the electron in the straight-line segment,

$$(5.13) \quad v_{\parallel} = \frac{h}{2\pi m} k_{\parallel} = \frac{\hbar}{m} k_{\parallel}.$$


And then we obtain

$$(5.14) \quad t_i = \frac{l_i}{v_{\parallel}},$$

and

$$(5.15) \quad \phi_i = \omega_B t_i = \frac{eB}{m} \frac{l_i}{v_{\parallel}} = \frac{eB}{m} \frac{l_i}{\frac{\hbar}{m} k_{\parallel}} = \frac{eB}{\hbar} \frac{l_i}{k_{\parallel}},$$

here v_{\parallel} is the velocity of the electron traveling in the straight-line segment, and t_i is the time spent by the electron traveling the whole segment, and ϕ_i is the precession angle of the spin of the electron under the both SIA and BIA spin splitting SOI effect.

Well, for this case, we define a length magnitude, L_{so} , which means the spin precesses a round after the electron travels along such length. That is

$$(5.16) \quad L_{so} = v_{\parallel} t_{\phi_i=2\pi}$$

where

$$(5.17) \quad t_{\phi_i=2\pi} = \frac{2\pi}{\omega},$$


so then by applying Eqs. 5.7, 5.9, 5.10, and 5.13, we get

$$(5.18) \quad L_{so} = \frac{\hbar^2 \pi}{m} \frac{k_{\parallel}}{k_B} \\ = \frac{\hbar^2 \pi}{m} \frac{k_{\parallel}}{\sqrt{[\alpha k_y + \eta k_x (k_y^2 - \langle k_z^2 \rangle)]^2 + [-\alpha k_x + \eta k_y (\langle k_z^2 \rangle - k_x^2)]^2}}$$

Well! we also must note that in this case even η , $\langle k_z^2 \rangle$ and k_{\parallel} (or v_{\parallel}) are fixed, the L_{so} is not a constant. It depends on the direction of the wave vector \mathbf{k}_{\parallel} .

Finally, we could get the equivalent spin evolution operator, S_{p_i} , for this straight-line segment by applying Eqs. 3.42, 3.44 and 3.45.

$$\begin{aligned}
 (5.19) \mathcal{D}(\mathbf{n}_B, \phi_i) &= \exp\left(\frac{-i\mathbf{S} \cdot \mathbf{n}_B \phi_i}{\hbar}\right) \\
 &\doteq \exp\left(\frac{-i\boldsymbol{\sigma} \cdot \mathbf{n}_B \phi_i}{2}\right) \\
 &= \mathbf{1} \cos\left(\frac{\phi_i}{2}\right) - i\boldsymbol{\sigma} \cdot \mathbf{n}_B \sin\left(\frac{\phi_i}{2}\right) \\
 &= \begin{pmatrix} \cos\left(\frac{\phi_i}{2}\right) - in_{B_z} \sin\left(\frac{\phi_i}{2}\right) & (-in_{B_x} - n_{B_y}) \sin\left(\frac{\phi_i}{2}\right) \\ (-in_{B_x} + n_{B_y}) \sin\left(\frac{\phi_i}{2}\right) & \cos\left(\frac{\phi_i}{2}\right) + in_{B_z} \sin\left(\frac{\phi_i}{2}\right) \end{pmatrix} \\
 &\equiv S_{l_i}.
 \end{aligned}$$

where \mathbf{n}_B parallel to \mathbf{B}_{eff, l_i} and $\phi_i = 2\pi \times (l_i/L_{so})$. We note that for the pure Rashba SOI effect (or the Dresselhouse linear term SOI effect case), as α (or β) is determined, the length L_{so} is fixed, too. But for the Dresselhouse (linear and cubic term) SOI effect case, we find that even η , $\langle k_z^2 \rangle$ and k_{\parallel} (or v_{\parallel}) are fixed, the L_{so} is not a constant. It depends on the direction of the wave vector \mathbf{k}_{\parallel} . We also find that if L_{so} is large, ϕ_i becomes smaller, since L_{so} is not a constant for the Dresselhouse (linear and cubic term) SOI effect case and the Rashba and Dresselhouse SOI effect case explored here, so in these cases the precession of the electron exhibits much more oscillation compared to the the cases of pure Rashba SOI effect and Dresselhouse linear term SOI effect.

5.3. Spin Evolution

Assume we have the same operation environment as the cases discussed in last section. Then according to the discussion of previous section, for one of the segments, we could get its corresponding spin-evolution operator S_{l_i} for segment l_i , Eq. 5.19. And due to the composition property of time-evolution operator, we could describe the spin evolution operator S_p along the p trajectory as:

$$(5.20) \quad S_p = S_{l_N} \cdot S_{l_{N-1}} \cdot \dots \cdot S_{l_3} \cdot S_{l_2} \cdot S_{l_1}$$

with

$$(5.21) \quad \begin{aligned} S_{l_i} &= D(\mathbf{n}_B, \phi_i) \\ &= \exp\left(\frac{-i\mathbf{S} \cdot \mathbf{n}_B \phi_i}{\hbar}\right) \\ &\doteq \exp\left(\frac{-i\boldsymbol{\sigma} \cdot \mathbf{n}_B \phi_i}{2}\right) \\ &= \mathbf{1} \cos\left(\frac{\phi_i}{2}\right) - i\boldsymbol{\sigma} \cdot \mathbf{n}_B \sin\left(\frac{\phi_i}{2}\right) \\ &= \begin{pmatrix} \cos\left(\frac{\phi_i}{2}\right) - in_{B_z} \sin\left(\frac{\phi_i}{2}\right) & (-in_{B_x} - n_{B_y}) \sin\left(\frac{\phi_i}{2}\right) \\ (-in_{B_x} + n_{B_y}) \sin\left(\frac{\phi_i}{2}\right) & \cos\left(\frac{\phi_i}{2}\right) + in_{B_z} \sin\left(\frac{\phi_i}{2}\right) \end{pmatrix} \end{aligned}$$

where

$$(5.22) \quad \phi_i = 2\pi \times \left(\frac{l_i}{L_{so}} \right),$$

and \mathbf{n}_B (or \mathbf{B}_{eff,l_i}) can be gained from Eq. 5.6.



CHAPTER 6

Semiclassical Approach

6.1. Chaotic Scattering

The study of a physical system from the viewpoint of Quantum Chaos usually starts with its classical dynamics. In open systems, e.g., the quantum transport, we must consider a classical scattering problem. Since the trajectory exit the scattering region after a finite amount of time in open systems, the concepts of chaos which developed for closed systems, and related to the long-time properties of the trajectories must be re-examined. Here, we don't attempt to review the field of Chaotic Scattering [56], but just roughly present the information needed to understand the quantum properties of ballistic cavities, and offer an example [57] to illustrate.

For a scattering problem, the *transient chaos* is characterized by the infinite set of trajectories that stay in the scattering region forever. The periodic unstable orbits of the scattering region (the *strange repeller*) and their stable manifold (the trajectories that converge to the previous ones in the infinite-time limit) form the set. Chaotic scattering is gained when the dynamics in the neighborhood of the repeller is chaotic in the usual sense, and this set has a fractal dimension in the space of classical trajectories. When an incoming particle enters the scattering

region it approaches the strange repeller, bounces around close to this set for a while and it is eventually ejected from the scattering region (if the initial conditions to be trapped is lost). If we scan a set of scattering trajectories (say, we fix the initial position y at the left entrance of the cavity of Fig. 0.1 (a) and we vary the initial injection angle θ) studying the time τ that the particle spends in the interaction region, then we could get a fractal curve for $\tau(\theta)$. We find an interesting aspect, the infinitely trapped trajectories give the divergences of $\tau(\theta)$ and determine its self-similar structure. To determine if our scattering is chaotic, the study of $\tau(\theta)$ is a quick way. The rate at which particles escape from the scattering region (ζ) results from a balance between the rate in which nearly trajectories diverge away from the repeller (it could be characterized by its largest Lyapunov exponent λ) and the rate at which the chaotic escaping trajectories are folded back into the scattering region (depending on the density of the repeller, that is measured by its fractal dimension d). More precise speaking, if we start (or inject) particles into the scattering region, the survival probability at time τ will be $p(\tau) = e^{-\zeta\tau}$, with $\zeta = \lambda(1 - d)$ [58]. We may interpret the escape rate as the inverse of the typical time spend by the particle in the scattering region. Let us see the examples [57] shown in Fig. 6.1, the length distribution (which in billiards is equivalent to the length distribution) for a cavity with the shape of stadium, and verify the exponential law (solid line), $p(L) = e^{-\zeta_{cl}L}$ (with $\zeta_{cl} = \zeta/v$ and v the constant velocity of the scattering particles). We notice that the exponential law sets in very fast, just after a length corresponding to a few bounces.

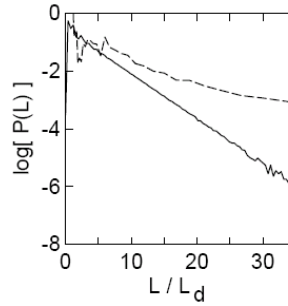


Figure 6.1. Classical distribution of length for stadium (solid line) and rectangular (dash line) billiards. In the stadium, the distribution is close to exponential after a short transient region and are very different from the distributions for the rectangle, which show the power-law behavior characteristic of non-chaotic systems.

We don't surprise the appearance of a single scale, since in chaotic scattering the particle moves ergodically over the whole energy surface while in the scattering region. We also can estimate the value of the escape rate from general arguments of ergodicity in the case of chaotic cavities with small openings, where the typical trajectory bounces around many times before it escapes [59]. Assuming that the instantaneous distribution of trajectories is uniform on the energy surface, the escape rate is simply given by $\zeta = F/A$, where F is the flux through the holes (equal to the size of the holes time v/π , the factor of π comes from integration over the departing angles), A is the area of the two-dimensional scattering domain. We find that in the case of small holes this simple estimate reproduces remarkably well the escape rates obtained from the numerical determination of the survival probability using classical trajectories.

The reason we talk about the escape rate is due to the fact that, the energy scale of the conductance fluctuation is given by this classical quantity. In addition, we also find that the conductance fluctuations as a function of magnetic field are governed by the area distribution.

6.2. Scattering Approach to the Electric Conductance

According to the Landauer-Büttiker approach, in the phase-coherent region the resistance is not an intensive resistivity of the type defined in standard condensed matter books [60], e.g., electron-phonon interaction, but arises from the elastic scattering that electrons suffer which traversing mesoscopic sample between the measuring devices. We treat the measuring devices as macroscopic electron reservoirs. They are characterized by an electrochemical potential μ which does not vary while giving and accepting electrons. The role of the reservoirs is important as they render the total system infinite, and the spectrum continuous. It is only in the reservoirs that the randomization of electron phases is assumed to take place.

Figure 0.1 shows the simplest experimental set up with two-probe measurement, where the sample is attached between two reservoirs whose electrochemical potentials differ by the value of the applied voltage V , which is supposed to be very small ($\mu_1 - \mu_2 = eV \ll \mu_1$).

The scattering description necessitates a set of asymptotic states. In this case such a set is provided by the propagating channels of the leads connecting the

sample with the reservoirs. The three key elements of ballistic transport are sample, reservoirs and leads.

Assuming the leads to be disorder-free, with hard walls (of width W) in the y -direction and infinite in the x -direction, their eigenstates with energy ε are products particle-in a box wave -function

$$(6.1) \quad \phi_a(y) = \sqrt{\frac{2}{W}} \sin\left(\frac{\pi a y}{W}\right)$$

(a is an integer) in the transverse direction and plane-waves propagating in the longitudinal direction, with wave-vectors k_a such that $\varepsilon = \hbar^2 / (2m) ((a\pi/W)^2 + k_a^2)$. The N transverse momenta which satisfy this relationship with $k_a^2 > 0$ define the $2N$ propagating channels of the leads with energy ε . Then we find that the incoming lead-state are

$$(6.2) \quad \phi_{1(2),\varepsilon,a}^{(-)}(\mathbf{r}) = \frac{1}{v_a^{1/2}} e^{\pm i k_a x} \phi_a(y), \quad \mathbf{r} = (x, y), \quad a = 1, 2, \dots, N$$

The normalization factor $v_a^{1/2} = (m/\hbar k_a)^{1/2}$ is chosen in order to have a unit of incoming flux in each channel. The subindex 1 (2) corresponding to channels propagating from the left (right) reservoir with longitudinal momenta k_a ($-k_a$), and k_a explicitly positive. The outgoing lead-state $\phi_{1(2),\varepsilon,a}^{(+)}$ (\mathbf{r}) are defined as in Eq. 6.2, but with the \pm of the exponent inverted. The time order of outgoing

and incoming lead-states is obtained by giving an infinitesimal positive (negative) imaginary part to k_a .

Then we get the scattering states corresponding to an electron incoming from lead 1 (2) with energy ε , in the mode a are given, in the asymptotic regions, by

$$(6.3) \quad \Psi_{1,\varepsilon,a}^{(+)}(\mathbf{r}) = \begin{cases} \frac{\phi_{1,\varepsilon,a}^{(-)}(\mathbf{r}) + \sum_{b=1}^N r_{ba} \phi_{1,\varepsilon,b}^{(+)}(\mathbf{r})}{\sum_{b=1}^N t_{ba} \phi_{2,\varepsilon,b}^{(+)}(\mathbf{r})}, & x < 0 \\ \phi_{2,\varepsilon,a}^{(+)}(\mathbf{r}), & x > 0 \end{cases},$$

$$(6.4) \quad \Psi_{2,\varepsilon,a}^{(+)}(\mathbf{r}) = \begin{cases} \frac{\sum_{b=1}^N t'_{ba} \phi_{1,\varepsilon,b}^{(+)}(\mathbf{r})}{\phi_{2,\varepsilon,a}^{(-)}(\mathbf{r}) + \sum_{b=1}^N r'_{ba} \phi_{2,\varepsilon,b}^{(+)}(\mathbf{r})}, & x < 0 \\ \phi_{1,\varepsilon,a}^{(+)}(\mathbf{r}), & x > 0 \end{cases}.$$

The $2N \times 2N$ scattering matrix S , relating incoming flux and outgoing flux, can be written in terms of the $N \times N$ reflection and transmission matrices r and t (r' and t') from the left (right) as

$$(6.5) \quad S = \begin{pmatrix} r & t' \\ t & r' \end{pmatrix}.$$

From the current conservation, we find that the incoming flux should be equal to the outgoing flux, and therefore S is unitary ($SS^\dagger = I$). In terms of the total transmission ($T = \sum_{a,b} |t_{ba}|^2$) and the reflection ($R = \sum_{a,b} |r_{ba}|^2$) coefficients, the unitarity condition is expressed as $T + R = N$. Also, unitarity dictates that $T = T'$

and $R = R'$. In the absence of magnetic field, time reversal invariance furthermore dictates that S is symmetric ($S = S^T$). For the case of cavities with geometrical symmetries (up-down or right-left) are described by scattering matrices with a block structure [61].

The set $\{\Psi_{1(2),\varepsilon,a}^{(+)}\}$ constitutes an orthogonal (but not orthonormal) basis [62][63],

$$(6.6) \quad \int d\mathbf{r} \Psi_{l,\varepsilon,a}^{(+)*}(\mathbf{r}) \Psi_{l',\varepsilon',a'}^{(+)}(\mathbf{r}) = \frac{2\pi}{v_a} \delta_{aa'} \delta(k_a - k_{a'}) \delta_{u'}$$

Using the spectral decomposition of the retarded Green function in this basis and taking into account the analytical properties of the transmission amplitudes in the complex k -plane, we can relate the Green function to the scattering amplitudes. Or alternatively, the formal theory of scattering (Lippmann-Schinger) can

be adapted to wave-guides and obtain [64].

$$(6.7) \quad t_{ba} = i\hbar (v_a v_b)^{1/2} \exp \left[-i \left(k_b x' - k_a x \right) \right] \int_{S_x'} dy' \int_{S_x} dy \phi_b^*(y') \phi_a(y) G(\mathbf{r}', \mathbf{r}; E),$$

$$(6.8) \quad -\delta_{ab} \exp \left(2ik_b x' \right) + i\hbar (v_a v_b)^{1/2} \exp \left[-i \left(k_b x' + k_a x \right) \right] \int_{S_x'} dy' \int_{S_x} dy \phi_b^*(y') \phi_a(y) G(\mathbf{r}', \mathbf{r}; E),$$

where the integration take place at the transverse cross sections S_x on the left lead and $S_{x'}$ on the right (left) lead for the transmission (reflection) amplitudes. We then have that the physical observables are obtained from the transmission and reflection coefficients ($T = |t_{ba}|^2$ and $R = |r_{ba}|^2$) between modes, which, by current conservation, do not depend on the choice of the transverse cross sections. And we will use this freedom to take S_x and $S_{x'}$ at the entrance and exit of the cavity (or both at the entrance for Eq. 6.8), and we will omit the x and x' dependences henceforth. The above equations give us an intuitive interpretation as a particle arriving at the cavity in mode a , propagating inside (through the Green function), and exiting in mode b is quite straightforward. Expressing the scattering amplitudes in terms of Green function is extremely useful for analytical and numerical computations. The diagrammatic perturbation theory, as well as semiclassical expansions, are built on Green functions.

We have presented the scattering theory for samples connected to wave-guides so far. Now, we reproduce the standard counting argument to relate conductance with scattering [65][1]. At the beginning of this section, we assume that the left reservoir has an electrochemical potential μ_1 slightly than the one of the right reservoir ($\mu_1 - \mu_2 = eV$). In the energy interval eV between μ_2 and μ_1 electrons are injected into right-going states emerging from reservoir 1, but none are injected into left-going states emerging from reservoir 2. Therefore, there is a net right-going current proportional to the number of states in the interval $\mu_1 - \mu_2$, given by

$$(6.9) \quad I = g_{spin} e \sum_{a=1}^N v_a \frac{dn_a}{d\varepsilon} eV \sum_{b=1}^N T_{ba} = g_{spin} \frac{e^2}{h} \left(\sum_{a,b=1}^N T_{ba} \right) V$$

N is the number of propagating channels at the energy μ_1 , the factor $g_{spin} = 2$ takes into account spin degeneracy, $\sum_{b=1}^N T_{ba}$ is the probability for an electron coming in the mode a to traverse the system, $dn_a/d\varepsilon$ quasi-one-dimensional density of states (which for noninteracting particles satisfies that $dn_a/d\varepsilon = 1/hv_a$). Then we find that the two-probe conductance is just proportional to the total transmission coefficient of the microstructure.

$$(6.10) \quad g = \frac{I}{V} = g_{spin} \frac{e^2}{h} T = g_{spin} \frac{e^2}{h} Tr \{tt^\dagger\}$$

where

$$(6.11a) \quad T = \sum_{a,b=1}^N T_{ba} = \sum_{a,b=1}^N t_{ba} t_{ba}^*$$

Note that the magnetic fields that we consider will always be very weak, and therefore the zero-field formulation of the conductance that we presented is sufficient for our purposes.

6.3. Semiclassical Transmission Amplitudes

The scattering formalism presented in the last section is the base for the semiclassical theory of ballistic transport that we develop here. Our goal is to calculate the conductance through a cavity (like one in Fig. 0.1) by using Eq. 6.10 and last part within a semiclassical approach. The Green function is the Laplace transform of the propagator. The Van Vleck expression, together with a stationary-phase integration on the time variable, leads to the semiclassical approximation for the Green function [13]

$$(6.12) \quad G(\mathbf{r}', \mathbf{r}; E) = \frac{2\pi}{(2\pi i\hbar)^{(d+1)/2}} \sum_{S(\mathbf{r}', \mathbf{r})} \sqrt{D_s} \exp \left[\frac{i}{\hbar} S_s(\mathbf{r}', \mathbf{r}; E) - i\frac{\pi}{2} \nu_s \right].$$

The sum is over classical trajectories S , with energy E , going between the initial and final points $\mathbf{r} = (x, y)$ and $\mathbf{r}' = (x', y')$. $S_s = \int_{C_s} \mathbf{p} \cdot d\mathbf{q}$ is the action integral along the path C_s . In the case of billiards without magnetic field $S_s/\hbar = kL_s$, where L_s is the trajectory length. The factor D_s describing the evolution of the classical probability can be expressed as a determinant of second derivatives of the action [13]. As the geometry shown in Fig. 0.1 (a), if we denote by θ and θ' the incoming and outgoing angles of the trajectory with the x -axis, $D_s = \left(v \left| \cos \theta' \right| / m \right)^{-1} \left| (\partial\theta / \partial y')_y \right|$. Here we include in the phase ν_s the Maslov index counting the number of constant-energy conjugate points and the phase acquired

at the bounces with the walls when those are giving by an infinite potential (hard wall). We will always take the spatial dimensionality $d = 2$ in our calculation.

In the case of hard-wall leads, the transverse wave-functions have the sinusoidal form of Eq. 6.1. Using the semiclassical expression, Eq. 6.12, of the Green function appeared in last section, we see that, for large integers a , integral over y will be dominated by the stationary-phase contribution occurring for trajectories starting at points y_0 defined by

$$(6.13) \quad \left(\frac{\partial s}{\partial y} \right)_{y'} = -p_y = -\frac{\bar{a}\hbar\pi}{W}, \quad \bar{a} = \pm a.$$

The dominant trajectories are those entering the cavity with the angles $\theta_{\bar{a}}$ such that $\sin \theta_{\bar{a}} = \bar{a}\pi/kW$. Thus, the initial transverse momentum of the trajectories equals the momentum of the transverse wave-function. As always in this type of reasoning, we have assumed that we could interchange the order of the integration and the sum over trajectories. Integrating the gaussian fluctuations we have

$$(6.14) \quad t_{ba} = i\sqrt{\frac{v_b}{2W}} \int dy' \phi_b(y') \sum_{\bar{a}=\pm a} \sum_{S(\theta_{\bar{a}}, y')} \text{sgn}(\bar{a}) \sqrt{\mathbf{D}_s} \exp \left[\frac{i}{\hbar} \mathbf{S}_s(\mathbf{y}', \theta_{\bar{a}}; E) - i\frac{\pi}{2} \nu_s \right]$$

The reduced action is

$$(6.15) \quad \mathbf{S}(\mathbf{y}', \theta_{\bar{a}}; E) = S(y', y_0(\theta_{\bar{a}}, y'); E) + \frac{\hbar\pi_{\bar{a}}}{W} y_0(\theta_{\bar{a}}, y').$$

The prefactor is now given by $\mathbf{D} = (v \cos \theta')^{-1} |(\partial y / \partial y')_{\theta}|$, and the new index \mathbf{v} (that we still call Maslov index) is increased by one if $(\partial \theta / \partial y')_{y'}$ is positive. At this intermediate stage we have a mixed representation, with trajectories starting with fixed angle $(\pm \theta_a)$ and finishing at points y' . A new stationary-phase over y' calls for. Here we will assume that trajectories are isolated and we can perform the y' integration by stationary phase. The final points y'_0 are selected according to

$$(6.16) \quad \left(\frac{\partial \mathbf{s}}{\partial y'} \right)_{\bar{a}} = \left(\frac{\partial s}{\partial y'} \right)_y = p_{y'} = -\frac{\bar{b}\hbar\pi}{W}, \quad \bar{b} = \pm b$$

implying that the trajectories have an outgoing angle $\theta_{\bar{b}}$ such that $\sin \theta_{\bar{b}} = \bar{b}\pi/kW$. Therefore the semiclassical expression for the transmission amplitude can then be casted as [66]

$$(6.17) \quad t_{ba} = -\frac{\sqrt{2\pi i \hbar}}{2W} \sum_{\bar{a}=\pm a} \sum_{\bar{b}=\pm b} \sum_{S(\bar{b}, \bar{a})} \text{sgn}(\bar{a}\bar{b}) \sqrt{\tilde{D}_s} \exp \left[\frac{i}{\hbar} \tilde{S}_s(\bar{b}, \bar{a}; E) - i \frac{\pi}{2} \tilde{\nu}_s \right]$$

The reduced action is

$$(6.18) \quad \tilde{S}(\bar{b}, \bar{a}; E) = S(y'_0, y_0; E) + \frac{\hbar\pi_{\bar{a}}}{W}y_0 - \frac{\hbar\pi_{\bar{b}}}{W}y'_0.$$

For billiards it can be written as $\tilde{S} = \hbar k \tilde{L}$, with $\tilde{L} = L + ky_0 \sin \theta_{\bar{a}} - ky'_0 \sin \theta_{\bar{b}}$.

The prefactor is now given by

$$(6.19) \quad \tilde{D}_s = \frac{1}{mv \cos \theta'} \left| \left(\frac{\partial y}{\partial \theta'} \right)_\theta \right|$$

and the Maslov index is

$$(6.20) \quad \tilde{\nu} = \nu + H \left(\left(\frac{\partial \theta}{\partial y} \right)_{y'} \right) + H \left(\left(\frac{\partial \theta'}{\partial y'} \right)_\theta \right),$$

where H is the Heaviside step function.

The similar arguments can be used to write the semiclassical reflection amplitude in terms of trajectories leaving and returning to the cross section at the left entrance with appropriate quantized angles. We note that there are two kinds of trajectories contributing to $G(y', y; E)$ in the case of reflected paths: those which penetrate into the cavity and those which go directly from y to y' staying on the cross section of the lead. It is only trajectories of the first kind which contribute to the semiclassical reflection amplitude, as trajectories of the second kind merely cancel the δ_{ba} of Eq. 6.8.

Here we notice that from the quantum point of view, since the Gutzwiller trace formula must reproduce a delta-function spectrum, it can be conditionally convergent at most, while the quantum transmission amplitude is a smooth function of the Fermi energy and so the semiclassical sum can be absolutely convergent. And we also find that the simple prescription for the Maslov indices makes possible the numerical evolution of the semiclassical transmission amplitude.

6.4. Spin Conductance

Following the point of view of scattering approach to the charge conductance to study the spin dependent conductance [67], we define

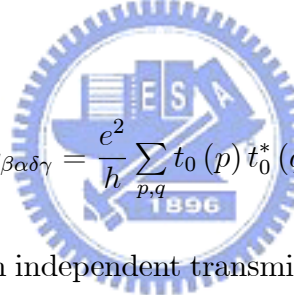
$$(6.21) \quad g_{\beta\alpha\delta\gamma} = \frac{e^2}{h} \sum_{a,b} t_{ba}^{\beta\alpha} t_{ba}^{\delta\gamma*}$$

where $t_{ba}^{\beta\alpha}$ is the transmission amplitude of an electron at Fermi energy E_F propagating from the channel (or mode) a and the spin state α in the injector to the channel (or mode) b and the spin state β in the collector, the same symbolization to $t_{ba}^{\delta\gamma}$. And $t_{ba}^{\beta\alpha}$ is the $\beta\alpha$ element of the matrix t_{ba} which operates on spin states. Then we have the usual spin independent electric conductance is simply $g = e^2/h \sum_{a,b,\alpha,\beta} |t_{ba}^{\beta\alpha}|^2$.

If from the injector a spin oriented in the x axis is injected, and its orientation turns to the y axis when the spin is collected at the collector, let g_{yx} represent this spin current passing through the loop. Then the matrix elements can then be written as

$$(6.22) \quad g_{ji} = \frac{e^2}{h} \sum_{a,b} Tr \left\{ \sigma_i t_{ba} \sigma_j t_{ba}^\dagger \right\}$$

where σ_i are Pauli matrices with $i = x, y, z$. By measuring the polarization of the emitted light [68][69][70], the spin orientation can be detected. In such an experiment, the polarization matrix of the emitted photons can be derived if we know g_{ji} . By applying the saddle point approximation to the path integral representation of the transmission amplitude, the quasiclassical expression of $g_{\beta\alpha\delta\gamma}$ can then be obtained as

$$(6.23) \quad g_{\beta\alpha\delta\gamma} = \frac{e^2}{h} \sum_{p,q} t_0(p) t_0^*(q) S_p^{\beta\alpha} S_q^{\delta\gamma*},$$


where $t_0(p)$ is the spin independent transmission amplitude for the p_{th} classical trajectory, $S_p^{\beta\alpha}$ is the matrix element of the operator of evolution of spin state along the p_{th} trajectory, the same symbolization to $S_q^{\delta\gamma}$. In Fig. 5.2, one such trajectory is schematically plotted as the zigzag line. The explicit expression [66][57][71] of $t_0(p)$ is not needed for the present work, because we only need to know its general statistical properties determined by the particle chaotic motions. The dependence of the transmission on spin degrees of freedom is represented by the spin evolution operator S_p along the p trajectory. From Eq. 5.1 S_p could be expressed as

$$(6.24) \quad S_p = T_s \exp \left[-\frac{i}{\hbar} \int_p H_{so} dt \right]$$

The symbol T_s means a T_s order such that the operators in the integrand in Eq. 6.24 are ordered along the path with the operator corresponding to the later part of the path length operating first. We also find for different spin-orbit interaction (SOI), the S_p can also be expressed as Eqs. 5.20 and 5.21.

In Equation 6.23 each quasiclassical amplitude $t_0(s)$ contains a phase factor $\exp(2\pi i l_s/\lambda)$. Since the path lengths l_p and l_q of the trajectories in Eq. 6.23 are much longer than the electron wavelength λ , in the sum the terms with $p \neq q$ oscillate rapidly even for a small variation of the particle energy, as well as for a slight change of the loop shape and/or the configuration of charged impurities. On the other hand, the terms with $p = q$ do not oscillate. If one is not interested in mesoscopic fluctuations of the spin conductance, only the terms with $p = q$ need to be retained. Accordingly, from Eq. 6.23 we obtain the so averaged spin conductance $\langle g_{\beta\alpha} \rangle$ as

$$(6.25) \quad \langle g_{\beta\alpha} \rangle = \frac{e^2}{h} \sum_p |t_0(p)|^2 D_{\beta\alpha}^p,$$

where

$$(6.26) \quad D_{\beta\alpha}^p = \langle x_\alpha | S_p^\dagger | S^\beta | S_p | x_\alpha \rangle,$$

and where x_α means the unit initial spinor with the spin state α , S^β is the spin operator for measure the spin state β .

For α means i , $i = x, y, z$, according to Eq. 6.22, we get the so averaged spin conductance $\langle g_{ji} \rangle$ as

$$(6.27) \quad \langle g_{ji} \rangle = \frac{e^2}{h} \sum_p |t_0(p)|^2 D_{ji}^p,$$

where

$$(6.28) \quad D_{ji}^p = \text{Tr} \{ \sigma_i S_p \sigma_j S_p^\dagger \}.$$

The so averaged electric conductance is simply $2e^2/h \sum_p |t_0(p)|^2$, and is spin independent.

In the semiclassical approximation, the spin independent transmission rate $|t_0(p)|^2$ in Eqs. 6.25 and 6.27 is approached by the transmission ratio of the classical trajectory ensemble, in which $|t_0(p)|^2$ is described by [57][66]

$$(6.29) \quad |t_0(p)|^2 = f_p(y, \theta_p) \cos(\theta_p) / N,$$

where N is the total number of the injected trajectories and $f_p(y, \theta_p) = 1$, if the trajectory with initial conditions (y, θ_p) is transmitted and $f_p(y, \theta_p) = 0$ otherwise.

6.5. Spin Evolution

Now, let us give the calculation basis of the simulation for spin relaxation case. The procedure of the deduction of the calculation formulae is almost similar to the one of spin conductance as listed above. The calculation basis for the simulation in spin relaxation case is deduced from equation

$$(6.30) \quad P_c^i(t) = \frac{P^j(0)}{2} \int R^{ij}(\mathbf{r}, \mathbf{r}', t) |\Phi(\mathbf{r}' - \mathbf{R})|^2 d^2 r'$$

here it is the expression of the semiconductor spin polarization. And

$$(6.31) \quad R^{ij}(\mathbf{r}, \mathbf{r}', t) = Tr \{ \sigma^i U(t, \mathbf{r}, \mathbf{r}') \sigma^j U^\dagger(t, \mathbf{r}, \mathbf{r}') \}$$

where $U(t, \mathbf{r}, \mathbf{r}')$ could be represented as

$$(6.32) \quad U(t - t', \mathbf{r}, \mathbf{r}') = \mathbf{T} \exp \left[-\frac{i}{\hbar} \int_p H_{so} dt \right],$$

it is the unitary matrix represents the spin dependence part of the Green's function, and H_{so} is the Hamiltonian of spin-orbit interaction under the effect of Rashba and Dresselhouse term case, see Eq. 5.1, and \mathbf{T} is time ordering operator, reference Eq. 6.24. Equation 6.30 describes the spin evolution of a particle initially distributed around the point \mathbf{R} with the probability density $|\Phi(\mathbf{r}' - \mathbf{R})|^2$. The particle starts its classical motion from the point \mathbf{r}' with the momentum $\hbar\mathbf{k}$ at time zero and arrives in the position \mathbf{r} at time t .

We do not intend to deduce detailedly the expression 6.30, the detail deduction procedure had been done by C.H. Chang et al [72], the basic idea about the deduction is given the two component spinor eigenfunction φ_n corresponding to the n_{th} quantized energy level E_n , and then by applying it we could get the time-dependent wave packet

$$(6.33) \quad \psi(\mathbf{r}, t) = \sum_n C_n \varphi_n(\mathbf{r}) e^{-iE_n t/\hbar},$$

where

$$(6.34) \quad C_n = \int \varphi_n^\dagger(\mathbf{r}) \psi(\mathbf{r}) d^2r$$

and then in terms of $\psi(\mathbf{r}, t)$ the time dependent spin polarization could be expressed as

$$(6.35) \quad \mathbf{P}(t) = \sum_{\alpha\beta} \int_{\alpha}^* \psi(\mathbf{r}, t) \boldsymbol{\sigma}_{\alpha\beta} \psi_{\beta}(\mathbf{r}, t) d^2r.$$

Then by introducing the retarded and advanced Green's function and their corresponding semiclassical approximation and using the saddle point approximation in them, we get the desired Green's function

$$(6.36) \quad G^r(t - t', \mathbf{r}, \mathbf{r}') = \frac{1}{2\pi} \sum_p \sqrt{J(\mathbf{r}, \mathbf{r}')} e^{i S_0(t-t', \mathbf{r}, \mathbf{r}')} U(t - t', \mathbf{r}, \mathbf{r}')$$

which it is a sum over all classical trajectories p , and $J(\mathbf{r}, \mathbf{r}')$ is the spin independent monodromy and $S_0(t - t', \mathbf{r}, \mathbf{r}')$ is the spin independent classical action, $U(t - t', \mathbf{r}, \mathbf{r}')$ is the spin dependent part of the Green's function shown in Eq. 6.32. And then by applying the Green's function into Eq. 6.35 we obtain a semiclassical expression for the spin polarization. Finally we proceed some simplified procedure in it, we get the final form, Eq. 6.30, which offers the ingredient to deduce the calculation basis of our simulation.

In our simulation we are interested in the spin evolution averaged over an ensemble of electrons with uniformly distributed coordinates \mathbf{R} and random directions of the initial momenta on the Fermi surface. So after averaged Eq. 6.30 over \mathbf{R} and the angular coordinate θ_k of the momentum \mathbf{k} , we obtain the simple expression

$$(6.37) \quad P_c^i(t) = \frac{P^j(0)}{4\pi} \int R^{ij}(\mathbf{r}, \mathbf{r}', t) d^2r' d\theta_k.$$

Eq. 6.37 is the basic equation for our numerical simulations of the spin polarization. We assume there are N particles initially with polarization in j direction at time $t = 0$, which each particle owns its corresponding trajectory and the spin should evolve as it travels along the trajectory as time goes by. Let $S_j^p(t)$ be the j component of the electron spin at time t for the p_{th} trajectory. Then in our simulation the integral in Eq. 6.37 could be replaced by the sum

$$(6.38) \quad P_c^i(t) = \frac{1}{N} \sum_{p=1}^N S_j^p(t)$$

where the sum runs over N individual trajectories.

The content shown above is the calculation basis of numerical simulation, it is deduced from the point of view of strict deduction of quantum mechanics and mathematical skill of semiclassical approach, here we should present an alternative

approach to *view* intuitively the spin polarization evolution to be the stop of Part I.

Reference last section of this chapter, we have the starting point (i.e. the Landauer-Büttiker approach) for the deduction of averaged spin conductance $\langle g_{ij} \rangle$, see Equations 6.21 and 6.25 ~6.29 etc. These equations are appropriate for the situation of open system. For closed system, we could imagine that both the inlet and outlet are lay in the closed system (or we could say the both inlet and outlet constitute the closed system itself), so for each electron at Fermi energy E_F propagating from the channel a and the spin state α in the injector (inlet) to the channel b and spin state β in the collector (outlet) for the calculation of spin conduction is just equivalent to one of electron of the ensemble with initial spinor state α to evolve to the final spinor state β in terms of the spin evolution operator S_p by traveling along the corresponding trajectory p . And for the electron ensemble, the distribution of the initial traveling direction is uniform (random), that is the weighting factor $|t_0(p)|^2$ could be treated as $1/N$, so spin conduction calculation of the ensemble in open system (i.e. right the spin polarization in closed system) is just the average spin polarization of the ensemble electrons for someone specific final spin polarization direction as Eq. 6.38 shown.

Part 2

Simulation and Discussion



CHAPTER 7

Spin Relaxation

As we mention in Part I, the key indicator in this thesis is that we treat the electrons transport in the mesoscopic system (e.g., regular or chaotic quantum systems, say circular quantum dot, quantum ring, etc.) as rigid balls travel in the cavity it may collide with the impurities and the wall of the cavity, that is we have a ballistic cavity since $\lambda_F \ll a \ll l_T \ll l_\phi$.

We note that for the spin relaxation simulation the main parameters are the categories of operation systems (e.g., regular or chaotic systems), operation cases (e.g., Rashba term case or Dresselhouse term case or the combination of Rashba and Dresselhouse terms cases, with various wave vectors, here we denote them as

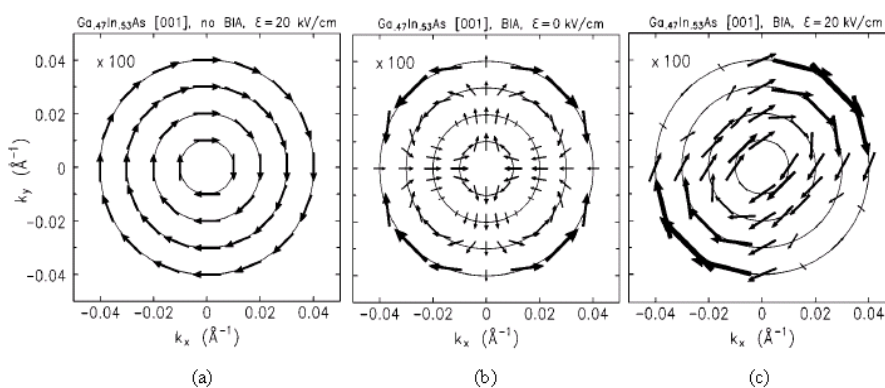


Figure 7.1. Configuration of \mathbf{B}_{eff} for various \mathbf{k} in real material.

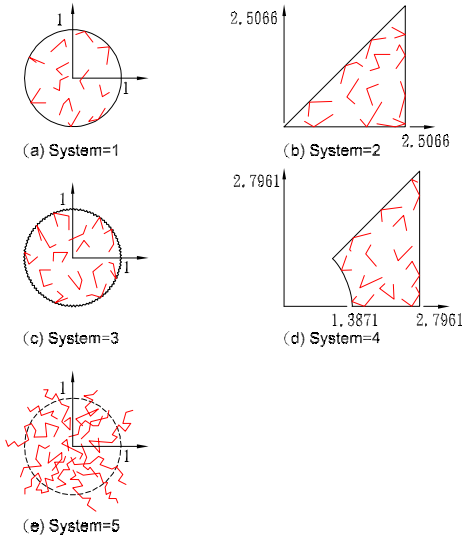


Figure 7.2. Five operation systems.

k_1 , k_2 , k_3 and k_4 , shown in Fig. 7.1), L_{so} (which means the strength of effective magnetic field \mathbf{B}_{eff}), the initial spinor (i.e., the direction of initial polarization), mean free path, l_m , the size of operation system, and the number of acting particles, and so on. In this chapter, we shall mainly talk about the following topics[73], (1) the overview of spin relaxation in the regular systems (include (A) circular dot with smooth boundary, Fig. 7.2, (B) triangular dot with smooth boundary, Fig. 7.2), and in the chaotic systems (include (C) circular dot with rough boundary, Fig. 7.2, (D) Sinai quantum dot, we create a triangle-like quantum dot but with a section cut in one of its acute angles, Fig. 7.2, and (F) two-dimensional bulk-like cavity, see Fig. 7.2, for this system we think there are impurities existing in the cavity), (2) the equivalence between Rashba term effect and Dresselhaus linear term effect in spin relaxation, (3) the equivalence between RMS of \mathbf{B}_{eff} and \mathbf{B}_{eff} configuration,

that is for different traveling segment-like trajectories, their corresponding \mathbf{B}_{eff} which with various magnitude and direction, could be treated as they own the same magnitude, i.e., the root-mean-square (*RMS*) value of the whole \mathbf{B}_{eff} , and their corresponding direction is the same as the original individual \mathbf{B}_{eff} , (4) cases of slow down spin relaxation and never relaxation of spin conductance, and so on.

7.1. Overview of Spin Relaxation Pattern (\mathbf{B}_{eff} Configuration Normalized Case)

At first let us see the overview of spin relaxation patterns for five different systems (we roughly divide them into regular systems, $Sys. = 1$, the circular dot with smooth boundary, $Sys. = 2$, the triangular dot, and chaotic systems, $Sys. = 3$, the circular dot with rough boundary, $Sys. = 4$, the Sinai billiard, and the more chaotic system, $Sys. = 5$, two-dimensional bulk-like system, we must note that in fact the system is a stochastic open system, but not closed system, the elastic collision length l distributed according to the Poisson law $Prob(l) = e^{-l/l_m}/l_m$, where l_m is the mean free path. This is just the system where the conventional D'yakonov-perel' spin relaxation has to be observed), and under the action of nine (or ten) different kinds of \mathbf{B}_{eff} configurations (we denote them as R case, Rashba term case, $D - k1 \sim D - k4$ cases, Dresselhouse linear and cubic terms cases, as \mathbf{k} (wave vector) varies from small to large, and $D - k1$ modified case, it is just the Dresselhouse linear term case, and $RD - k1 \sim RD - k4$ cases, the combination of Rashba term and Dresselhouse linear and cubic terms cases, as \mathbf{k} varies from

small to large). In generally, here we assume $L_{so} = 2$ (indicator of strength of \mathbf{B}_{eff} , we normalize the whole \mathbf{B}_{eff} configurations for nine operation cases, that is the maximum of \mathbf{B}_{eff} denoted by $L_{so} = 2$), l_m (mean free path) = 1, R (radius of circular dot) = 1, and adjust the size of triangular dot and Sinai billiard in order to get the all five systems with the same area, and we also assume about 1000 particles (electrons) to be operated initially, finally we treat the polarization of initial spinor orientated in z direction and the spin detection also orientated in z direction, the situation is symbolized by P_c^z .

Well! at first glance, what do we see in Fig. 7.3? We find the resembles between the nine cases except for $RD - k1$ case, this phenomena seem to mean that the dominated factor which causes the relaxation pattern is the operation system, not operation cases. In general speaking, the regular system (black and red lines), after quick drop of the magnitude of initial spinor, we set $P_c^z(t = 0) = 1$, they remain as constant as time goes by. And the drop magnitudes for the two regular systems, circular dot and triangular dot, depend on the operation cases. it's a so magic thing that we observe that in $D - k2$, $RD - k1$ cases, the spin conductance of circular dot system drops more large than that of triangular dot system. Does it mean the \mathbf{B}_{eff} configuration has something deep implication with the shape of operation system? For chaotic systems (green and blue lines), they exhibit relaxation aspects as time goes by. But we note that the more sensitive to operation cases for $Sys. = 3$ (green line), since it behaves like more chaotic system ($Sys. = 5$) under the more fluctuated operation cases (e.g. $D - k2 \sim D - k4$, $RD - k2 \sim RD - k4$). This is a

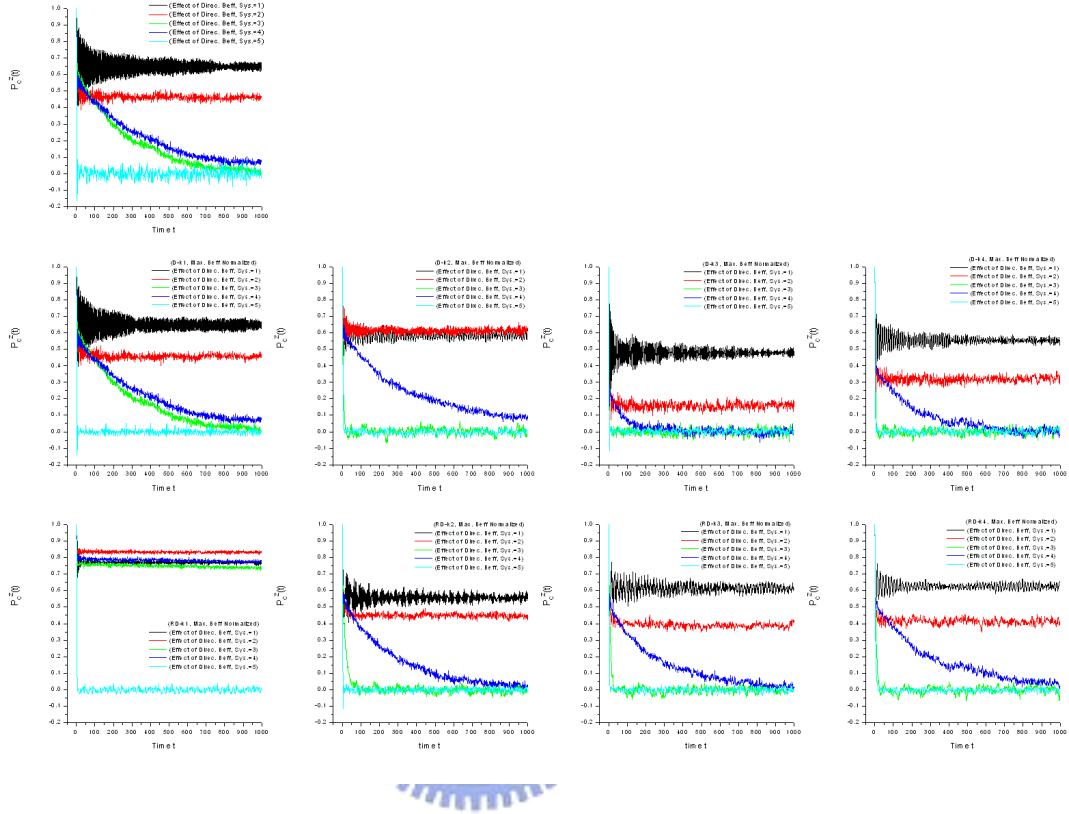


Figure 7.3. Spin relaxation rate under the viewpoint of effect of direction of \mathbf{B}_{eff} in the five operation systems.

so interesting phenomenon worth studying advancedly. And we also note that the almost same aspect between R and $D - k1$ cases. Yes! it is true, R and $D - k1$ cases are equivalent, we should mention them in Sec. *Equivalence between R and $D - k1$ Modified Cases* below. We also find the most special case, $RD - k1$ case, it seems to own the ability to retain the spin polarization regardless the operation systems what they belong. Of course this is due to the special \mathbf{B}_{eff} configuration for this case, we also should discuss it more detailedly in Sections *Relaxation Rate*

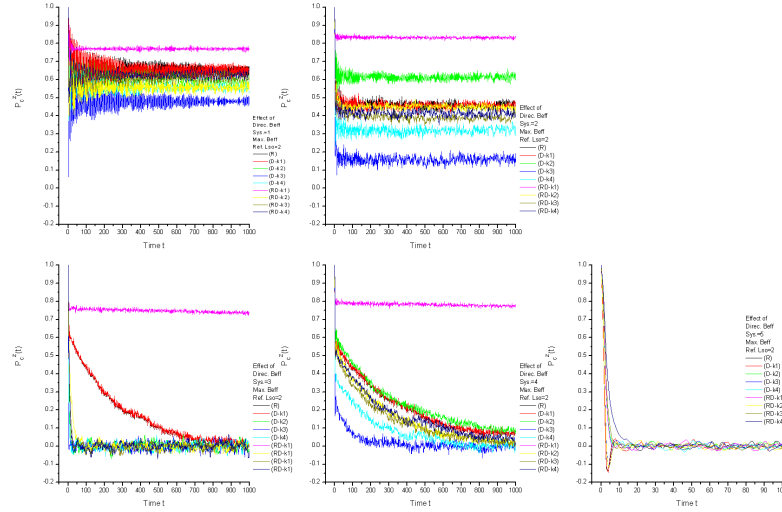


Figure 7.4. Sum up of nine operation cases into one under the view-point of effect of direction of \mathbf{B}_{eff} in the five operation systems.

Slow Down Case and *Relaxation Rate Never Decay Case* below. Finally we see the very fast relaxation system, $Sys. = 5$, the more chaotic system constitutes a particular category of systems. Since in basically it belongs to open system, it owns its special relaxation pattern, we should talk about it latter.

Fig. 7.4 shows the sum up of nine different operation cases into one for different systems. From the figure we could obviously distinguish the effect of systems. For $Sys. = 1$, it dominates the relaxation pattern regardless the operation cases, but for $Sys. = 2$, intrinsically it dominates the relaxation pattern, but the operation cases could affect the spin polarization drop significantly. And for $Sys. = 3$, we find the significant role of operation cases, different \mathbf{B}_{eff} configuration could causes various relaxation pattern, we see that the more *regular* \mathbf{B}_{eff} configuration, the

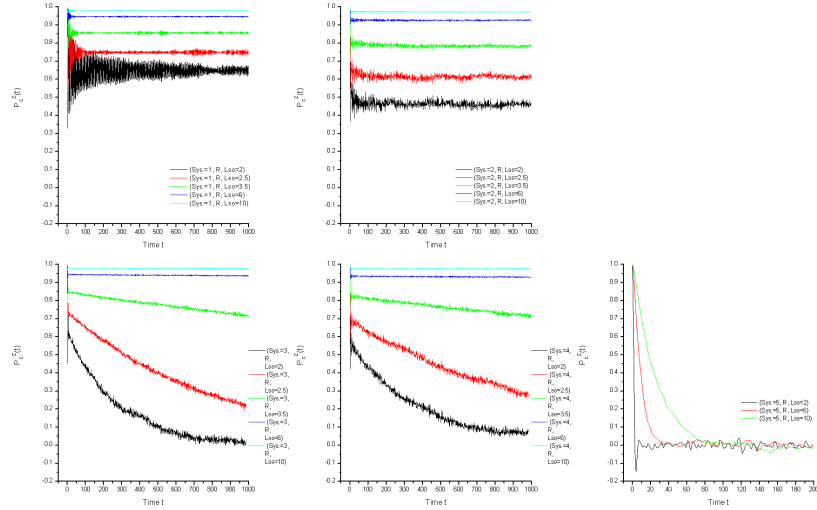


Figure 7.5. The effect of L_{so} in relaxation rate.

more *slow down* relaxation aspects appeared. $Sys. = 4$ shows the typical character of chaotic system, it is less affected by operation cases. $Sys. = 5$ also show the dominated role of the system, we should talk about it more detailedly in Sec. *Equivalence between RMS of B_{eff} and B_{eff} Configuration* below.

Next let's see what happened as we vary the L_{so} (that is we vary the correspondent magnitude of L_{so} with the magnitude of the normalized maximal \mathbf{B}_{eff}). It is obvious that the more larger L_{so} , the more less relaxation trend appeared, Fig. 7.5.

We also get that if we vary the direction of polarization of initial spinor and the direction of polarization of detection, the much different relaxation patterns appeared. Fig. 7.6 shows the so much informations about the effect of the direction

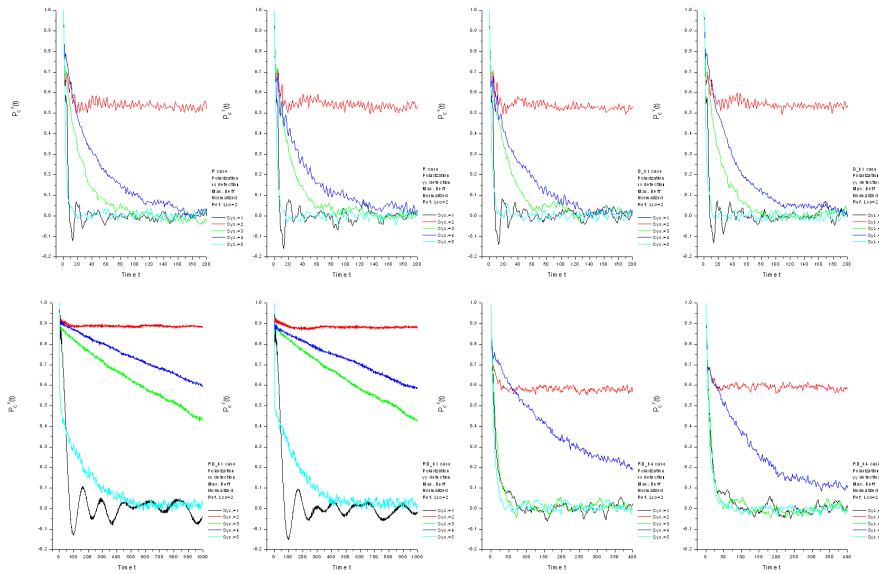


Figure 7.6. The initial spinor input in $+x$ and $+y$ directions for R , $D - k1$, $RD - k1$ and $RD - k4$ cases in all five operation systems.

of initial spinor input. We maybe retain the advanced research about it in other thesis in future, so here we just indicate few astonishing aspects come from it. We find that the equivalence between R and $D - k1$ cases in all five systems both for the initial spinor input in $+x$ and $+y$ directions, it is not so surprised. The surprised thing is that the much different relaxation patterns between different kinds of categories of regular and chaotic systems, say circular-dot-like systems (e.g. $Sys. = 1$ and $Sys. = 3$) and triangular-dot-like systems (e.g. $Sys. = 2$ and $Sys. = 4$), we find that the aspect of faster relaxation rate in circular-dot-like systems than that of triangular-dot-like systems in R , $D - k1$, $RD - k1$ and $RD - k4$ cases and the aspect of reversed relaxation rate for the regular and chaotic cases

of circular-dot-like systems compared with that of triangular-dot-like systems in R , $D - k1$ and $RD - k1$ cases. And the so astonishing relaxation patterns in R , $D - k1$ and $RD - k1$ cases in $Sys. = 1$, they show so quick drop and oscillated aspects about the relaxation patterns. I think that the reason is due to since cases of R , $D - k1$, $RD - k1$ exhibit more *regular* configuration, they influence the intrinsic character of regular and chaotic systems. And for R , $D - k1$, $RD - k1$ and $RD - k4$ cases in $Sys. = 5$ we also find a so much interesting phenomenon which seems to relate to spin relaxation time T_1 (often called longitudinal or spin-lattice time, it seems to be the case of initial spinor input in $+z$ direction) and spin dephasing time T_2 (also called transverse or decoherence time, it seems to be the case of initial spinor input in $+x$ and $+y$ directions), look at these cases and compare them with Fig. 7.9 in $Sys. = 5$, if we add the effect of B_0 (in our simulation $B_0 = 0$, the existence of B_0 should slow down the relaxation rate in the case of initial spinor input in $+z$ direction in $Sys. = 5$) as described in subsection *Spin Relaxation Time and Spin Dephasing Time* of chapter 1 we seem to be able to get the consistency about the statement $T_2 \leq 2T_1$. Well! we stop to discuss it more, but we must note that it is not a simple thing to indicate the correlation between the relaxation pattern and the various operation factors.

Before we end this section, we indicate an interesting thing, we find a similar *motional narrowing* aspect for spin relaxation, we observe that as we reduce the size of the system, the less relaxation aspect happened. The same phenomenon

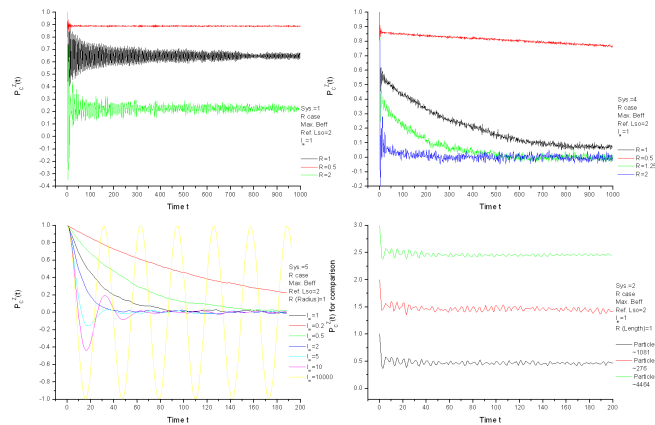


Figure 7.7. The effects of l_m (length of mean free path) and size of system in relaxation rate.

also be observed as we change the length of the mean free path l_m in $Sys. = 5$, the more longer the l_m , the less relaxation trend exhibited, see Fig. 7.7.

Fig. 7.7 also shows the effect of number of particles (electrons) for simulation, the much larger amount of particles, the relaxation curve exhibits less fluctuant aspect.

7.2. Some Aspects of Spin Relaxation Patterns (B_{eff} Configuration in Real Material)

Before we discuss the other interesting aspects about the relaxation patterns, now let's represent the case of spin relaxation in real material.

Fig. 7.1 shows the nine different operation cases in real material, here we assume the strength of B_{eff} of R case as the reference, that is it corresponds to

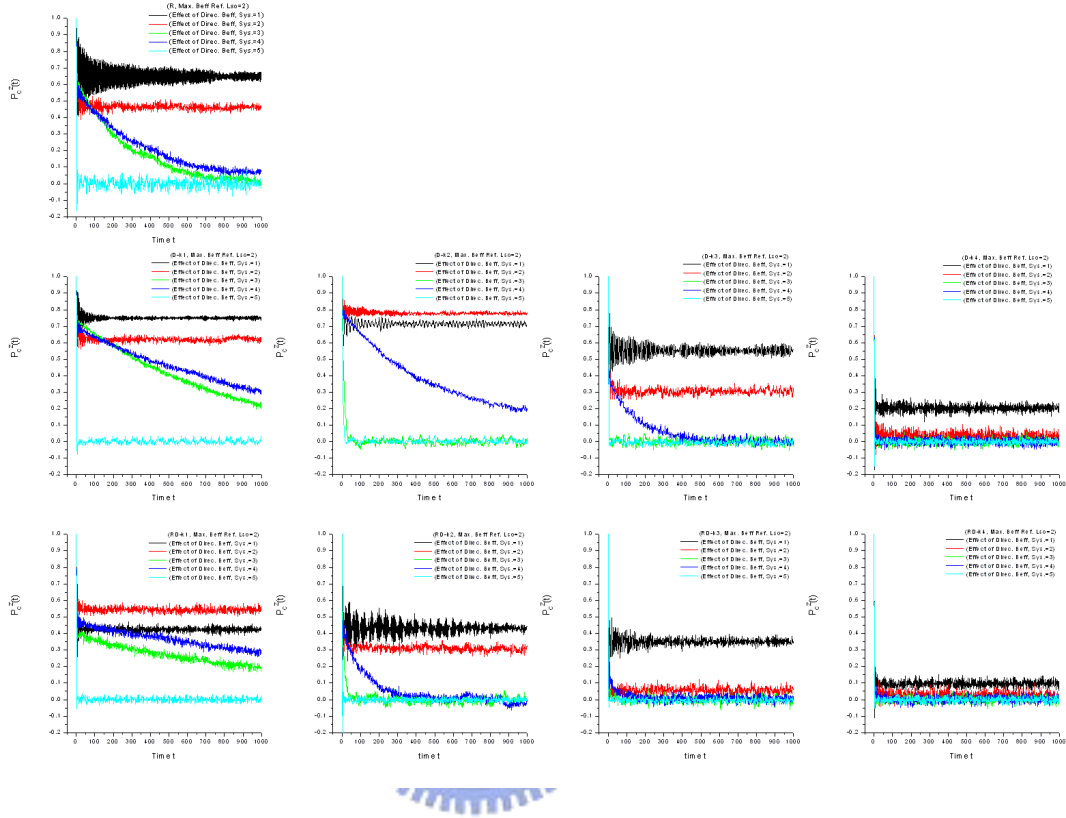


Figure 7.8. Spin relaxation rate under the viewpoint of effect of real (calculated) aspect of \mathbf{B}_{eff} in the five operation systems.

$L_{so} = 2$, for the stronger \mathbf{B}_{eff} , the corresponding L_{so} is smaller, and reversely the weaker \mathbf{B}_{eff} corresponds to larger L_{so} .

At first glance these relaxation patterns shown in Fig. 7.8 seem to exhibit less correspondence. Compare with Fig. 7.3 and look at Fig. 7.1, for systems 1~4, we find that since the \mathbf{B}_{eff} configurations are weaker in $D - k1$ and $D - k2$ cases, so their spin relaxation patterns exhibit slow down aspect, but for $D - k4$, $RD - k1 \sim RD - k4$ cases, the more stronger \mathbf{B}_{eff} configuration, the more quick relaxation

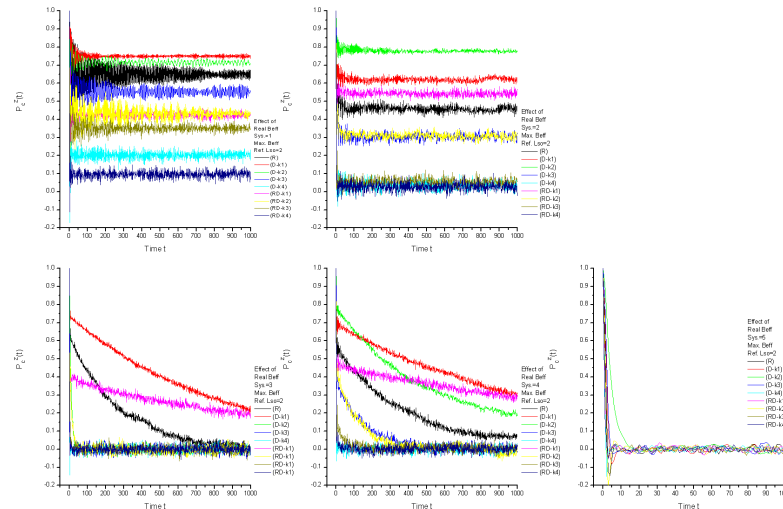


Figure 7.9. Sum up of nine operation cases into one under the viewpoint of effect real (calculated) aspect of \mathbf{B}_{eff} in the five operation systems.

patterns appeared. And for $Sys. = 5$, the variation of strength of \mathbf{B}_{eff} also plays the same role as statement above. We should see the details latter.

Fig. 7.9 shows the sum up of nine different operation cases into one for different systems. Compare with Fig. 7.4, we observe the similar trend between them. The most difference is the variation of \mathbf{B}_{eff} configuration reduces the intrinsic character of systems, especially for $Sys. = 1$ and $Sys. = 4$. these aspects imply that the strength of \mathbf{B}_{eff} configuration owns the more powerful ability to affect the relaxation pattern than the various \mathbf{B}_{eff} configuration itself for some typical operation systems. Another important thing should be noted is that in our simulation we use unitless time parameter. In order to indicate the reasonableness about our

simulation, we should convert the unitless time parameter into real unit. We find that for chaotic system the spin relaxation time (up to zero) is about $20(ns)$, for more chaotic system the relaxation time (up to zero) is estimated about $100(ps)$. Well! they lie in the reasonable spin relaxation time which spans from several pico-seconds to several micro-seconds [21].

7.3. Equivalence between R and $D - k1$ Modified Cases

See Fig. 7.3 we find the spin relaxation patterns in Rashba term case (R case) and Dresselhouse linear and cubic terms case ($D - k1$ case) (here $D - k1$ modified case (Dresselhouse linear term case) is almost the same as $D - k1$ case) are almost the same. The reason is due to the configuration of \mathbf{B}_{eff} for R case and $D - k1$ case are almost the same except for the rotation trend, for R case if we view the wave vector variation in counter-clock-wise (C.C.W.), the corresponding \mathbf{B}_{eff} rotates in C.C.W. and they all have the same magnitude, and for $D - k1$ case if we view the wave vector variation in C.C.W., we find the corresponding \mathbf{B}_{eff} rotates clockwise (C.W.) and they also own the same magnitude Fig. 8.24. We then find that for the ensemble electrons which own different propagating direction individually, the C.C.W. or C.W. rotation of \mathbf{B}_{eff} doesn't matter at all about the ensemble results of spin evolution, so we get the interesting result. We should discuss it more detailedly in Chapter 8.

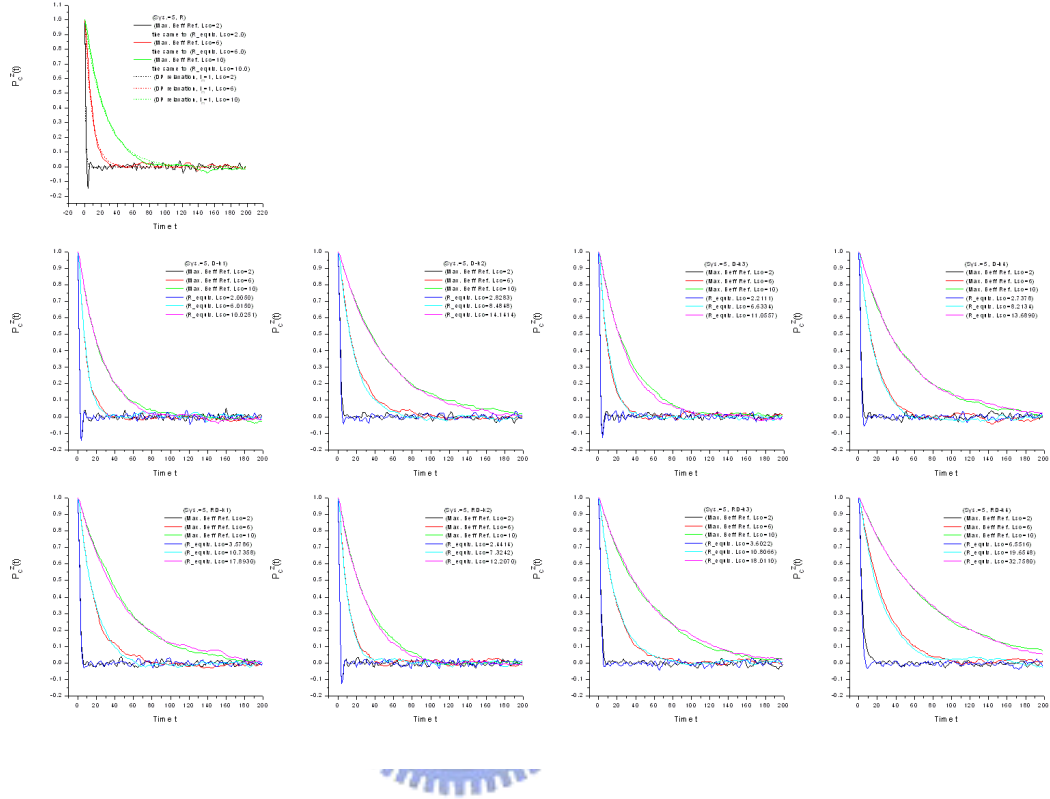



Figure 7.10. Equivalence between RMS of \mathbf{B}_{eff} and \mathbf{B}_{eff} configuration in the relaxation under various operation cases in two-dimensional bulk-like system.

7.4. Equivalence between RMS of \mathbf{B}_{eff} and \mathbf{B}_{eff} Configuration

Reference Fig. 7.10 we find that in the two-dimensional bulk-like system the spin relaxation patterns under the action of each operation cases are almost the same as that under the action of their corresponding root-mean-square (RMS) magnitude of the effective magnetic field \mathbf{B}_{eff} . The reason is due to, for example the $RD - k3$ case, in someone moment each particles in the two-dimensional

bulk-like system own various propagating direction, and regardless of the corresponding direction of \mathbf{B}_{eff} for someone specific propagating direction (i.e. the *configuration* of \mathbf{B}_{eff}), each particles suffered different degree of precession, we assume the equivalence between the RMS of \mathbf{B}_{eff} and the \mathbf{B}_{eff} configuration for someone operation case is meant that we assume the effect of the average of the more fluctuated degree of precession for each particles in $RD - k3$ case is almost the same as that of the average of the less fluctuated degree of precession for each particles in the RMS of \mathbf{B}_{eff} of $RD - k3$ case. Then we obtain the funny result and the mathematical representation is shown below

$$(7.1) \quad \frac{\sum_{n=1}^N P_{n, \text{someone-specific-operation-case}}^z(t)}{N} \approx \frac{\sum_{n=1}^N P_{n, \text{RMS-of-}\mathbf{B}_{eff}\text{-of-someone-specific-operation-case}}^z(t)}{N}$$


where N is the number of particles used in simulation, $N \approx 1000$ in our simulation.

Look at the R case of this figure, we also find the excellent fit between simulation result and theoretical prediction of longitudinal DP relaxation, that is the dash lines indicate the results of well-known expression for the longitudinal DP relaxation $P_{DP}(t) = \exp(-4tl_m/L_{so}^2)$, the relevant discussion could be found in the thesis of C.H. Chang et al. [72]

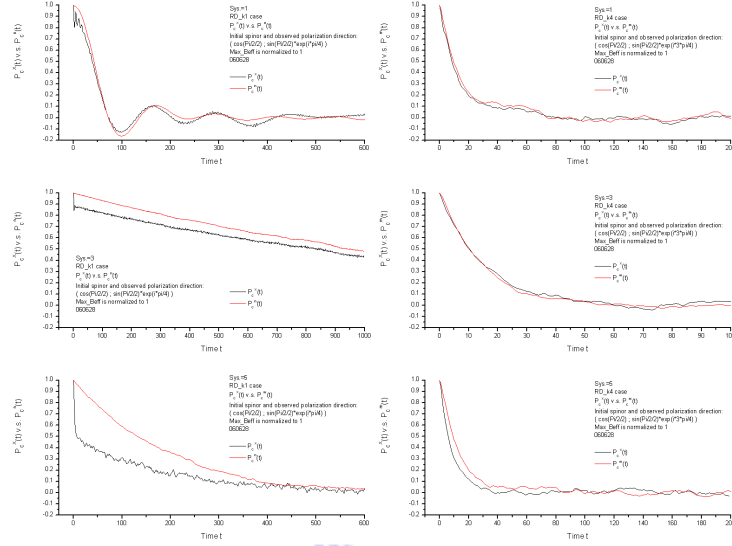


Figure 7.11. Relaxation rate slow down case under specific operation cases with specific initial spinors input in three different systems.

7.5. Relaxation Rate Slow Down Case

From the B_{eff} configuration, Fig. 7.1, we get a hint that if we assume someone special initial polarization direction, maybe we could get something special results, we should continue this talk in Chapter 8. Fig. 7.11 shows three systems, $Sys. = 1, 3$ and 5 , each with two different initial spinors input, spinor $p^n \doteq (\cos(\pi/2/2); \sin(\pi/2/2) \exp(i\pi/4))$ and spinor $p^m \doteq (\cos(\pi/2/2); \sin(\pi/2/2) \exp(i3\pi/4))$, acting on $RD - k1$ and $RD - k4$ cases individually. From this figure we observe the trend that if the adequate match between initial spinor and operation case existence, we could get the relaxation slow down aspects. The aspects is more astonishing in systems 3 and 5 under the operation of $RD - k1$ case. In fact, we should find in

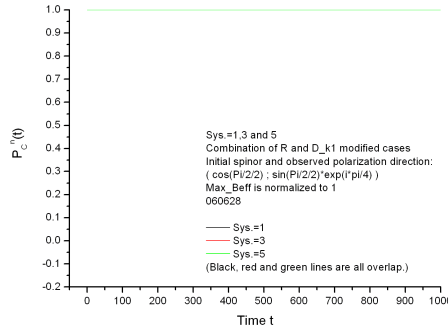


Figure 7.12. Relaxation rate never decay case under specific operation cases with specific initial spinors input in three different systems.

next section and Chapter 8, the key role which causes such aspect is the operation case, that is if we could create someone special spinor evolution behavior which owns something special correlation with operation case, theoretically we could get many various relaxation aspects (patterns) as we desire.

7.6. Relaxation Rate Never Decay Case

O.K. let us end this chapter by a never decay case in terms of practical application. We will give the mathematical description in Chapter 8. Here we just represent the simulation results. Fig. 7.12 shows a never relaxation (decay) case as we create a special \mathbf{B}_{eff} configuration, that is the combination of the same strength of R case and $D - k1$ modified case, the direction of \mathbf{B}_{eff} of such special operation case always direct in the same direction (or in opposite direction). Then if we input a corresponding initial spinor which parallels (or anti-parallel) to this

direction, we get a never relaxation polarization output as the spinor evolution. In fact it is the ideal goal which the engineers desire to create in spintronics in future.



CHAPTER 8

Spin Transport

Now let us see the simulation results of spin transport in following four kinds of operation systems, and discuss some interesting phenomena revealed by them. Here the operation conditions are similar to that of the previous chapter *Spin Relaxation*, that is we have $\lambda_F \ll a \ll l_T \ll l_\phi$, where l_ϕ is the phase relaxation length, l_T is the transport mean-free-path, a is the size of the operation system, λ_F is the Fermi wavelength, so that we can treat the transport cases in terms of ballistic cavities viewpoint and then apply semiclassical approximation to solve them as the statement in Chapter 6 of Part I.

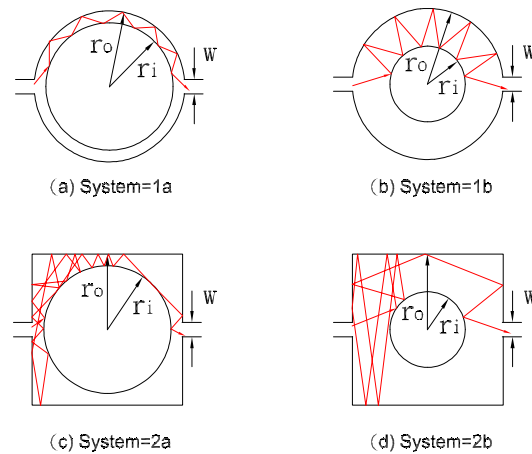


Figure 8.1. Four kinds of operation systems for spin transport simulation.

In our simulation the main purpose is to find out some significant implication of the simulation results (that is the simulation patterns) related to the main simulation parameters. They are the operation systems[73] (here we divide them into four kinds, Fig. 8.1, (a) and (b) are ring-like open systems, they belong to regular system, the main difference between them is the ratio of the radius of inner circle and the radius of outer circle, for (a) we have $r_i : r_o = 29/30 : 1$, for (b), $r_i : r_o = 9/10 : 1$, (c) and (d) are chaotic systems, the main difference between them is the ratio of the radius of inner circle and the half length of the outer square, for (c) we have $r_i : r_o = 9/10 : 1$, (d) $r_i : r_o = 8/10 : 1$), the operation cases (here as the conditions discussed in Chapter 8 *Spin Relaxation*, we divide the operation cases into nine (or ten) kinds, they are Rashba term case, Dresselhouse term cases (they include linear and cubic terms) for different magnitude of wave vector, and the combination of Rashba and Dresselhouse terms cases for different magnitude of wave vector, Fig. 7.1, and we also consider a special case of operation case, which is the combination of Rashba term and Dresselhouse linear term, and the strength (or magnitude) of the effective magnetic field for both cases are the same), the initial spinor (mainly we vary the initial spinor from expectation value in $+x$ direction, expectation value in $+y$ direction, expectation value in $+z$ direction to the expectation value in arbitrary direction), and the scale of the operation cases (that is we divide this parameter into two situation, one is we treat the maximal magnitude of the \mathbf{B}_{eff} for various operation cases correspond to the same magnitude of a new parameter L_{so} which it means the

degree of precession and we assume $|\mathbf{B}_{eff}| \propto 1/L_{so}$, the purpose of such treatment is to offer the information of the effect of the configuration of \mathbf{B}_{eff} related to the simulation patterns, another is we treat the various operation cases as a whole, we assume the magnitude of \mathbf{B}_{eff} in operation case, R case, as a reference, that is we assume that it corresponds to a specific L_{so} value, and then depending on the real situation of \mathbf{B}_{eff} for different operation cases, the different magnitude of \mathbf{B}_{eff} corresponding to a scaled magnitude of L_{so} , we execute such simulation is try to offer the information to see what happened about the effect of real configuration of \mathbf{B}_{eff} for various operation case related to simulation patterns), and so forth.

In this chapter we mainly divide it into three parts, part one says the overview of the simulation patterns, it talks about the characters and implication of the simulation patterns for all operation parameters, etc., in part two we talk about the equivalence of Rashba term case (i.e. R case) and Dresselhouse linear case (generally speaking, it is the $D - k1$ case), and in part three we represent a special case, that is the combination of Rashba term and Dresselhouse linear term case which the strengths of the maximal \mathbf{B}_{eff} for the two cases are the same, we find a never decay interesting phenomena in simulation pattern.

8.1. Overview of the Conductance Decay Patterns (\mathbf{B}_{eff} Configuration Normalized Case)

In principle the conductance pattern is governed by the following factors, system categories, system size, \mathbf{B}_{eff} configuration and the initial input of spinor, and

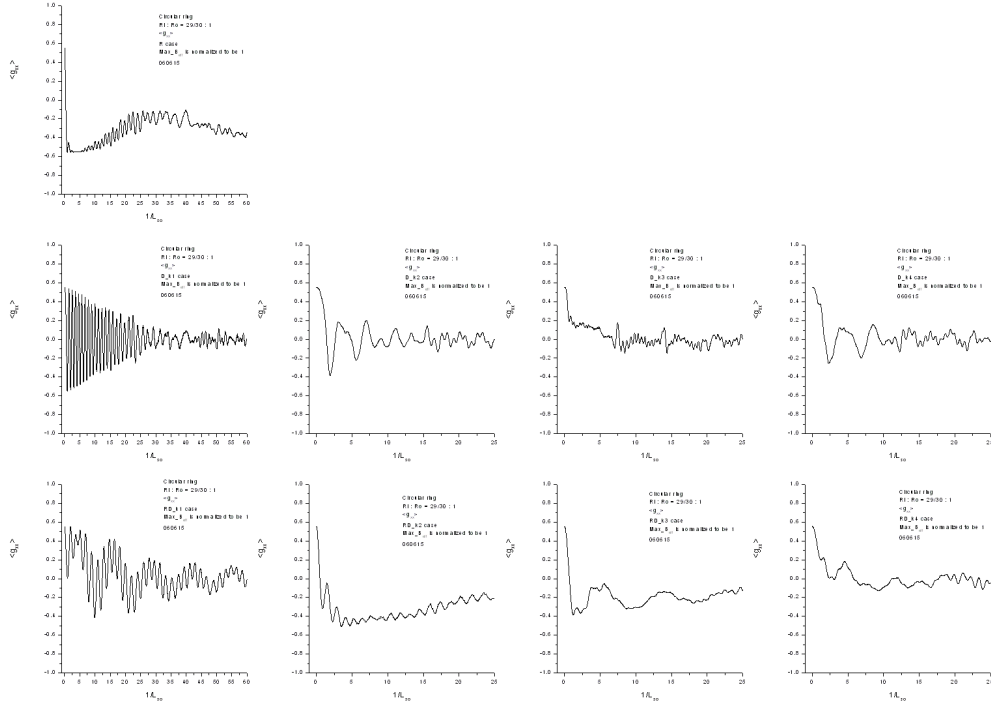


Figure 8.2. Spin conductance $\langle g_{xx} \rangle$ v.s. $1/L_{so}$ under the action of normalized B_{eff} in more narrow circular ring system.

so on. Figures 8.2, 8.3 and 8.4 show the conductance versus $1/L_{so}$ in circular ring with inner radius $R_i = 29/30$, outer radius $R_o = 1$ and the width of both inlet and outlet $w = 0.1$ for initial spinor (or polarization) in x , y and z direction under the action of various \mathbf{B}_{eff} configuration. Here we have normalized the maximum of \mathbf{B}_{eff} to be 1 for various kinds of operation cases. In Fig. 8.2 we find the similarity between R case and $RD - k2$ case, they show the $\langle g_{xx} \rangle$ decays very fast to the $-x$ direction and then gradually comes back to someone minus $\langle g_{xx} \rangle$ value, that is

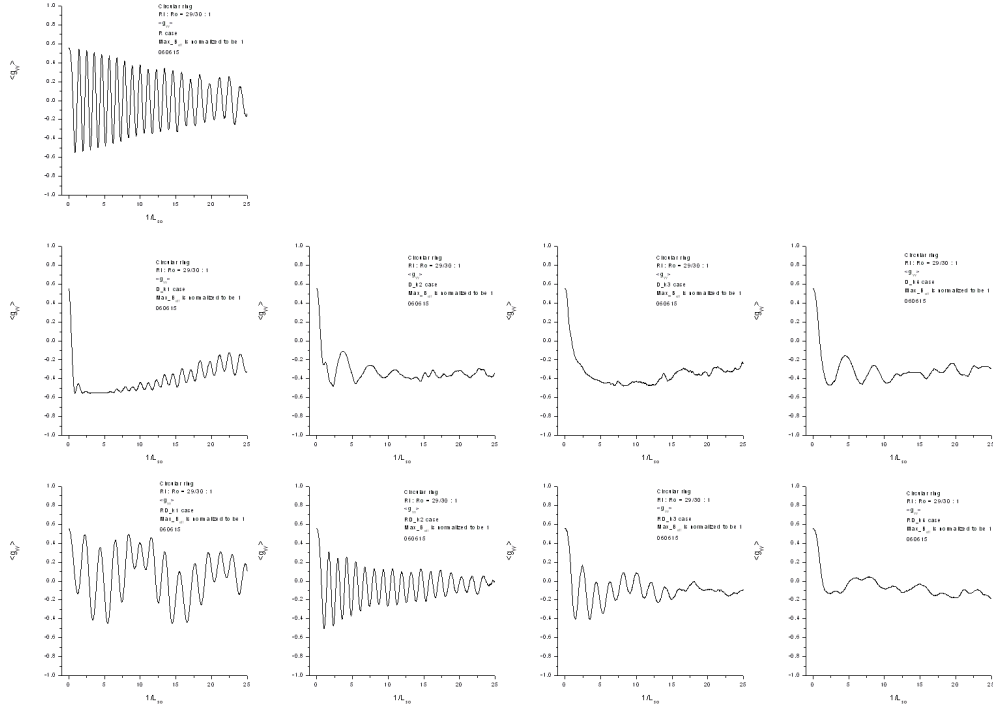


Figure 8.3. Spin conductance $\langle g_{yy} \rangle$ v.s. $1/L_{so}$ under the action of normalized B_{eff} in more narrow circular ring system.

very interesting that the $\langle g_{xx} \rangle$ seems not to approach zero even in the very large strength of B_{eff} , i.e. in large value of $1/L_{so}$. We also find the similarity between $D - k2$ and $D - k4$ cases, they show the oscillated decay to zero as $1/L_{so}$ goes by. And we also find the slightly decay pattern in $D - k3$ and $RD - k4$ cases, they don't exhibit the suddenly *deep* decay behavior at the decay portion. We also find the tendency of different oscillation decay period between $RD - k2$, $RD - k3$ and $RD - k4$ cases, and for the three cases they seem to exhibit the similar decay

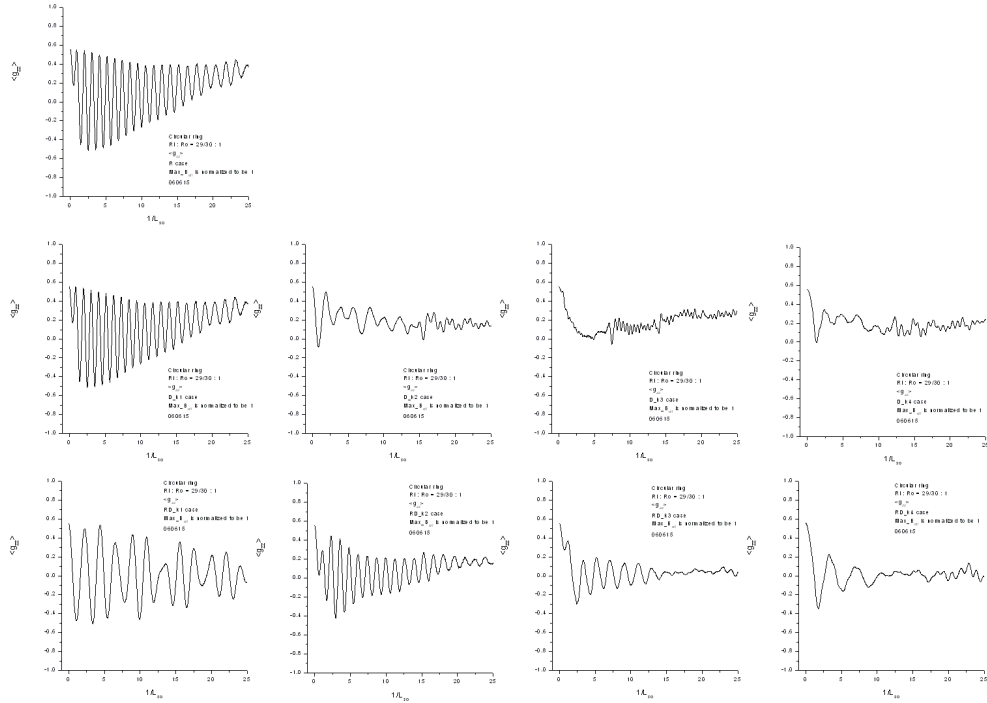


Figure 8.4. Spin conductance $\langle g_{zz} \rangle$ v.s. $1/L_{so}$ under the action of normalized B_{eff} in more narrow circular ring system.

pattern. The most interesting decay pattern is $D - k1$ case and $RD - k1$ case, in $D - k1$ case the decay pattern shows a very beautiful cone shape with almost the same period of oscillation, the theoretical prediction has been done by A.G. Mal'shukov et al. [67], and the simulation has been shown by C.H. Chang et al. [72], the special regular behavior exhibits great applicability in future. For the $RD - k1$ case, it shows a very special decay oscillation pattern. It seems to exhibit a tendency similar to the pattern of $D - k1$ (or $D - k4$) case, but with

an oscillation tendency attached in this decay pattern. In principle it shows a deep implication that if we vary the initial spinor input, we could obtain the very slowly decay pattern, or even create a never decay pattern (we should discuss this situation in below sections). Well! anyhow these various kinds of decay pattern response the various \mathbf{B}_{eff} configuration of different operation cases, see Fig. 7.1. I think that the reason is very obvious, but it implies that we could create various conductance pattern as possibly as we could by create various \mathbf{B}_{eff} configuration for the possible application in future.

Now let's focus on Fig. 8.3 and see what happened. At first glance we have a strong impression about the similarity and strong correlation between the $\langle g_{yy} \rangle$ of R , $D - k1$, $RD - k1$ cases and $\langle g_{xx} \rangle$ of R , $D - k1$, $RD - k1$ cases, Fig. 8.2. The reason is due to the equivalence between pure Rashba term effect and pure Dresselhouse linear term effect, we should give a detailed explanation for them in below section. We also find the similarity between R and $RD - k2$ cases, the phenomena also be exhibited in Fig. 8.2, the reason is due to the similarity of \mathbf{B}_{eff} configuration of R and $RD - k2$ cases, Fig. 7.1. Besides we also find an obvious difference between $\langle g_{yy} \rangle$ of $RD - k1$ case and $\langle g_{xx} \rangle$ of $RD - k1$ case, it implies that we can't ignore the effect of initial spinor input, and it also implies that someone deep correlation between operation system, operation case (i.e. the configuration of \mathbf{B}_{eff}), and initial spinor input, and so on. For other operation cases they show the similar decay pattern to that of Fig. 8.3.

Next let's see the pattern of Fig. 8.4. Well! it seems to exhibit a particular decay pattern of its own. At first we find the similarity between R and $D - k1$ cases, it seems to tell us that something *symmetry* implication between the circular ring operation system and R and $D - k1$ cases. And we find a very interesting phenomena that for R , $D - k1 \sim D - k4$ and $RD - k2$ cases, they exhibit a residue decay value, the final decay value $\langle g_{yy} \rangle$ seems not to approach to be zero. It seems to tell us that if the \mathbf{B}_{eff} configuration exhibits an *equal* distribution with respect to different \mathbf{k} , the residue character exhibited. And if the \mathbf{B}_{eff} configuration owns an un-equal distribution, like $RD - k1$, $RD - k3$ and $RD - k4$ cases, the conductance should approach zero as $1/L_{so}$ goes by. Of course this suggestion is happened under the circular ring system and the initial spinor in z direction, we don't see the tendency for the initial spinor input in x and y direction, see Figures 8.2 and 8.3.

Of course, for these all patterns shown in Figures 8.2, 8.3 and 8.4, the universal conductance oscillation phenomenon is very obvious, it can be realized easily by the point of view of the technique of the semiclassical approach analysis.

Now let us look at what happened as we vary the width of the circular ring. The more details about the effect of the size and the width of the circular ring related to the oscillation pattern should be described in Chapter 10. Figures 8.5, 8.6 and 8.7 show the conductance pattern in circular ring which with the same operation conditions except for $R_i = 9/10$ and $R_o = 1$. In Fig. 8.5 we find almost the same decay feature to the corresponding case of the wider circular ring

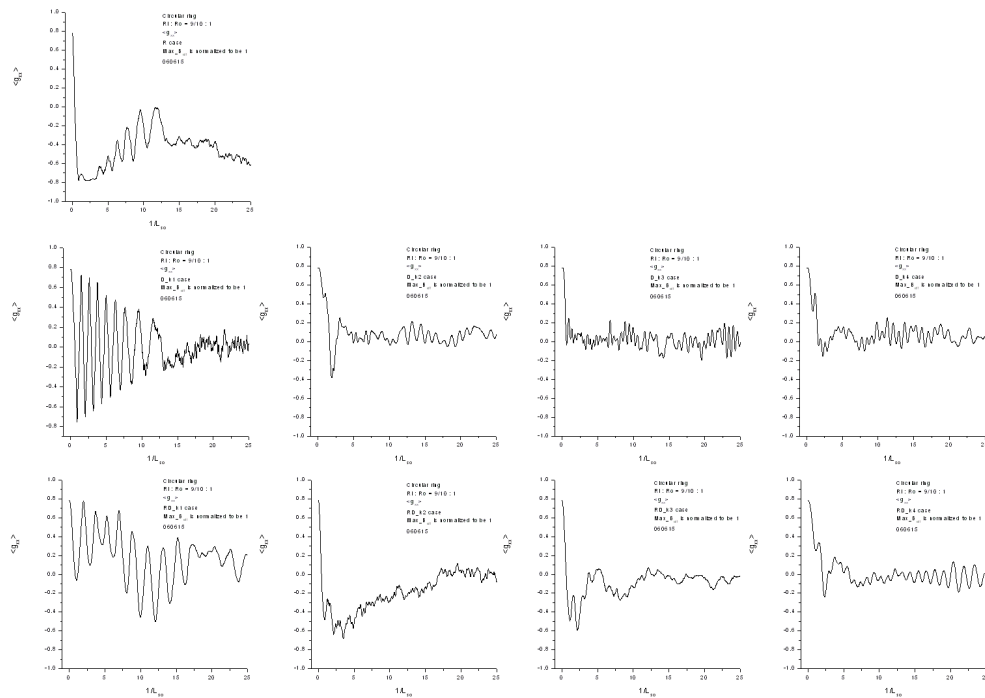


Figure 8.5. Spin conductance $\langle g_{xx} \rangle$ v.s. $1/L_{SO}$ under the action of normalized B_{eff} in less narrow circular ring system.

operation system, see Fig. 8.2, the main differences are the conductance is larger and the conductance oscillation is faster and more radical, so they show indented oscillation feature. These features reflect that as we increase the width of the ring, more electrons can go through the outlet after they orbit several times of the ring, and since the width is increased, the oscillation behaviors of the trajectories of the electrons exhibit more radical aspects. Well! we also note a very interesting aspect

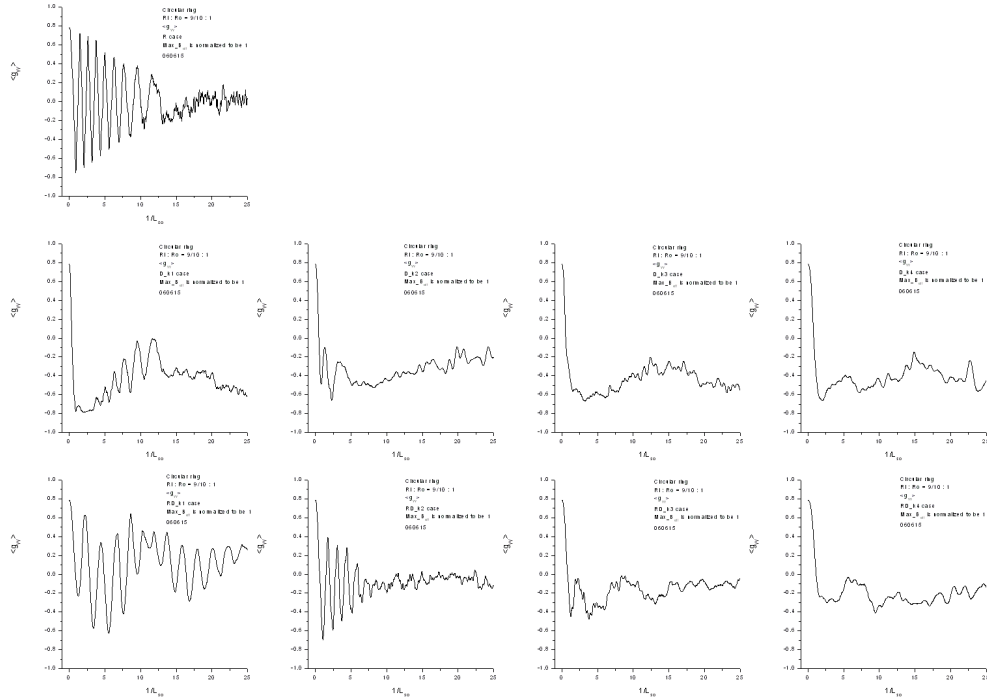


Figure 8.6. Spin conductance $\langle g_{yy} \rangle$ v.s. $1/L_{so}$ under the action of normalized B_{eff} in less narrow circular ring system.

in R case, the conductance $\langle g_{xx} \rangle$ exhibits arc-like shape decrement as $1/L_{so}$ goes by.

Next we find that Fig. 8.6 exhibits the same tendency to Fig. 8.3. The same phenomenon also happens between Fig. 8.7 and Fig. 8.4. But wait a moment, from Figures 8.3, 8.4 and Figures 8.6, 8.7, and even from Figures 8.2, 8.5, we find the $RD - k2$ case seems to show a diminutive conduction pattern compared with R case. From the \mathbf{B}_{eff} configuration we could realize the phenomenon, since they

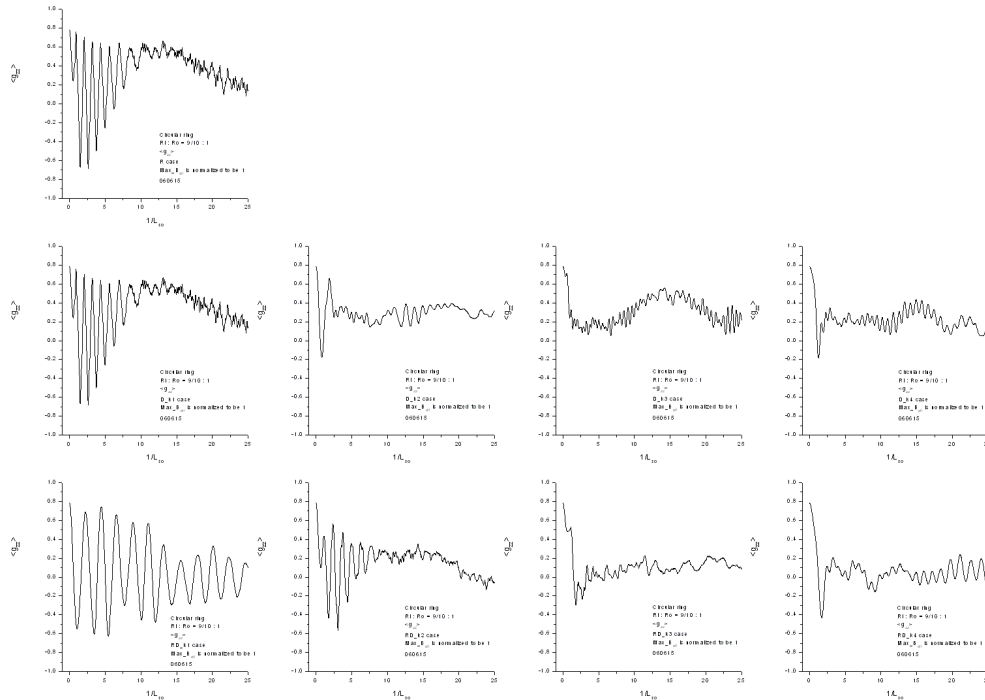


Figure 8.7. Spin conductance $\langle g_{zz} \rangle$ v.s. $1/L_{so}$ under the action of normalized B_{eff} in less narrow circular ring system.

exhibit the similar \mathbf{B}_{eff} configuration, see Fig. 7.1, but I think it is interesting to theorize these phenomena.

Now let us turn our focus to another operation system, Sinai billiard, to see what happened about their conductance decay patterns. Here we explore two different sizes of Sinai billiard, in Figures 8.8, 8.9, 8.10, and 8.11, 8.12, 8.13, the $R_i = 9/10$ and $R_o = 1$, the widths of both inlet and outlet are 0.2, and in Figures 8.14, 8.15, 8.16 and 8.17, 8.18, 8.19, the $R_i = 8/10$ and $R_o = 1$, the widths of

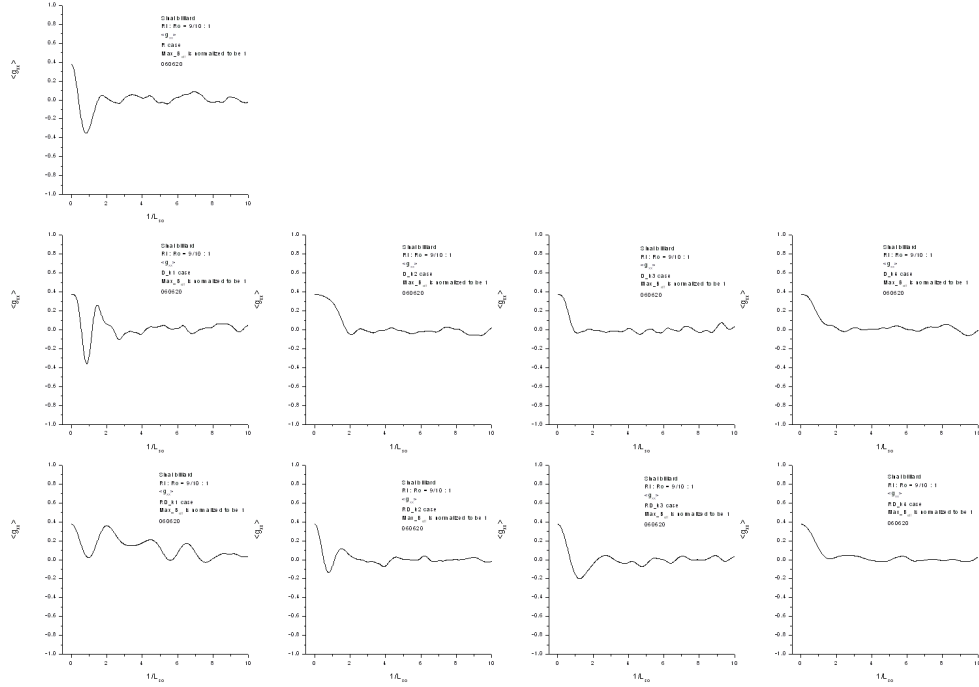


Figure 8.8. Spin conductance $\langle g_{xx} \rangle$ v.s. $1/L_{SO}$ under the action of normalized B_{eff} in more narrow Sinai billiard system.

both inlet and outlet are 0.2. Compare Fig. 8.8 with Fig. 8.2, Fig. 8.9 with Fig. 8.3, Fig. 8.10 with Fig. 8.4, Fig. 8.14 with Fig. 8.5, Fig. 8.15 with Fig. 8.6, Fig. 8.16 with Fig. 8.7 each other, we find the almost the same tendency between these paired patterns. The most striking aspect is in the $D - k2$ case, we observe the appearance of most slow decay pattern. Reference to the \mathbf{B}_{eff} configuration, see Fig. 7.1 we could understand the aspect, the reason is due to the \mathbf{B}_{eff} disappeared in some region of \mathbf{k} , so the spin in these region doesn't relax.

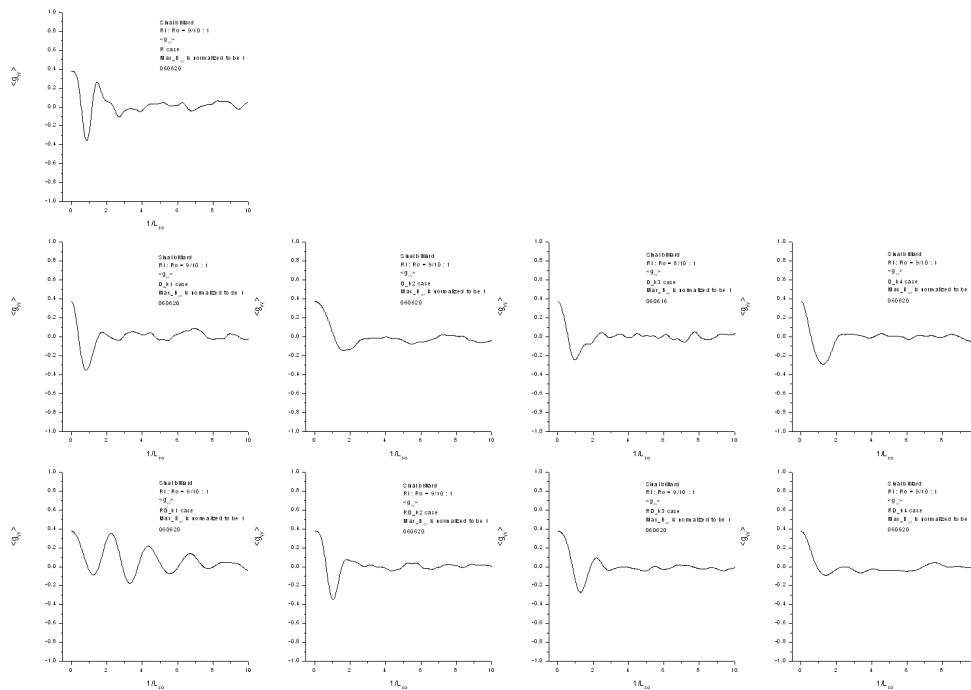


Figure 8.9. Spin conductance $\langle g_{yy} \rangle$ v.s. $1/L_{SO}$ under the action of normalized B_{eff} in more narrow Sinai billiard system.

And we also find the particular decay aspects in R , $D - k1$ and $RD - k1$ cases, they exhibit the most chiseled decay pattern. For R and $D - k1$ cases, they also show the correlation implication between their own patterns, the reason is due to the equivalence between R and $D - k1$ cases. For $D - k1$ case, the special \mathbf{B}_{eff} configuration causes the particular decay pattern. We will discuss that the special \mathbf{B}_{eff} configuration could create a never decay conductance aspect in the section below. Figures 8.11, 8.12, 8.13 and 8.17, 8.18, 8.19 show the sum up aspects of the

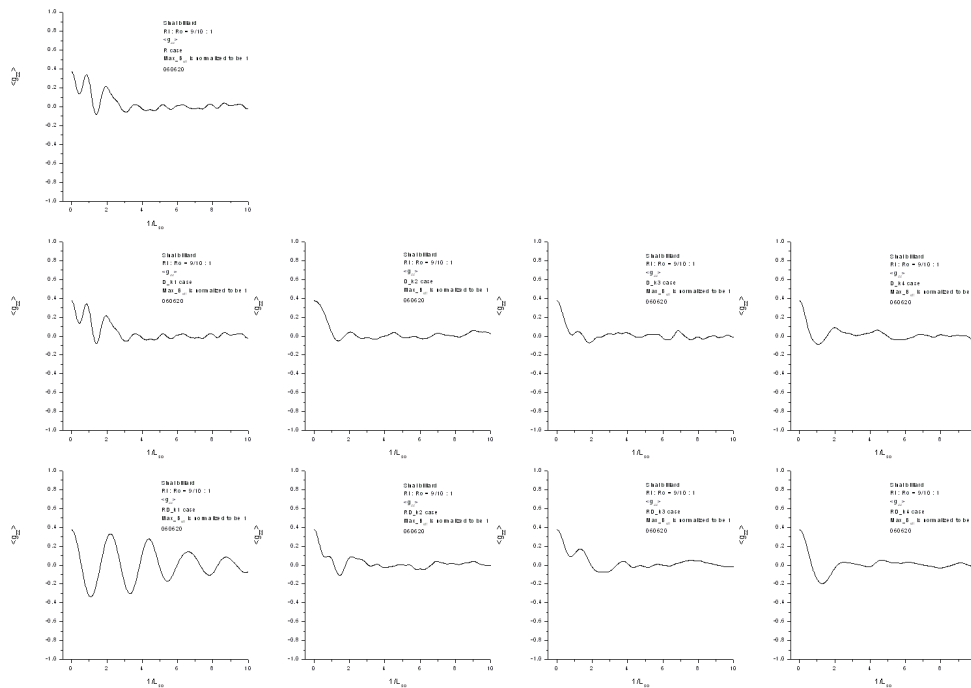


Figure 8.10. Spin conductance $\langle g_{zz} \rangle$ v.s. $1/L_{so}$ under the action of normalized B_{eff} in more narrow Sinai billiard system.

conductance patterns for each different initial spinor input cases of the different size of Sinai billiard. We could clearly see the special aspects for the $D - k2$ case (light green line), it exhibits the most slow decay aspects, and the most clean up decay pattern in R (black line), $D - k1$ (red line) and $RD - k1$ (purple line) cases. Finally we observe that in Sinai billiard system, as $1/L_{so}$ goes by, the conductance decays to zero for all operation cases. It seems to imply that the particular aspects is due to the operation system is *chaotic* system, we could see that the conductance

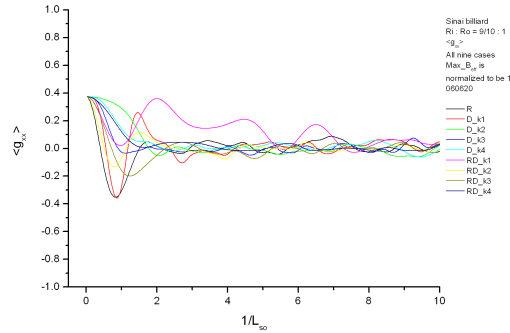


Figure 8.11. Sum up of spin conductance $\langle g_{xx} \rangle$ v.s. $1/L_{so}$ under the action of nine kinds of normalized B_{eff} in more narrow Sinai billiard system.

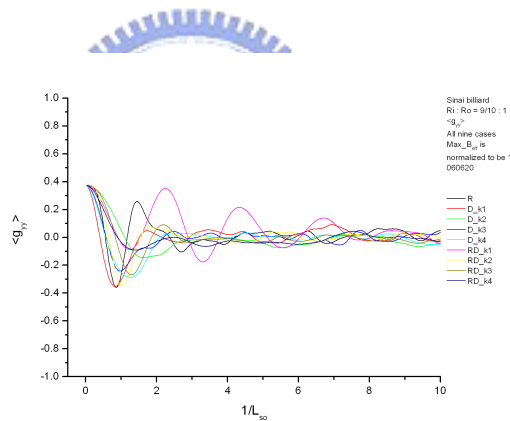


Figure 8.12. Sum up of spin conductance $\langle g_{yy} \rangle$ v.s. $1/L_{so}$ under the action of nine kinds of normalized B_{eff} in more narrow Sinai billiard system.

decay doesn't always approach zero for various operation cases in circular ring system, since it belongs to *regular* system. We also find the same appearance for spin relaxation simulation in last chapter.

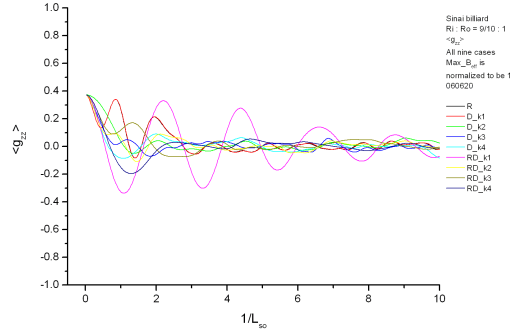


Figure 8.13. Sum up of spin conductance $\langle g_{zz} \rangle$ v.s. $1/L_{so}$ under the action of nine kinds of normalized B_{eff} in more narrow Sinai billiard system.

8.2. Some Aspects of Conductance Decay Patterns (B_{eff} Configuration in Real Material)

In last section we talk about the decay patterns under the action of normalized B_{eff} configuration, that is we treat the maximum of B_{eff} as 1. The purpose of such treatment is to try to offer the information about the effect of B_{eff} configuration related to the decay pattern. Well! as the statement of last section we found out many interesting phenomena. Here we want to see what happened about the conductance decay pattern under the action of B_{eff} configuration in real material (although it is also deduced from theoretical calculation). Fig. 7.1 shows the B_{eff} configuration in real material, the larger and bolder arrow means the larger (stronger) B_{eff} , so under different standpoint of these B_{eff} (i.e. not to be normalized aspect) the decay patterns may be reflected something different and interesting aspects.

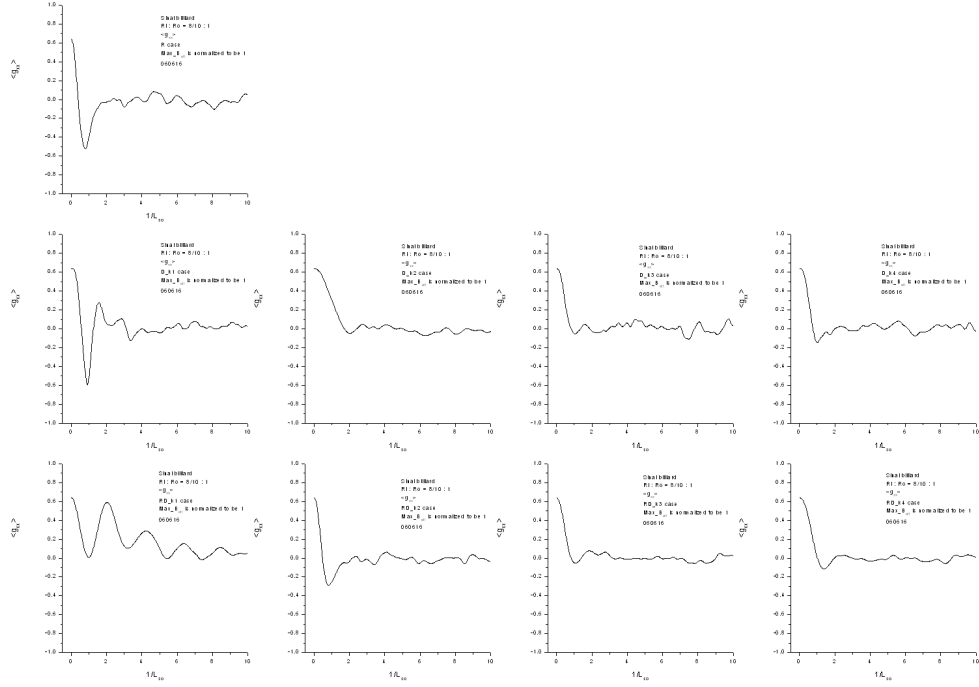


Figure 8.14. Spin conductance $\langle g_{xx} \rangle$ v.s. $1/L_{so}$ under the action of normalized B_{eff} in less narrow Sinai billiard system.

Here we don't intend to give an overview about the effect of \mathbf{B}_{eff} configuration in real material, we just pick some representative operation cases to indicate the effect of \mathbf{B}_{eff} configuration in real material. Fig. 8.20 indicates the obvious difference between the normalized \mathbf{B}_{eff} configuration and \mathbf{B}_{eff} configuration in real material for $D - k2$ case in circular ring system with $R_i = 29/30$, $R_o = 1$ and widths of both inlet and outlet $w = 0.1$. As Fig. 7.1 shown, in $D - k2$ case the maximum of \mathbf{B}_{eff} is smaller than one of \mathbf{B}_{eff} in R case (which the magnitude of

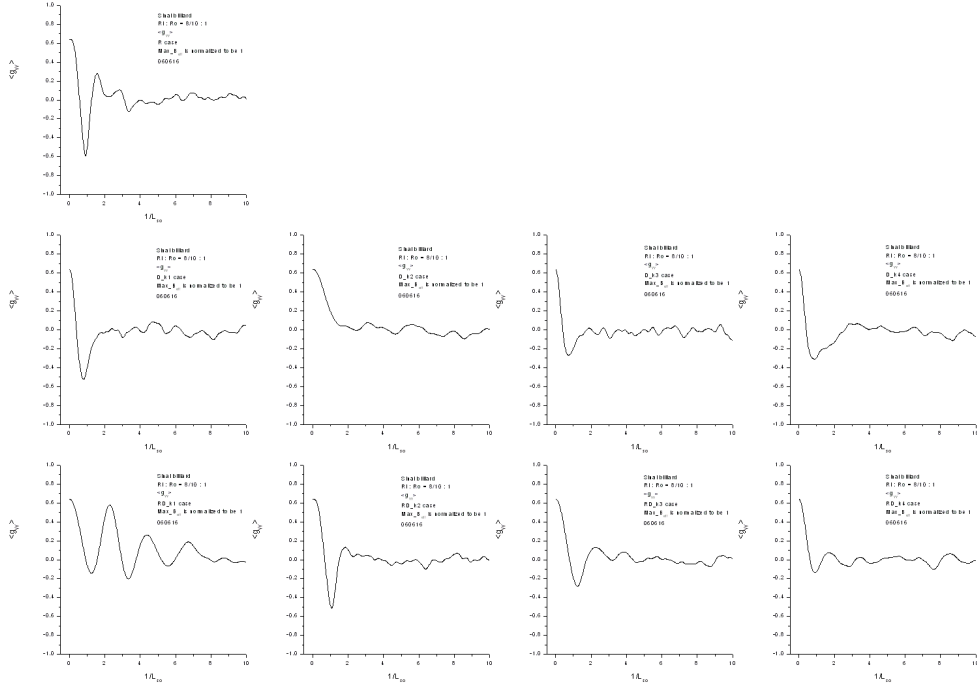


Figure 8.15. Spin conductance $\langle g_{yy} \rangle$ v.s. $1/L_{so}$ under the action of normalized B_{eff} in less narrow Sinai billiard system.

\mathbf{B}_{eff} is setted to be 1), so we obtain a slow down decay pattern, i.e. we obtain a stretched-out and shifted toward right decay pattern (red line) as comparison with the decay pattern of normalized \mathbf{B}_{eff} configuration (black line). Fig. 8.21 shows a reversed trend, since we find the maximum of \mathbf{B}_{eff} in $RD - k4$ case is much larger than the one in R case, that is meant that the effect of \mathbf{B}_{eff} is much stronger in \mathbf{B}_{eff} configuration in real material. So the decay pattern exhibits contracted and

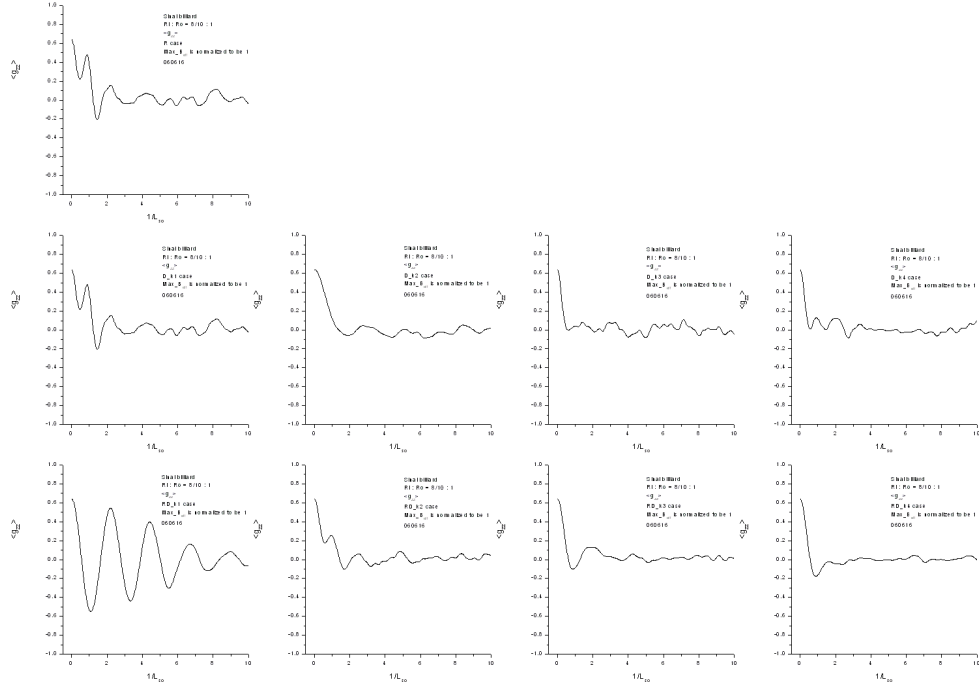


Figure 8.16. Spin conductance $\langle g_{zz} \rangle$ v.s. $1/L_{so}$ under the action of normalized \mathbf{B}_{eff} in less narrow Sinai billiard system.

shifted toward left decay aspects (red line) compared with the decay pattern of normalized \mathbf{B}_{eff} configuration (black line).

The same trend happened in Figures 8.22 and 8.23, for them we proceed the simulation in Sinai billiard with $R_i = 8/10$, $R_o = 1$ and widths of both inlet and outlet $w = 0.2$ under $D - k1$ and $RD - k4$ cases. For $D - k1$ case we find out the smaller magnitude of \mathbf{B}_{eff} than the one of \mathbf{B}_{eff} in R case from Fig. 7.1, so we predict to obtain a slow down decay pattern as Fig. 8.22 shown. Note that for

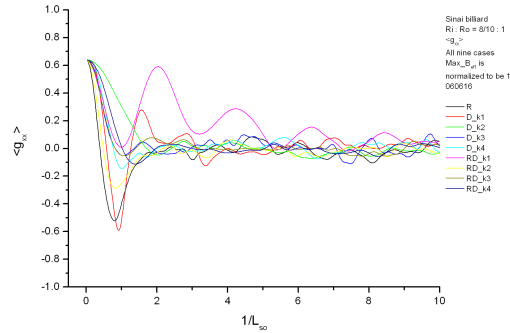


Figure 8.17. Sum up of spin conductance $\langle g_{xx} \rangle$ v.s. $1/L_{so}$ under the action of nine kinds of normalized B_{eff} in less narrow Sinai billiard system.

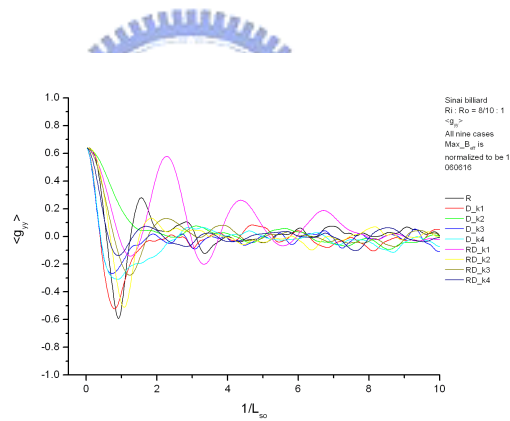


Figure 8.18. Sum up of spin conductance $\langle g_{yy} \rangle$ v.s. $1/L_{so}$ under the action of nine kinds of normalized B_{eff} in less narrow Sinai billiard system.

these two paired cases, the initial conductances don't vary, the reason is obvious since the variation of the magnitude of \mathbf{B}_{eff} doesn't affect the number of electrons which leave off the outlet, so we get the same conductance initial values.

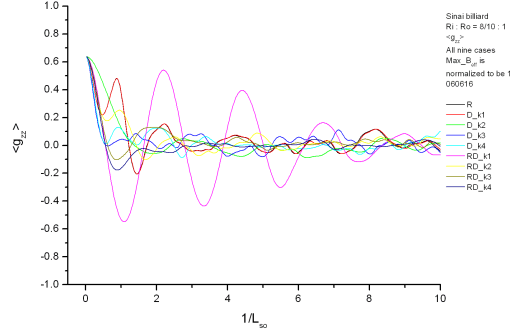


Figure 8.19. Sum up of spin conductance $\langle g_{zz} \rangle$ v.s. $1/L_{so}$ under the action of nine kinds of normalized B_{eff} in less narrow Sinai billiard system.

8.3. Equivalence between R and $D - k1$ Modified Cases

Now let us talk about the very interesting topic, the equivalence between R case and $D - k1$ modified case (i.e. we just consider the linear term of Dresselhaus Hamiltonian).

See Fig. 8.24, we find out the result

$$(8.1) \quad S_{R,x_y_z} P_{n,R,x_y_z} = S_{D,y_x_z} P_{n,D,y_x_z} = S_{D,x_y_z} P_{n,D,x_y_z}$$

where we set P_{n,R,x_y_z} as the initial spinor for Rashba term case (R case)

$$(8.2) \quad P_{n,R,x_y_z} = \begin{pmatrix} \cos \frac{\theta}{2} \\ \sin \frac{\theta}{2} e^{i\phi} \end{pmatrix},$$

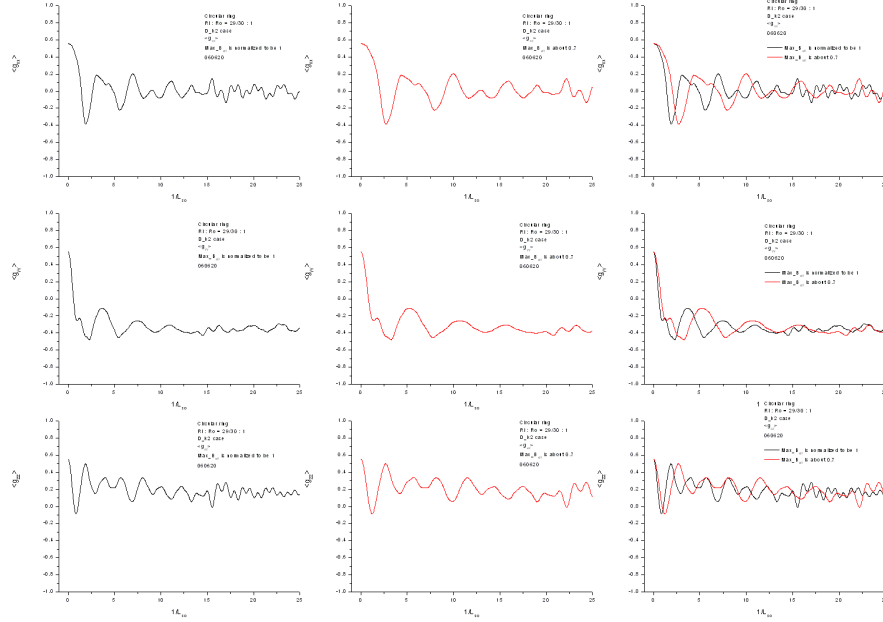


Figure 8.20. Comparison between the normalized \mathbf{B}_{eff} configuration and \mathbf{B}_{eff} configuration in real material for $D - k2$ case in circular ring system.

and the corresponding P_{n,D,x_y_z} as the initial spinor for Dresselhouse linear term case ($D - k1$ modified case)

$$(8.3) \quad P_{n,D,x_y_z} = \begin{pmatrix} \cos \frac{1}{2}(\pi - \theta) \\ \sin \frac{1}{2}(\pi - \theta) e^{i(\frac{\pi}{2} - \phi)} \end{pmatrix}.$$

S_{R,x_y_z} is the equivalent rotation operator for someone specific electron travels half-tour of circular ring under the action of R case viewed in x_y_z coordinates

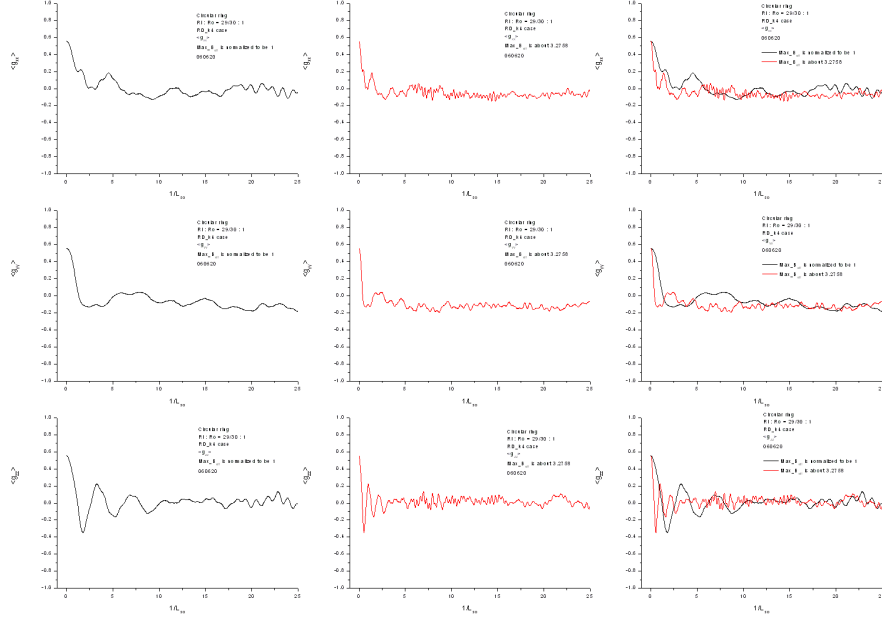


Figure 8.21. Comparison between the normalized \mathbf{B}_{eff} configuration and \mathbf{B}_{eff} configuration in real material for $RD - k4$ case in circular ring system.

system, and S_{D,x_y_z} is the equivalent rotation operator for someone specific electron travels half-tour of circular ring under the action of $D - k1$ modified case viewed in x_y_z coordinates system. And S_{D,y_x_z} is the equivalent rotation operator for someone specific electron travels half-tour of circular ring under the action of $D - k1$ modified case viewed in y_x_z coordinates system, here we find that S_{R,x_y_z} is the same as S_{D,y_x_z} , reference Eq. 3.30. And P_{n,D,y_x_z} is the initial spinor viewed in y_x_z coordinates system, it has the same form as P_{n,D,x_y_z} which viewed in x_y_z coordinates system.

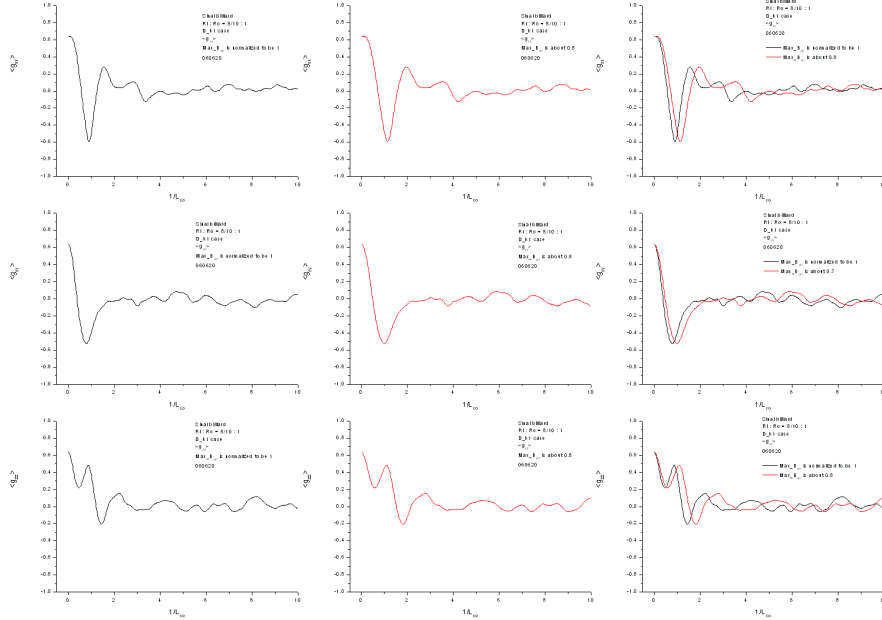


Figure 8.22. Comparison between the normalized \mathbf{B}_{eff} configuration and \mathbf{B}_{eff} configuration in real material for $D - k1$ case in Sinai billiard.

Then let us apply the above result to give two examples for illustration. See Fig. 8.25, the first example we proceeded is the circular ring system with $R_i = 29/30$, $R_o = 1$ and widths of both inlet and outlet $w = 0.1$ in R case, the initial spinor input is

$$(8.4) \quad P_{n,R,x_y_z} = \left(\frac{\cos \frac{4.7\pi/12}{2}}{\sin \frac{4.7\pi/12}{2} e^{i3.83\pi/12}} \right),$$

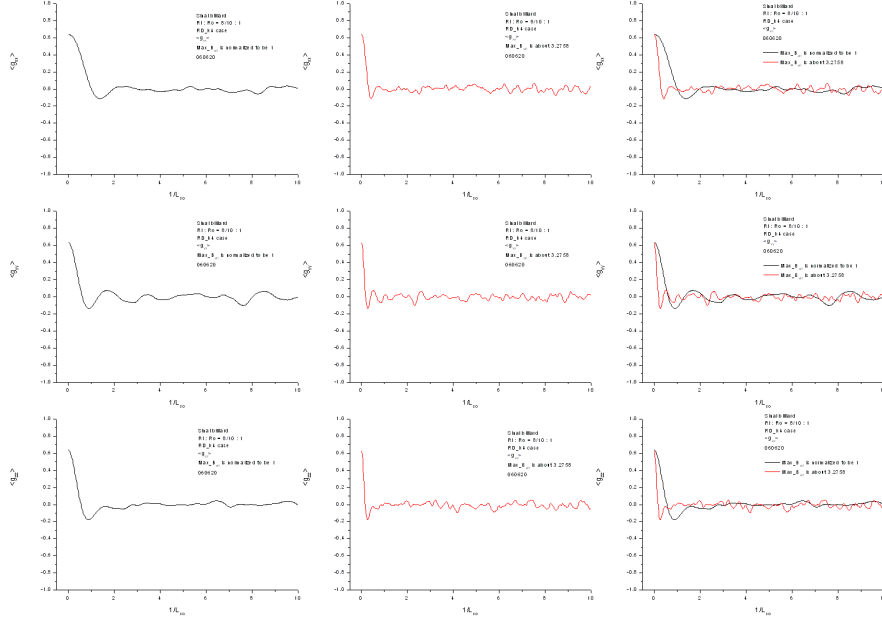


Figure 8.23. Comparison between the normalized \mathbf{B}_{eff} configuration and \mathbf{B}_{eff} configuration in real material for $RD - k4$ case in Sinai billiard.

and from the above discussion we should obtain the corresponding initial spinor input in $D - k1$ modified case as

$$(8.5) \quad P_{n,D,x-y-z} = \left(\frac{\cos \frac{1}{2} (\pi - 4.7\pi/12)}{\sin \frac{1}{2} (\pi - 4.7\pi/12) e^{i(\frac{\pi}{2} - 3.83\pi/12)}} \right) = \left(\frac{\cos (7.3\pi/12/2)}{\sin (7.3\pi/12/2) e^{i2.17\pi/12}} \right).$$

And then by applying Eq. 3.30 and look at Fig. 8.24, we find that

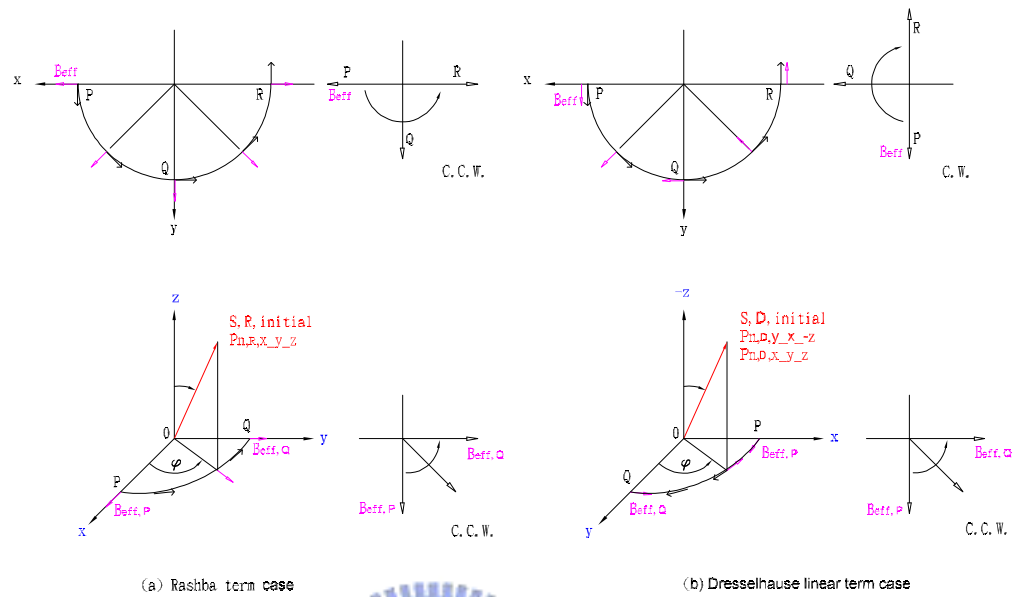


Figure 8.24. Equivalence between R and $D - k1$ modified cases.



$$(8.6) \quad \langle g_{nx} \rangle = \langle g_{my} \rangle, \langle g_{ny} \rangle = \langle g_{mx} \rangle \text{ and } \langle g_{nz} \rangle = -\langle g_{mz} \rangle,$$

they coincide with the correlation relation which coordinates x (in R case) corresponds to coordinates y (in $D - k1$ modified case), coordinates y (in R case) corresponds to coordinates x (in $D - k1$ modified case), and coordinates z (in R case) corresponds to coordinates $-z$ (in $D - k1$ modified case).

Finally let us see a very interesting thing that extends our understanding about spin transport. Fig. 8.26 shows the spin decay pattern for Sinai billiard with $R_i = 9/10$, $R_o = 1$ and widths of both inlet and outlet $w = 0.2$, we find that the

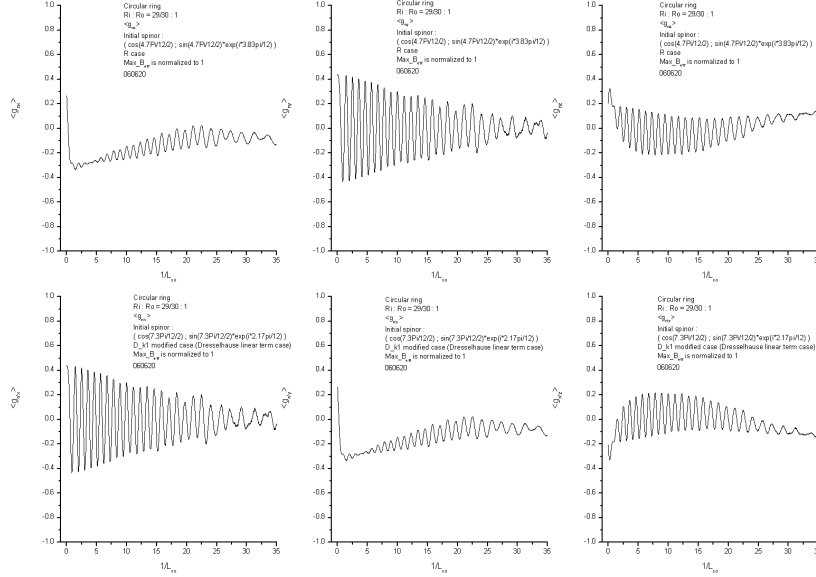


Figure 8.25. Example of equivalence between R and $D - k_1$ modified cases in circular ring system.

correspondence relationship is also exactly appeared, i.e. we get the correct relationship $\langle g_{nx} \rangle = \langle g_{my} \rangle$, $\langle g_{ny} \rangle = \langle g_{mx} \rangle$ and $\langle g_{nz} \rangle = -\langle g_{mz} \rangle$. Well! this operation system is chaotic system, in principle we can't get the equivalent rotation operators, that it S_{R,x_y_z} , S_{D,y_x_z} and S_{D,x_y_z} as Eq. 3.30 shown. In principle we just could obtain the approximate equality relationship between $\langle g_{nx} \rangle$, $\langle g_{ny} \rangle$, $\langle g_{nz} \rangle$ and $\langle g_{my} \rangle$, $\langle g_{mx} \rangle$, $-\langle g_{mz} \rangle$, but here we get the exact equality relationship! This phenomenon means that S_{R,x_y_z} , S_{D,y_x_z} and S_{D,x_y_z} are the rotation operators for each individual segments of electrons' orbitals. Reference Fig. 8.24 we could assert such guess is correct, since for someone segment the $\mathbf{B}_{eff,R}$ for Rashba term case in coordinates x_y_z is the same to $\mathbf{B}_{eff,D}$ for Dresselhaus linear term

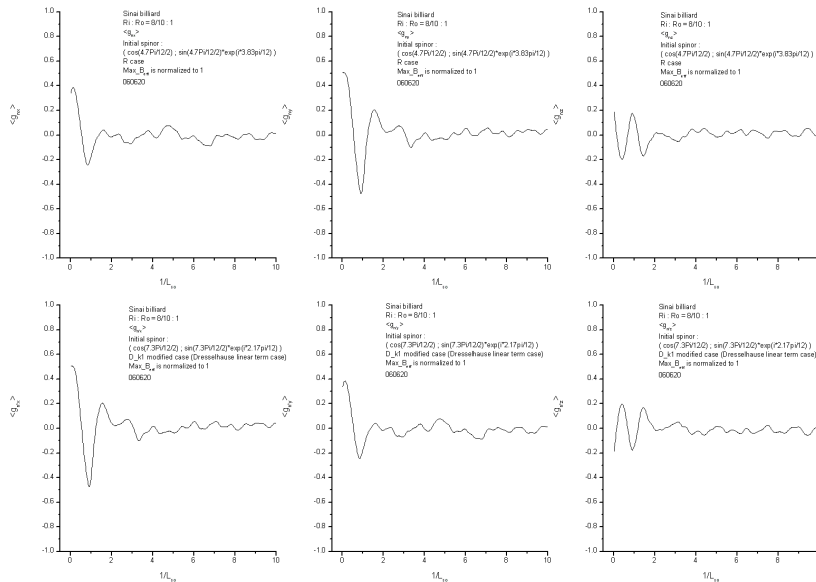


Figure 8.26. Example of equivalence between R and $D - k1$ modified cases in Sinai billiard system.

case in coordinates y_x_z , so we could get the exactly same conductance decay patterns as we remember the corresponding coordinates replacement relationship.

8.4. Slow Down Conductance Decay Pattern Case

In this section we turn slightly our viewpoint of academic research to the viewpoint of application. By look at the \mathbf{B}_{eff} configuration in Fig. 7.1 we find that some configurations are more special, for example R , $D - k1$, $RD - k1$, $RD - k4$ and so on. (In fact all \mathbf{B}_{eff} configurations are special.) If we could create some-one special man-made initial spinor input which interacts with these special \mathbf{B}_{eff}

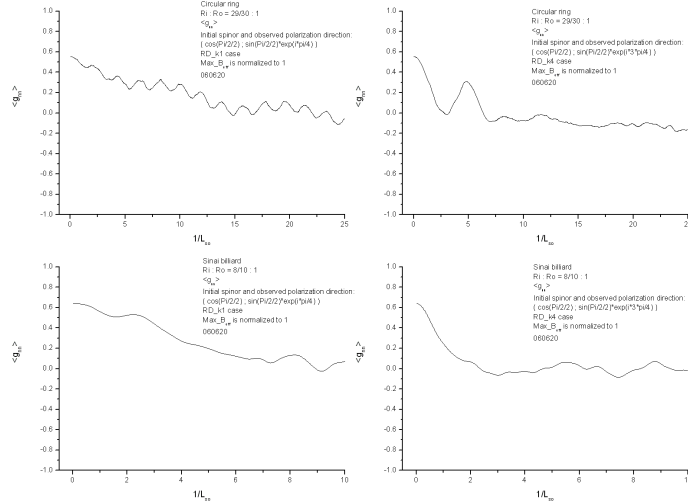


Figure 8.27. Example of slow down conductance decay pattern case in $RD - k1$ and $RD - k4$ cases in circular ring system and Sinai billiard.

configurations, in principle we could create many amazed decay patterns for application. For example if we could create someone time vary spinor input which corresponds to the variation of \mathbf{B}_{eff} in someone form for each traveling trajectories, in principle we could get any kinds of decay patterns (even though never decay pattern, we would talk about the interesting case in next section) as possibly as we like. Here we present two funny cases which they exhibit slow down decay patterns. Fig. 8.27 shows the circular ring system with $R_i = 29/30$, $R_o = 1$ and widths of both inlet and outlet $w = 0.1$, proceeded in $RD - k1$ case under the initial spinor input $(\cos(\pi/2/2); \sin(\pi/2/2) \exp(i\pi/4))$ and in $RD - k4$ case under the initial spinor input $(\cos(\pi/2/2); \sin(\pi/2/2) \exp(i3\pi/4))$. What the reasons for such treatment is to offer the corresponding initial spinor input to the pattern of

\mathbf{B}_{eff} configuration and the maximum of $|\mathbf{B}_{eff}|$. We find the appearance of slow down decay pattern compared with Figures 8.2, 8.3 and 8.4. We also proceed the simulation in Sinai billiard with $R_i = 9/10$, $R_o = 1$ and widths of both inlet and outlet $w = 0.2$, as the proceeding listed above, we also find out the slow down decay patterns compared with Figures 8.8, 8.9 and 8.10.

8.5. Never Decay Pattern Case

Finally we talk about a very interesting and ideal case. Go back to the content of Section *Rashba and Dresselhouse SOI Effect*, we find the Hamiltonian is

$$(8.7) \quad H_{so} = [\alpha k_y + \eta k_x (k_y^2 - \langle k_z^2 \rangle)] \sigma_x + [-\alpha k_x + \eta k_y (\langle k_z^2 \rangle - k_x^2)] \sigma_y$$

and the corresponding \mathbf{B}_{eff} is

$$(8.8) \quad B_x = \frac{2m}{e\hbar} [\alpha k_y + \eta k_x (k_y^2 - \langle k_z^2 \rangle)]$$

$$(8.9) \quad B_y = \frac{2m}{e\hbar} [-\alpha k_x + \eta k_y (\langle k_z^2 \rangle - k_x^2)]$$

$$(8.10) \quad B_z = 0$$

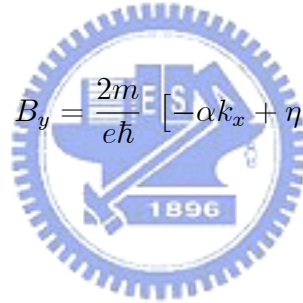
If we neglect the k^3 term in the Hamiltonian, we obtain

$$(8.11) \quad H_{so} = [\alpha k_y + \eta k_x (-\langle k_z^2 \rangle)] \sigma_x + [-\alpha k_x + \eta k_y \langle k_z^2 \rangle] \sigma_y$$

that is we get the corresponding \mathbf{B}_{eff} as

$$(8.12) \quad B_x = \frac{2m}{e\hbar} [\alpha k_y + \eta k_x (-\langle k_z^2 \rangle)]$$

$$(8.13) \quad B_y = \frac{2m}{e\hbar} [-\alpha k_x + \eta k_y \langle k_z^2 \rangle]$$



$$(8.14) \quad B_z = 0.$$

And then if we advancedly assume that

$$(8.15) \quad \alpha = \eta \langle k_z^2 \rangle,$$

we get that

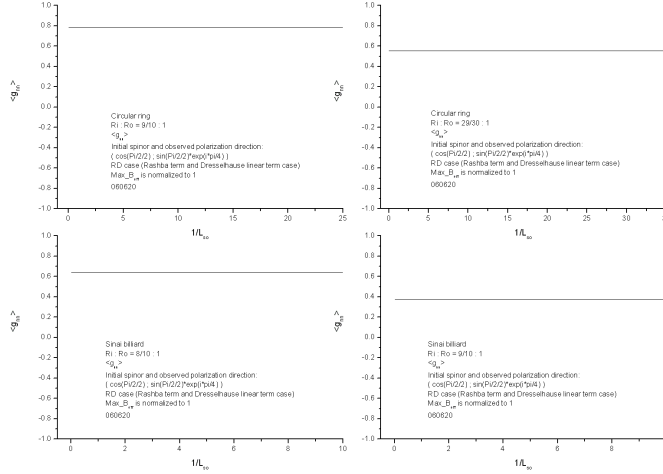


Figure 8.28. Examples of never decay spin conductance pattern case.



$$(8.16) \quad B_x = B_y, B_z = 0.$$

This result means that the \mathbf{B}_{eff} is always lay in the same (or opposite) direction of $k = \left\langle \frac{1}{\sqrt{2}}, \frac{1}{\sqrt{2}}, 0 \right\rangle$, regardless of the directions of each segments of electron traveling trajectories. This peculiar aspect give us a hint, we project the initial spinor input parallel (or anti-parallel) to this direction, we should obtain a response of never decay pattern. This is true, Fig. 8.28 tells us the wonderful results, here we proceed the simulation in circular ring and Sinai billiard system, with initial spinor as

$$(8.17) \quad P_0 = \left(\frac{\cos(\pi/2/2)}{\sin(\pi/2/2) \exp(i\pi/4)} \right),$$

and with the final polarization detection parallel to this initial spinor. This result indicates a greatly possible ability of application, that is if we could create something \mathbf{B}_{eff} configuration like this, we could well control the spin evolution behavior in future.



CHAPTER 9

Spin Waveform Editor (SWE)

Well! let us propose a funny device, *Spin Waveform Editor (SWE)* to end up this thesis. For narrow width circular ring system under the action of Rashba term case (R case), the spin conductance was derived analytically as [67][74].

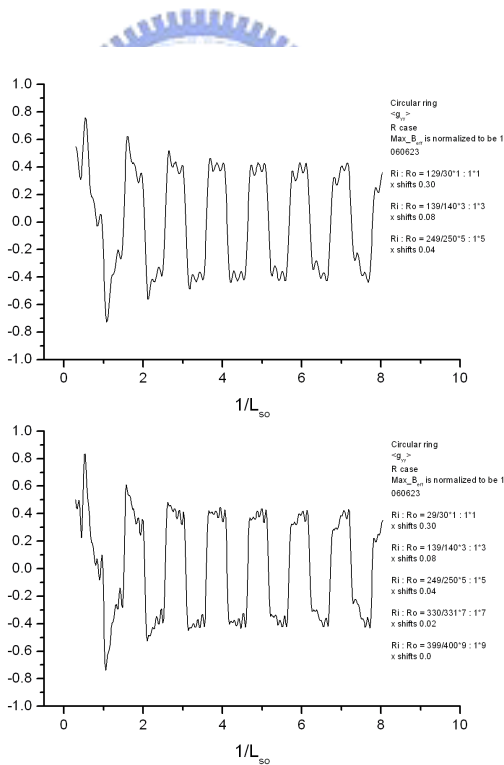


Figure 9.1. Square waveform patterns.

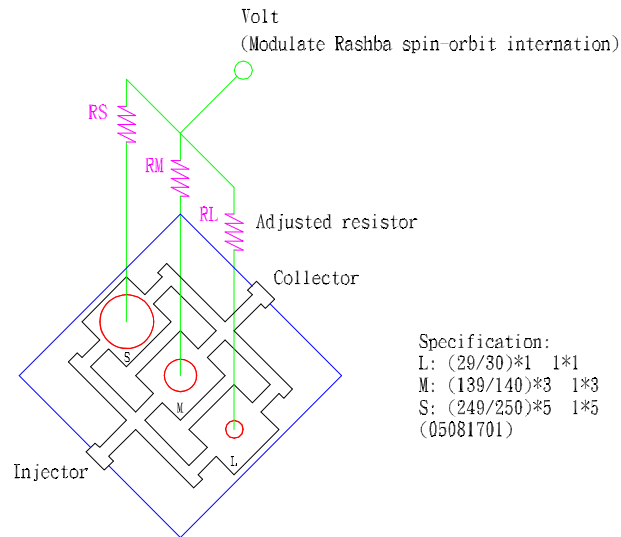


Figure 9.2. Design of Spin Waveform Editor (SWE) device 1.

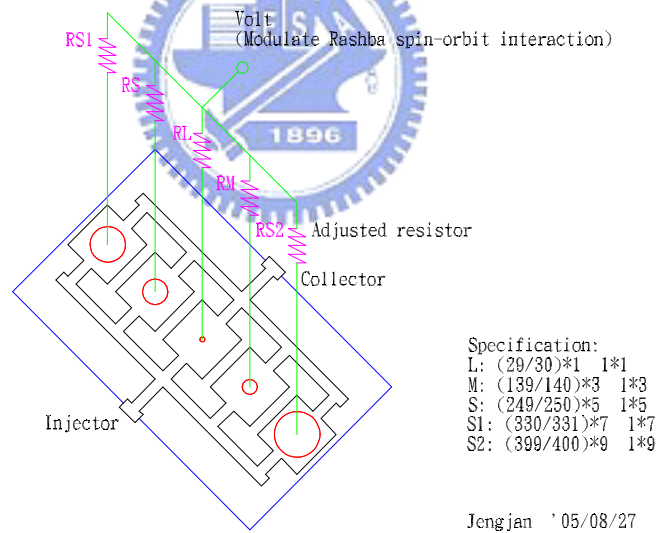



Figure 9.3. Design of Spin Waveform Editor (SWE) device 2.

$$(9.1) \quad \langle g_{yy} \rangle = \frac{-g_0 \kappa^2 \cos \left[\pi \sqrt{1 + 4(d/L_{so})^2} \right]}{\kappa^2 + 4 \sin^2 \left[\pi \sqrt{1 + 4(d/L_{so})^2} \right]}$$

(here we just present conductance $\langle g_{yy} \rangle$ to give an example to be as an illustration) where g_0 is the spin independent conductance, $d = \sqrt{(R_i^2 + R_o^2)}/2$ is the averaged radius, $\kappa = \sqrt{2T_w/\tau}$ is determined by the mean escape time τ and the average duration T_w for one winding. We find that g_0 could be determined by Equations 6.27, 6.28 and 6.29 as represented in Section *Spin Conductance* of Chapter 6, and we note that as we vary the width of the ring and the averaged radius d , we could control the magnitude of $\langle g_{yy} \rangle$ and the oscillation period of $\langle g_{yy} \rangle$, this aspect give us a hint to apply Fourier series to make any shape of waveform output. That's why we call such device as *Spin Waveform Editor (SWE)*. Here we just present an example, we try to make a square waveform output. The Fourier series for square wave is



$$\begin{aligned}
 (9.2) \quad F_N(x) &= \sum_{n=1}^N \frac{1}{2n-1} \sin[(2n-1)x] \\
 &= \frac{1}{1} \sin(x) + \frac{1}{3} \sin(3x) + \frac{1}{5} \sin(5x) + \dots
 \end{aligned}$$

by adjust the width of the ring and the averaged radius d , we could adjust the magnitude of the coefficients and the arguments for each terms, and then by combining several circular ring systems and adequately shift these conductance patterns relatively each other (by applying these *adjusted resistors* shown in Figures 9.2 and 9.3) we obtain the desired square waveform pattern as shown in Fig. 9.1. And the corresponding devices design is shown in Figures 9.2 and 9.3. It's a

good idea to apply this device in practical industrial usage and instruction tool in future.



Part 3

Conclusion and Outlook



CHAPTER 10

Conclusion and Outlook

Well! it's so excited to touch the wonderful topics *Spintronics*, *Spin Relaxation* and *Spin Transport* which try to reveal the mechanism and details of the interaction between spin and micron (or submicron) structure. There are still many topics and details worth and waiting for researching advancedly related to the contents of this thesis, but here we just indicate three representative key points to be as the conclusion and outlook of this thesis.

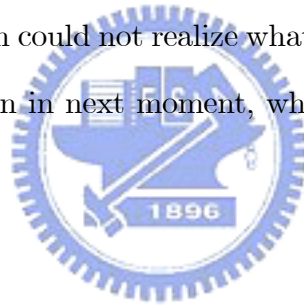
The first point is the effectiveness and advantage of the usage of the semiclassical approach. It is above suspicion about the advantage of the application of semiclassical approach, the semiclassical approach offers an intuitive viewpoint and convenient handling about the behavior of submicron structure action, but I think that the behavior of the action of submicron structure (e.g. spin relaxation of electrons in real material, etc.) is so subtle and complicated, the questions of the effectiveness of such semiclassical treatment are raised. The connection and/or correlation between classical mechanics viewpoint and quantum mechanics viewpoint still waiting for exploring more advancedly.

The second point is the plenty aspects about the topics *spin relaxation* and *spin transport* and so on. As the contents of this thesis we found that there are so many

factors which could affect the spin evolution of the traveling electrons. Well! such aspects offer a so wonderful and plenty region to explore them more detailedly and completely. I think there are many magic and unexpected unknowns will be appeared as we touch such topics more advancedly. Basically speaking the reason is due to the *spin* is so novel to our intuition and realization. So it is well above suspicion the complexity of interaction between spin and environment. Finally let us turn our focus from academic viewpoint to the point of view of application to end up the thesis.

The last point about the conclusion and outlook of this thesis is the information about the control the spin offered from the thesis. *Spintronics* is so fascinating and with great application potential in next generation electronic industry, whether or not the success in application of spintronics maybe determine whether the improvement of the civilness of mankind in future. I feel a little suspicious and cheerful about the application potential in terms of the approach of *spin control* from the research of the thesis. Let us give an example to illustrate the viewpoint of suspicion, in fact the simulation in our thesis is totally lay under the *ideal* situation, and even in such ideal situation the wavevectors (velocities) of electrons exhibit an adequately broad distribution aspect, reference Fig. 7.1, so we could expect the spin relaxation rate is more fast when we proceed the operation (simulation) under the action of combination of many operation cases, see Fig. 7.8 et al. If this aspect is true, well! unfortunately the possibility of the application of spintronics, especially for in terms of the spin control approach is lowered. About the part of

cheer, the reason comes from that we find the *enough* long about the relaxation time which exhibited from our thesis. From the point of view of the improvement of modern industrial techniques, such long relaxation time owns the so great potential in practical application. Anyhow there are existing many problems which obstruct the advancement of the practical application in the point of view of spin control, e.g. the injection of nonequilibrium electronic spin is still a big problem nowadays and so on. However the experimental exploration and demonstration and the theoretically fundamental research are still necessary hurry-scurry in future! In one word nature is so novel and unexpected inspired by the nature exploration history, at present we even could not realize what happened about and even predict the position of an electron in next moment, who know what happened about the nature in future!?



References

- [1] S. Datta, *Electronic Transport in Mesoscopic Systems* (Cambridge University Press, Cambridge, 1995).
- [2] S. Das Sarma *et al.*, Phys. Rev. B **32**, 8442 (1988).
- [3] M. L. Roukes *et al.*, Phys. Rev. Lett. **59**, 3011 (1987).
- [4] C. J. B. Ford *et al.*, Phys. C **21**, L325 (1988).
- [5] C. J. B. Ford *et al.*, Phys. Rev. Lett. **62**, 2724 (1989).
- [6] C. M. Marcus *et al.*, Phys. Rev. Lett. **69**, 506 (1992).
- [7] M. J. Berry *et al.*, Phys. Rev. B **50**, 8857 (1994).
- [8] A. M. Chang *et al.*, Phys. Rev. Lett. **73**, 2111 (1994).
- [9] R. M. Clarke *et al.*, Phys. Rev. B **52**, 2656 (1995).
- [10] R. P. Taylor *et al.*, Phys. Rev. Lett. **78**, 1952 (1997).
- [11] A. G. Huibers *et al.*, Phys. Rev. Lett. **81**, 1917 (1998).
- [12] A. S. Sachrajde *et al.*, Phys. Rev. Lett. **80**, 1948 (1998).
- [13] M. C. Gutzwiller, *Chaos in Classical and Quantum Mechanics* (Springer-Verlag, Berlin, 1990).
- [14] S. Datta *et al.*, Appl. Phys. Lett. **56**(7), 665 (1990).
- [15] S. J. Pearton *et al.*, J. Appl. Phys. **93**, 1 (2003).

- [16] H. Ohno, *Science* **281**, 951 (1998).
- [17] V. Dediu et al., *Solid State Commu.* **122**, 181 (2002).
- [18] D. A. Pejaković *et al.*, *Phys. Rev. Lett.* **88**, 057202 (2002).
- [19] K. Tsukagoshi *et al.*, *Nature (London)* **401**, 572 (1999).
- [20] B. Zhao et al., *Appl. Phys. Lett.* **80**, 3144 (2002).
- [21] I. Zutic et al., *Rev. Mod. Phys.* **76**, 323 (2004).
- [22] F. Bloch, *Phys. Rev.* **70**, 460 (1946).
- [23] H. C. Torrey, *Phys. Rev.* **104**, 563 (1956).
- [24] J. I. Kaplan, *Phys. Rev.* **115**, 575 (1959).
- [25] D. Loss *et al.*, *Phys. Rev. A* **57**, 120 (1998).
- [26] M. A. Brand *et al.*, *Phys. Rev. Lett.* **89**, 236601 (2002).
- [27] S. Namba, *J. Phys. Soc. Jpn.* **63**, 224 (1994).
- [28] J. Nitta *et al.*, *Phys. Rev. Lett.* **78(7)**, 1335 (1997).
- [29] J. M. Elzerman *et al.*, *Nature* **430**, 431 (2004).
- [30] D. J. Griffiths, *Introduction to Quantum Mechanics* (Prentice Hall, Inc. 1995).
- [31] H. C. Ohanian, *Am. J. Phys.* **54**, 500 (1986).
- [32] D. Hestenes, *Am. J. Phys.* **47(5)** (1979).
- [33] D. Griffiths, *Introduction to Electrodynamics*, 3rd ed. (Prentice-Hall International, Inc. 1999).
- [34] H. Goldstein, *Classical Mechanics* (Addison-Wesley Publishing Company, 1980).
- [35] J. J. Sakurai, *Modern Quantum Mechanics*, revised ed. (Addison-Wesley Publishing Company, Inc. 1994).

- [36] J. J. Sakurai, *Advanced Quantum Mechanics* (Addison-Wesley, Reading, MA, 1967).
- [37] R. J. Elliot: See E. N. Adamas, II, Phys. Rev. **92**, 1063 (1953), reference 7.
- [38] G. Dresselhause *et al.*, Phys. Rev. **95**, 568 (1954).
- [39] R. H. Parmenter, Phys. Rev. **100(2)**, 573 (1995).
- [40] G. Dresselhause, Phys. Rev. **100(2)**, 580 (1995).
- [41] S. V. Kravchenko *et al.*, Phys. Rev. B. **50(11)**, 8039 (1994).
- [42] V. M. Pudalov, JETP Lett. **66**, 175 (1997).
- [43] S. J. Papadakis *et al.*, Science **283**, 2056 (1999).
- [44] H. Ohno (Ed.), vol. **10** of Physica E (2001).
- [45] C. Kittel, *Quantum Theory of Solids* (Wiley, New York, 1963).
- [46] Y. A. Bychkov *et al.*, J. Phys. C: Solid State Phys. **17**, 6039 (1984).
- [47] U. Rössler *et al.*, Solid State Commun. **121**, 313 (2002).
- [48] G. Goldoni *et al.*, Phys. Rev. Lett. **69(17)**, 2567 (1992).
- [49] R. Winkler, *Spin-Orbit Coupling Effects in Two-Dimensional Electron and Hole Systems* (Springer, 2003).
- [50] The main idea to make such connection is due to Hui-Fen Lo *et al.* from private communication (2006).
- [51] M. Cardona *et al.*, Phys. Rev. B. **38(3)**, 1806 (1988).
- [52] D. G. Seiler *et al.*, Phys. Rev. B. **16(6)**, 2822 (1977).
- [53] H. Riechert *et al.*, Phys. Rev. Lett. **52(25)**, 2297 (1984).
- [54] R. Eppenga *et al.*, Phys. Rev. B. **37**, 10923 (1988).
- [55] R. Winkler, Phys. Rev. B. **69**, 045317 (2004).

- [56] C. Jung *et al.*, J. Phys. A. **21**, 2301 (1988).
- [57] H. U. Baranger *et al.*, Chaos. **3**, 665 (1993).
- [58] P. Gaspard *et al.*, J. Chem. Phys. **90**, 2225; 2242; 2255 (1989).
- [59] R. V. Jensen, Chaos. **1**, 101 (1991).
- [60] N. W. Ashcroft *et al.*, *Solid State Physics* (Holt Rhinehart, and Winston, New York, 1976).
- [61] H. U. Baranger *et al.*, Phys. Rev. B. **54**, R14297 (1996).
- [62] D. C. Langreth *et al.*, Phys. Rev. B. **24**, 2978 (1981).
- [63] H. U. Baranger *et al.*, Phys. Rev. B. **40**, 8169 (1989).
- [64] D. S. Fisher *et al.*, Phys. Rev. B. **23**, 6851 (1981).
- [65] M. Buttiker, Phys. Rev. Lett. **57**, 1761 (1986).
- [66] R. A. Jalabert *et al.*, Phys. Rev. Lett. **65**, 2442 (1990).
- [67] A. G. Mal'shukov *et al.*, Phys. Rev. B **66**, 081311(R) (2002).
- [68] R. Fiederling *et al.*, Nature (London) **402**, 787 (1999).
- [69] A. T. Hanbicki *et al.*, con-mat/0110059.
- [70] J. C. Egues, Phys. Rev. Lett. **80**, 4578 (1998).
- [71] R. Blümel *et al.*, Phys. Rev. Lett. **60**, 477 (1988).
- [72] Cheng-Hung Chang *et al.*, Phys. Rev. B **70**, 245309 (2004).
- [73] The prototype of simulation programs for spin relaxation topic is mainly come from Cheng-Hung Chang, and that for spin transport topic is partially come from Cheng-Hung Chang (2006).
- [74] Cheng-Hung Chang *et al.*, Physics Letter A **326**, 436-441 (2004).

Vita

Jengjan Tsai, a boy was born in 1968 in Tainan city of the Republic of China (R.O.C.). His learning process is B.S. (Mechanical Engineering) in National Taiwan University of Science and Technology (1999), M.S. (Physics) in National Chiao Tung University (2006) et al. He is a boy who likes and loves the natural world. He likes the life with a simple way since he is not a wheeler-dealer. At present there are still many tasks waiting for running after for him. He strongly desires to execute his dream in his life, a nice job (which offer just enough income for living), a nice residence, a lovely girl, enjoy the world, enjoy math and physics, help others (families, people, living objects, environment, the world et al.) and so on.